DESIGN AND PERFORMANCE EVALUATION OF AN IMPROVED PHOTOVOLTAIC THERMAL (PVT) COLLECTOR POWERED DRYER

BY

MUNKAILU, ABUBAKAR AHMED SADIQ

(Reg. No: 20134873228)

A THESIS SUBMITTED TO THE POSTGRADUATE SCHOOL

FEDERAL UNIVERSITY OF TECHNOLOGY OWERRI

IN PARTIAL FULFILMENT OF THE REQUIREMENTS FOR

THE AWARD OF MASTER OF ENGINEERING (M.ENG.)

IN

MECHANICAL ENGINEERING

(ENERGY AND POWER OPTION)

JANUARY, 2022

CERTIFICATION

This is to certify that this research work on "Design and Performance Evaluation of an Improved Photovoltaic Thermal (PVT) Collector Powered Dryer" carried out by **MUNKAILU ABUBAKAR AHMED SADIQ (B.ENG)** with registration number **20134873228**, is a thesis submitted to the Postgraduate School, Federal University of Technology, Owerri, in partial fulfilment for the award of Master of Engineering in Energy and Power Engineering in the Department of Mechanical Engineering of the Federal University of Technology Owerri.

05/01/2022

Engr. Prof. Nnamdi V. Ogueke
(Project Supervisor)

05/01/2022
Date

05/01/2022

Engr. Dr. O. C. Nwufo
(Co-Project Supervisor)

05/01/2022
Date

09/02/2022

Engr. Dr. Osita O. Obiukwu
(Ag. Head of Department)

09/02/2022
Date

Engr. Prof. J. C. Ezeh
(Dean, SEET)

Date

Engr. Prof. C. C. Eze
(Dean, Postgraduate School)

Date

5 January, 2022

External Examiner
Engr. Prof. O. V. Ekechukwu

Date

DEDICATION

I dedicate this work to Almighty Allah for his unconditional love and guidance in my life and also to my beloved parents for their unrelenting support in my career path.

ACKNOWLEDGEMENTS

May all praises and thanks be ascribed to Almighty Allah for the gift of life, and the wisdom to excel in my career path.

My sincere appreciation goes to my project supervisor Engr. Prof. Nnamdi V. Ogueke for his continuous support, encouragement, and advice all through the course of this work. You remain the pillar behind the success of this work and will forever remain blessed. I sincerely thank the head of department, Engr. Dr. Osita O. Obiukwu, Prof. E. E. Anyanwu and Dr. O. C. Nwufo for the key roles they played throughout the course of this work. Also, I wish to acknowledge all other lecturers of Mechanical Engineering Department for the unrelenting roles they played in making this work a success.

Special thanks to the Deans of School of Engineering and Engineering Technology (SEET) and Post Graduate School (PGS) for the unconditional access they granted me whenever their attention was needed.

To my parents, siblings, and wife, I say God bless you all for your support in every aspect of my life.

A special appreciation goes to my friend and colleague; Engr. Boniface Ugochukwu, for his unconditional support throughout the course of this work. My appreciation to Engr. Emukah Nnamdi C. for his assistance in the fabrication and safe-keeping of the experimental rig, and I also thank Mr. James Daniel for his unwavering assistance all through the period of data collection.

Grateful I am, and may Allah bless you all (Ameen).

ABSTRACT

This work involves the design, construction and testing of an improved Photovoltaic thermal collector (PVT) powered dryer used in the drying of agricultural products. The setup consists of a 0.989m^2 PV panel, an air flow channel modified by fitting twenty curved aluminium vanes, each of height 50mm with a curvature radius of 31mm, thus covering a distance of 37mm from its base, a charge controller, temperature probes, thermo-couple temperature reader, a DC fan, a 12V battery and a 0.078m^3 drying chamber constructed using a ply-wood. The PVT collector is formed by the assembly of the modified air-flow channel and the PV panel. The PVT collector outlet is connected to the drying chamber at an angle of 8.48° for maximum harvesting of solar radiation at the test location, with the setup facing due south. Air is drawn beneath the PV panel and subjected to a serpentine flow pattern through the configuration of the aluminium vanes in the air-flow channel. The air flow regime is aided by the use of a DC fan installed directly on the exit vent of the drying chamber thereby enabling the heated air drawn in from the PVT collector to be used for drying 5kg of cassava from the initial moisture content of 65% to the final moisture content of 15% wet basis. Temperature probes are fitted to the inlet and outlet region of the air flow channel, likewise in the drying chamber and the temperature readings are displayed on the digital thermo-couple temperature reader. The 12V battery powers the fan and the temperature reader during periods of low solar insolation while the charge controller ensures that the battery is continuously charged and at the same time protects the battery from being over charged. The PVT powered solar dryer was tested for a total of thirteen days: five days unloaded test and eight days of loaded test under the meteorological conditions of FUTO from 8:00h to 17:00h daily. The maximum recorded PV surface temperature for the loaded and unloaded tests are 49°C and 50°C respectively. The upper and lower regions of the drying chamber recorded identical maximum temperatures readings of 49°C during the unloaded test which corresponds to an 11°C rise from ambient temperature. Also, during the loaded test, the upper and lower region of the drying chamber recorded maximum temperatures of 47°C and 46°C respectively, corresponding to 9°C and 8°C rise in ambient temperature respectively. The PVT collector recorded an average thermal efficiency of 48.52% while the drying chamber efficiency ranged from 44.96 – 82.72% at a moisture removal rate of 0.07 – 0.21Kg/hr. Therefore addition of the curved aluminium vanes in the air-flow channel has significantly improved waste heat recovery efficiency from PV panel leading to overall PVT powered dryer performance improvement.

KEY WORDS: PVT collector, air-flow channel, drying chamber, temperature, thermal efficiency, drying chamber efficiency.

TABLE OF CONTENTS

LIST OF FIGURES

LIST OF TABLES

NOMENCLATURE

A_c = Collector area (m^2)

A_{dc} = Surface area of drying bed (m^2)

a_w = Water activity

$\mathcal{B}$ = Dimensionless parameter whose value ranges between 0.14 – 0.25

B_{dc} = Breadth of the drying chamber (m)

C_{pa} = Specific heat of air (kJ/kgK)

C_{pg} = Specific heat capacity of cassava (kJ/kgK)

F' = Collector fin efficiency factor (%)

F_R = Collector heat removal factor

H = Monthly mean daily global radiation incident on a horizontal surface (MJ/m^2daily)

HR = Humidity ratio (kg_w/kg_a)

H_b = Beam radiation on a tilted surface (MJ/m^2daily)

H_d = Diffused radiation (MJ/m^2daily)

H_f = Final moisture content for safe storage of the cassava after drying (Kg)

H_{hac} = Height of hot air column (m)

H_o = Monthly average daily extraterrestrial radiation on a horizontal surface (MJ/m^2daily)

H_T = Monthly average daily solar radiation on a tilted surface (MJ/m^2daily)

h_w = Wind heat transfer coefficient (W/m^2C)

I_o = Maximum intensity of the solar radiation/solar constant; 1367 (W/m^2)

I_t = Intensity of radiation incident on the plane of the collector (W/m^2)

K = Extinction coefficient of cover material (glass)

K_T = Clearness index

L = Glass thickness (mm)

L_c = Collector length (m)

L_{dc} = Length of the drying chamber (m)

L_v = The latent heat of vaporization (KJ/Kg)

M = Equilibrium moisture content (kg_w/kg_a)

m_f = Final moisture content (Kg)

m_i = Initial moisture content (Kg)

m_p = Initial mass of product to be dried (Kg)

M_T = Total mass of air needed for drying (Kg)

m_w = Amount of moisture content to be removed (Kg)

$\dot{m}$ = Mass flow rate (kg/s)

n = Julian day number

$n_1 \& n_2$ = Average refractive index in solar spectrum

P_a = Partial pressure of dry air in the atmosphere (N/m^2)

P_c = Critical pressure of water (Pa)

Q_u = Useful energy gain received by the drying air (kJ/s)

R_a = Specific gas constant (J/kg K)

R_b = Ratio of beam radiation on a tilted surface to that of a horizontal surface

R_g = Gas constant for water vapour (J/kg K)

$r_{\parallel}$ = Parallel component of reflection

$r_{\perp}$ = Perpendicular component of reflection

S = Average monthly solar radiation absorbed by the collector per unit area of the absorber (W/m^2)

T_a = Ambient temperature (°C)

T_b = Boiling temperature of water at atmospheric pressure (°C)

T_c = Critical temperature of water (°C)

t_d = Drying time required (s)

T_f = Temperature of air leaving the drying bed (°C)

T_{fr} = Freezing temperature of water at atmospheric pressure (°C)

T_i = Inlet air temperature (°C)

T_m = Mean temperature of the liquid (°C)

T_o = Outlet air temperature (°C)

T_{pm} = Mean absorber plate temperature (°C)

T_{pt} = Temperature of the product (°C)

T_t = Total drying time (s)

U_L = Overall heat loss coefficient (W/m^2K)

V_a = Volume of air required for drying (m^3)

$\dot{v}$ = Volume flow rate (m^3/s)

W_c = Collector width (m)

$\eta_{(c)PVT}$ = Thermal efficiency of the PVT collector (%)

η_s = Solar dryer efficiency (%)

GREEK SYMBOLS

α = Angular absorptance of the absorber plate of the incident energy

β = Collector slope/tilted angle (degrees)

δ = Angle of declination (Degree)

θ_i = Incident angle (Degree)

θ_z = Zenith angle (Degree)

$(\theta_1 = \theta_i)$ = Angle of incidence (Degree)

θ_2 = Angle of refraction (Degree)

ρ = Density (Kg/m^3)

ρ_d = Reflectance of the cover system for diffused radiation incident from the bottom side

ρ_g = Ground reflectance

τ = Transmittance of the cover system at the desired angle of incidence

τ_a = Transmittance considering absorption losses alone

τ_r = Transmittance due to reflection losses

$(\tau\alpha)$ = Transmittance-absorptance product

$(\tau\alpha)_e$ = Effective transmittance-absorptance coefficient

ω = Hour angle (Degree)

ω_s = Sunset angle (Degree)

ABBREVIATIONS

Ave = Average

Diff = Difference

ERH = Equilibrium relative humidity

Max = Maximum

Temp = Temperature

CHAPTER ONE
INTRODUCTION

1.1 Background of the study

The need for alternative renewable energy sources as a result of increasing fossil fuel prices, energy security challenges due to depleting fossil fuel reserves, and the environmental and health problems caused by the over-dependence on fossil fuel as a global energy source, have led to the increased search for environmentally friendly and renewable energy sources to address these challenges. One of such possible energy source is the Sun.

Exploiting the energy of the sun as an alternative source of green fuel looks very promising, hence its global acceptance as a possible energy source for compensating the global energy demand, considering that the earth's exposure to a small fraction of the sun's total energy output for about 30 minutes is estimated to be equal to the world's energy demand for one year (Nalis, 2012). Although solar energy has been identified as a cheap and inexhaustible source of renewable energy, researchers and designers have struggled to develop efficient collector models for harnessing and converting this energy into various uses such as electricity and heat generation.

Technological advances using stand-alone photovoltaic (PV) and solar thermal (ST) collectors in harnessing the energy of the sun are associated with operational defects. For instance, higher cell temperature in stand-alone PV systems leads to lower electrical conversion efficiency (Ogueke & Anyanwu, 2017). The poor electrical efficiency is because most of the absorbed solar radiation is dumped on the PV module as waste heat causing a further drop in efficiency per degree rise in temperature of the module (Karan, 2015). This undesirable effect may lead to extreme cell working temperature which may also cause a permanent structural damage to the module if the thermal stress remains for prolonged period (Chow, 2010).

The challenges of using stand-alone (PV) modules gave rise to modified proto-types known as photovoltaic thermal (PV/T) collectors. A PV/T system integrates a photovoltaic module and a solar thermal collector into a single unit that is used for co-generation of electricity and heat energy simultaneously. The advent of PVT systems using air or water as a working fluid for heat recovery has led to the extraction and conversion of what was once referred to as waste heat dumped on the PV surface into different useful purposes. This recovered heat can be used in applications such as solar drying, space heating and cooling, domestic water

heating (DWH), etc. PV/T systems have the advantage of requiring less space compared to standalone collectors. However, the need to optimize the electrical and thermal efficiencies for best results has led researchers and designers proposing different configurations and material selection for use in constructing a PV/T system. Various approaches adopted in trying to improve the efficiency of PV/T systems have been carried out. One of such works explained that one way to achieve considerable improvement in collector efficiency is to use an extended heat transfer area using corrugated surfaces, finned absorber, matrix type absorber, compound honeycomb collector, absorber with slats, and porous media (Fudholi, Othman, Ruslan, Yahya, Zaharim & Sopian, 2012). Similarly, the work of Hegazy (2000) used four PV/T air collector configurations to investigate the thermal, electrical, hydraulic and the overall performance of the system. Payman, Yahaya, Shamsollah & Hossein (2016) applied computational fluid dynamics to investigate the performance of four different fins geometries (rectangular, trapezoidal, curved, and pin) to ascertain the setup that extracted more heat from the PV panel while Deepali & Tiwari (2014) gave the efficiencies and temperature coefficient specifications for silicon and non-silicon based PV modules. Glazing has also been used in a channel above the PV panel setup in trying to improve the thermal efficiency of the system as sighted in the work of Ogueke, Njokuocha & Anyanwu (2017).

With successes recorded in the application of PV/T systems in domestic water heating, space heating and cooling, electricity generation, etc, its poor global implementation of three percent (3%) in solar drying (Jee, Iniyan & Suganthi, 2015), has left its potential largely un-tapped in the agricultural sector. Sun drying has been widely practiced by rural farmers in Nigeria due to its inexpensive nature. This system of preservation has led to these farmers battling with how to deal with minimizing agricultural wastes caused by unfavourable sun drying characteristics. Sun drying is unhygienic and unreliable due to its entire dependence on the weather conditions, non-uniform drying, loss of nutritional value, labour intensive and time consuming. An improved PV/T powered drier can play an important role in preserving agricultural products thereby reducing agricultural wastes likewise maintaining the nutritional value of the product.

1.2 Statement of problem

Most of the PVT powered dryers are characterized by poor performance as a result of poor heat extraction from the PV panel. This defect can be attributed to a poorly configured cooling medium/channel failing to generate the required turbulence in order to achieve efficient heat extraction from the PV panel. The challenge being that denser air in the lower

region of the flow channel is allowed to exit the flow channel without absorbing sufficient heat. This has resulted to achieving lower than possible exit air temperature from the system which also affects the quality of drying for most of the PVT powered dryers. Different flow configurations considered by some authors achieved varying degrees of energy extraction from the PV surface and subsequent exit air temperature. However, most of them have not been applied to a PVT powered dryer while those applied have not yielded the desired performance improvement that will lead to the general acceptance of PVT powered dryer. This work will introduce further modification in the airflow channel of PVT collector, hitherto not applied, with potential of increased energy recovery from the PV collector and subsequently used for crop drying and powering other accessories to be fitted into the PVT powered dryer.

1.3 Objectives of the study

The major objective of this work is the design and performance evaluation of an improved PVT powered dryer. The specific objectives of this work include:

i. To design and construct an agricultural produce dryer and select an appropriate PV panel area to deliver the desired drying temperature.
ii. To retrofit a PV panel into a PVT system, incorporating the modified air flow channel.
iii. To assemble the PVT and agricultural produce dryer to achieve a PVT powered dryer.
iv. To test the performance of the PVT powered dryer.

1.4 Justification of Study

The temperature of PV collectors increases during operation. This affects their operational efficiency and subjects the panel to extreme working condition. An effective heat removal technique will improve the thermal, electrical and overall efficiency of the PV collector while the waste heat recovered can be used for agricultural drying thereby discouraging open air drying which has severely exposed agricultural produce to poor healthy conditions for use.

1.5 Scope of study

This work is limited to the design, construction and performance testing of the PVT dryer system. Performance analysis carried out on the PVT dryer is based on parameters such as solar intensity, PV panel surface temperature, wind speed, relative humidity, inlet and outlet temperature of the flow channel, and drying chamber temperature.

CHAPTER TWO

LITERATURE REVIEW

2.1 Overview

Remarkable progress has been made in applying various renewable sources for energy generation, but environmental concern, health hazards, availability, and the soaring cost of conventional energy as well as its finite nature, led to the major drive behind studies in combined PVT systems as a means of energy supply (Ogueke & Anyanwu, 2017). Studies on PVT for energy generation began after the 1973/1974 oil embargo with the primary aim of reducing dependence on fossil fuel for electricity and thermal energy generation (Zondag, 2008).

However, there has been a poor implementation of PVT systems in solar drying as was reflected in the works of Jee et al. (2015) when they rated the application of solar thermal technologies as follows: tap water heating (39%), solar air heating (45%), solar cooling (7%), industrial heating (6%), **drying (3%)** and pool heating (0.2%). The progress made in advancing PVT technology and its application in solar drying will greatly improve food preservation techniques to sustainable heights.

The setup required for solar drying using PVT system consists of a PVT collector and a drying chamber. The PVT system has an air duct installed behind or above the PV module. The PV module can be manufactured using different materials such as mono-crystalline, poly-crystalline and amorphous silicon with each of them having varying electrical efficiency capability. The thermal absorber while extracting heat from the PV module surface simultaneously introduces a cooling effect on the module surface. This helps to improve its electrical efficiency while the hot air is channelled to the drying chamber in the form of thermal energy and used to reduce the moisture content of agricultural and other related products to acceptable levels. Thus, they can be preserved for a longer period of time. With the PV module having a poor electrical conversion efficiency of between 6%–15% (Deepali & Tiwari, 2014), designing an efficient flow channel will lead to the recovery of more heat energy that would have been lost to the environment. This will help improve the overall efficiency of the system as well as preserving the life span of the PV module.

Adopting PV/T systems for solar drying will tremendously minimise the challenges of agricultural wastes faced due to lack of adequate storage facilities for most perishable goods.

2.2 Classification of energy source

Based on their mode of generation, energy sources can be classified into renewable and non-renewable sources.

2.2.1 Non-renewable source

These are energy sources drawn from finite sources. Fossil fuels which include coal, crude oil, and natural gas are categorised under this energy sources. They are not eco-friendly and are available in limited supplies due to the time it takes to replenish.

2.2.2 Renewable source

These are energy sources that are constantly replenished and are inexhaustible. Some of their sources include solar energy, wind energy, geothermal energy, tidal energy, and hydropower. Renewable energy sources are used to produce clean energy thereby addressing most challenges faced using non-renewable sources. Some of their advantages include;

- Their sources are inexhaustible
- Economically viable
- They do not pollute the environment

All the renewable energy sources directly or indirectly depend on the heat from the sun's energy (solar energy) since it is the only source of heat in the universe. Also, human existence would have been impossible because earth as a planet would have been too cold to support human life likewise unavailability of food due to lack of photosynthesis.

2.3 Solar energy

This is the radiant energy emitted from the Sun which is harvested using special devices called collectors to generate electrical and heat energy. The Sun energy is generated from a nuclear fusion reaction which occurs deep in the core of the Sun. Nayeem-Ur-Rahman (2013), in his work, described the spectrum of the sun's radiation as one similar to the one of a blackbody at approximately 5777K with spectrum's emissivity considered as unity. He also disclosed that the solar radiation incident on the outside of the earth's atmosphere is $1367W/m^2$ with approximately $1000W/m^2$ reaching the earth and experiences a reducing effect as it passes through the atmosphere due to absorption of certain wavelengths by molecules in the atmosphere and diffusion by atmospheric pollutants. Nalis (2012) reported also that the Sun has a total energy output of about 3.8×10^{20} MW, which is equal to $63MW/m^2$ on the Sun's surface. However, only a small fraction (1.7×10^{14} kW) of the total radiation emitted is received by the earth, and the earth's exposure to this small fraction of

solar radiation for about 30 minutes is estimated to be equal to the world's energy demand for one year. This shows that solar energy can sustain global energy demands in all sectors. However, the only limitation is the lack of standard technological know-how in optimally harnessing it. Some solar energy applications includes crop drying, space heating and cooling through solar architecture, day lighting, domestic water heating, solar cooking, etc. The solar energy technology has many advantages compared to others energy sources. These advantages include;

- It is noiseless in operation.
- Does not produce any unwanted waste such as radioactive materials.
- Reliable performance.
- A credible system.
- Low maintenance system.

2.3.1 Solar energy characterisation

Solar technologies can either be photovoltaic or thermal. Photovoltaic systems convert sun energy into electricity while the thermal systems directly use the sun energy for heating, cooling, etc. The solar thermal systems are broadly characterized as either passive solar energy generation or active solar energy generation depending on the way they capture, convert, and distribute solar energy (Deepali & Tiwari, 2014).

2.3.2 Active solar energy generation

Active solar systems use mechanical means to convert solar radiation into usable energy for different applications such as solar drying, space heating, water heating and other uses. These systems require mechanical devices such as a pump, sensors or fan to collect the sun's energy (DOE 2010). The use of these mechanical devices helps in harnessing a large amount of available energy by activating the system immediately a reasonable temperature difference becomes present within the system.

Active solar techniques generally employ photovoltaic (PV) panels to generate electricity to drive the mechanical components of the solar thermal systems. Solar cells are known to convert only a small part of the solar energy that they absorb into electricity with efficiency ranging from 6%–15% depending on the type of cells (Deepali & Tiwari, 2014).

2.3.3 Passive solar energy generation

Passive solar techniques require designing spaces that naturally circulate air such that the air will start circulating when a certain amount of internal energy has built up within the system.

They do not require mechanical devices such as pumps, fans and sensors during their operation (DOE 2010). Passive solar energy generation can be categorized into direct gain and indirect gain systems. Direct gain involves directly heating the space of the building using solar energy absorbed through the south-facing windows of a building in the northern hemisphere or the north-facing windows of a building in the southern hemisphere. Indirect gain requires a storage mass that intercedes between the solar energy and the building (DOE 2010). Thus, the stored energy moves through internal spaces and then slowly delivered into the building.

2.4 Solar collectors and their classification

Collectors are special devices used to capture and convert the energy of the sun into electrical and heat energy. The collector geometry is very important in its application as it defines the mode of operation, and the quality of energy generated. Collectors are generally categorized as flat plate or concentrating collectors.

2.4.1 Concentrating collectors

Zondag (2008) reported that the quest for replacing expensive photovoltaic collectors (PVC) with cheap reflectors led to conceiving the design for concentrating collectors. Concentrating collectors use concentrating ratio (C.R) to increase flux radiation on the energy absorbing surface thereby leading to increased temperature at which energy can be delivered. They require tracking to maintain the quality of energy generated. They generate higher temperatures compared to flat plate collectors and could be used for various applications if active cooling is adopted.

2.4.2 Flat plate collectors

Flat plate collectors are used for low temperature applications (less than 60 °C) or medium temperature (less than 100°C). Flat plate collectors have a wide view and absorb up to 70% of the day light from the sun and their geometry enables them absorb both beam and diffuse solar irradiance encountering the collector (Tyagi, Kaushik & Tyagi, 2012). Hence, these types of collectors do not necessarily require a tracking mechanism.

2.5 The PV module: Composition and operational defects

Silicon and Germanium are two semi-conductors mostly used in making solar cells with silicon being more widely used. Mono-crystalline silicon (c-Si), poly-crystalline silicon (pc-Si), and amorphous silicon (a-Si) are the three major types of solar cells used in constructing silicon based solar panels (Deepali & Tiwari, 2014). However, these panels are faced with

operational defects such that absorbed radiation increases the cell temperature of a PV module up to a point where further increase in temperature will result to decrease in electrical efficiency. Ogueke et al. (2017) highlighted that during operation, the temperature of a PVC increases very significantly leading to reduced efficiency caused by an inverse relationship between its efficiency of conversion of solar radiation into electrical energy and temperature. Hence, the highest efficiencies of PVCs are obtained at low operating temperatures. Similarly, Karan (2015) reported that loss in electrical efficiency of a PV panel is due to an increase in short circuit current with a resultant decrease in the open circuit voltage which decreases the maximum power output. Hence, more that 50% of the solar energy not converted into electricity is converted to heat, which may lead to extreme cell working temperature, as high as 50°C above the ambient environment, and may also cause a permanent structural damage of the module if the thermal stress remains for prolonged period (Chow, 2010). Mono-crystalline and poly-crystalline silicon solar panel electrical efficiency decreases about 0.45% per degree rise in temperature while amorphous silicon electrical efficiency decreases about 0.25% per degree rise in temperature (Chow, 2010). In general, silicon-based PV modules have an electrical efficiency of about 12∼16% under standard test condition (STC: air mass 1.5, irradiation intensity 1000 W/m^2, and cell temperature 25°C) (Karan, 2015).

2.6 Photovoltaic thermal (PV/T) systems

A hybrid photovoltaic thermal solar system (PV/T system) is a combination of photovoltaic (PV) and solar thermal systems which produce both electricity and heat simultaneously from one integrated component or system (Chow, 2010). Figure 2.1 depicts the comparison of a PV, thermal and hybrid PV/T systems.

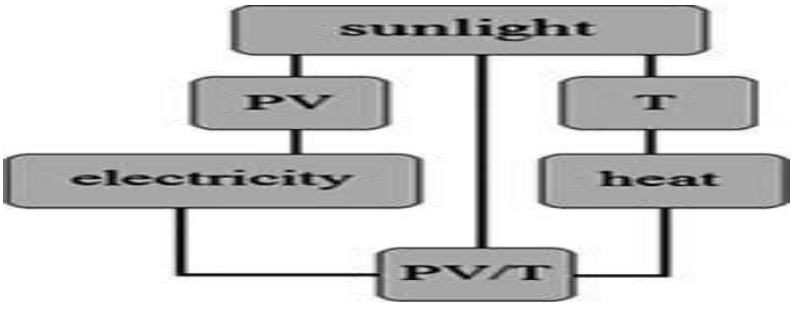

Fig. 2.1: Comparison of PV, thermal and hybrid PV/T systems (Source: Saffa, Riffat & Erdem, 2011)

PV/T collectors produce more energy per unit surface area than side-by-side PV modules and solar thermal collectors. Therefore, these systems are especially appropriate for the

applications where the available surface area is limited (Saffa et al., 2011). Figure 2.2 shows the main features of a flat plate PV/T collector.

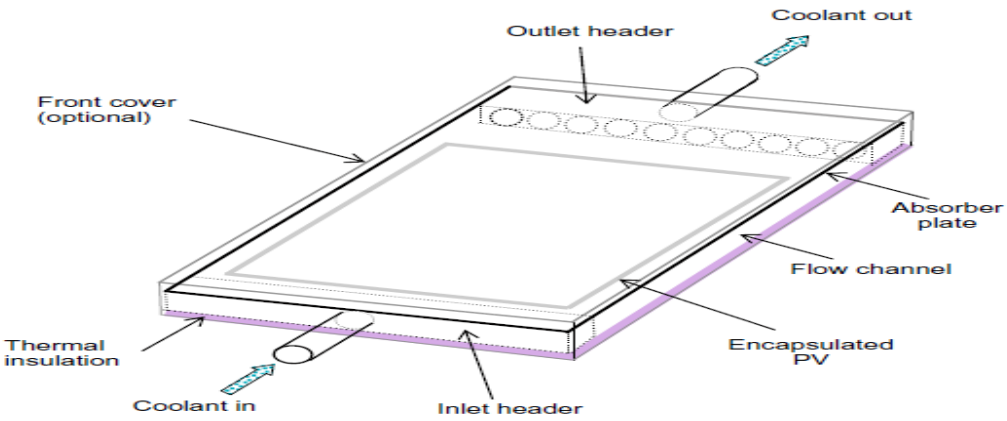

Fig.2.2: Main features of a flat-plate PVT collector (Source: Chow, 2010)

2.7 Classification of PV/T collector

PV/T collectors can either be used for liquid or air heating. According to Ogueke & Anyanwu (2017), they are generally classified based on the working fluid used which includes: PV/T water collector, hybrid water/air PV/T collector, and PV/T air collector. Figure 2.3 shows the major classification of PVT collectors.

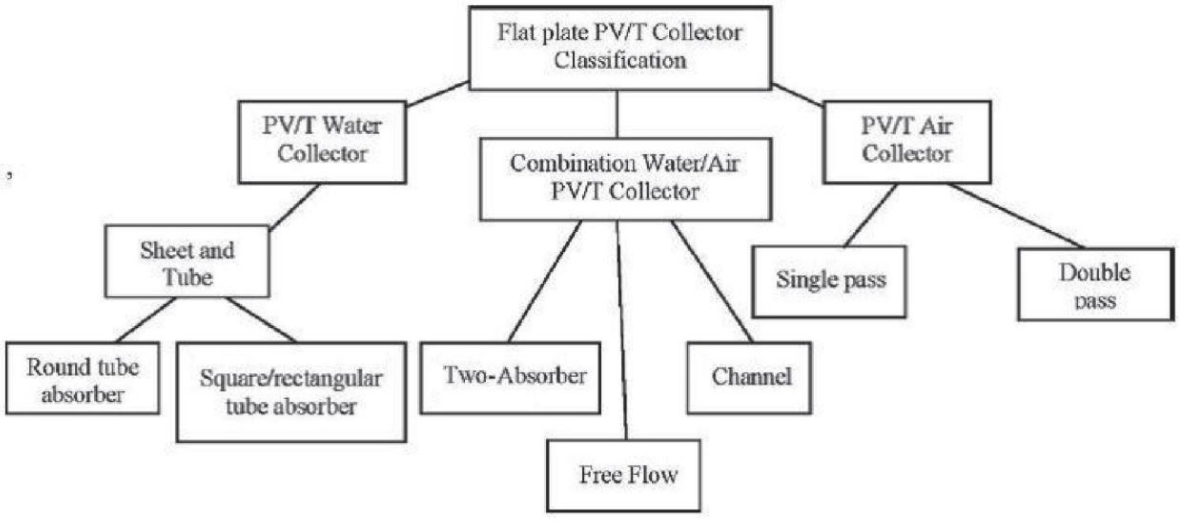

Fig. 2.3: Major classifications of PVT collectors (Source: Ogueke & Anyanwu, 2017)

2.7.1 PVT water collector

An extensive review carried out by Saffa et al. (2011) has shown that the first works on water PV/T collectors were performed by Kern and Russell at MIT in 1978 and ever since, various modifications using mono-crystalline silicon (c-Si), poly-crystalline silicon (pc-Si), and amorphous silicon (a-Si) have been carried out. Water is an available, clean and affordable

fluid used in various designs by researchers for optimizing the performance of PV/T systems. From Figure 2.3, it is shown that there are generally four categories for water based PV/T collectors classified in terms of the heat transfer techniques. They include the sheet and tube, channel, free flow, and two absorbers. These geometries are as shown in Figure 2.4.

Saffa et al. (2011) reported that the yield of nine design concepts of PVT water collectors classified in four categories as earlier mentioned were studied by Zondag, De Vries, Van Helden, Van Zolingen & Van Steenhoven (2003) and their electrical and thermal efficiencies found to be below the efficiencies of the corresponding standalone photovoltaic and solar thermal collectors. Furthermore, it was noted that the configuration that yielded increased thermal efficiency gave reduced electrical efficiency (Ogueke & Anyanwu, 2017). Saffa et al. (2011) also reported that the sheet and tube type among the water based PV/T collectors is the most promising for practical applications with both cost and effectiveness considered.

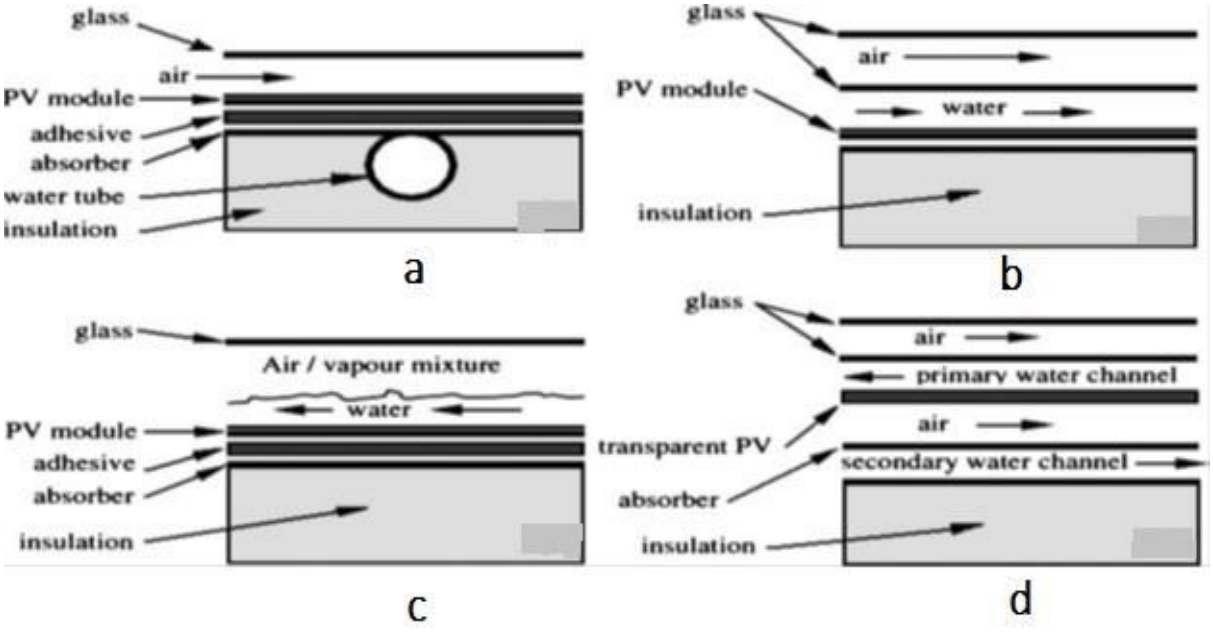

Fig. 2.4: Types of PVT collectors: (a) Sheet and tube (b) Channel (c) Free flow (d) Dual absorber (Source: Saffa et al., 2011)

2.7.2 Air type collectors

An extensive review performed by Zondag (2008) reported that the first PVT-air facility was the 'Solar One' house built in 1973/ 1974 at the University of Delaware by Professor Bo¨er and it was the first house which enabled the direct conversion of sunlight into both electricity and heat for domestic use. The air-type PV/T design provides a simple and economical solution to PV cooling with Figure 2.5 showing a sectional and exploded view of the PVT air collector having a channel above the absorber configuration.

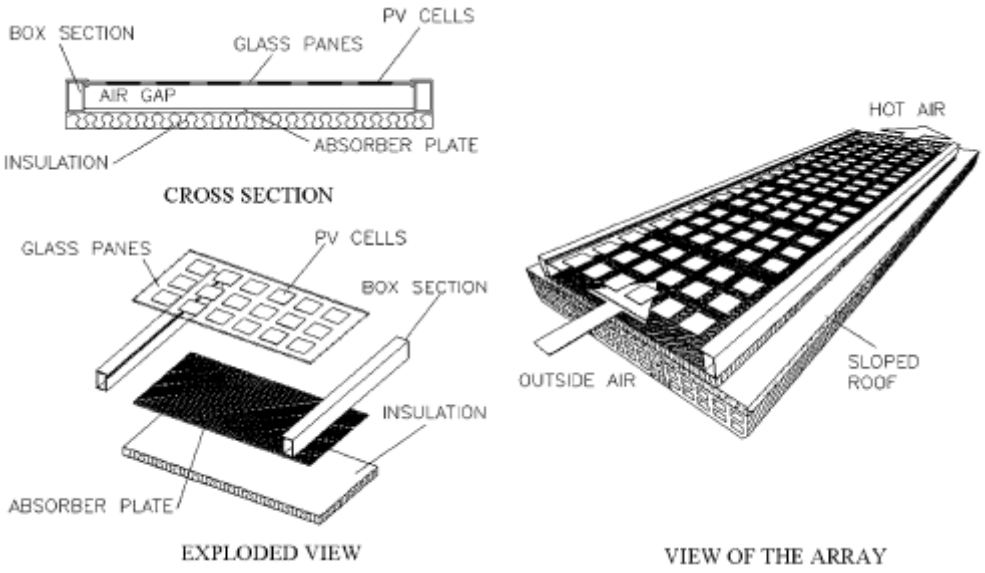

Fig. 2.5: Preliminary sketch of the collector (source: Aste, Giancarlo & Francesco 2008)

The collector has a channel above the absorber configuration, consisting of a glass pane which houses the PV cells, an absorber plate, an air gap separating the PV cells from the absorber plate and a back insulator preventing heat loss from the absorber material. The panel looks like a chessboard composed of squares with the PV cells embedded on it. Forced flow using a fan or natural flow through buoyancy effect can be used for air circulation through the air gap. Forced circulation is more efficient than natural circulation considering that it improves convective and conductive heat transfer properties of the cooling medium. Fresh air removes the heat absorbed by the collector, cooling in the same time the rear of the PV cells with the effect of an increment in the electrical conversion efficiency (Aste et al. 2008). Unfortunately, fan power reduces the net electricity gain of the PV/T air systems (Chow 2010). The air type collectors do not have specific classification; rather they are defined by how the air as the thermal fluid is used, such as in channel above the absorber, channel below the absorber and channel on both sides of the absorber in single or double pass ways (Chow 2010).

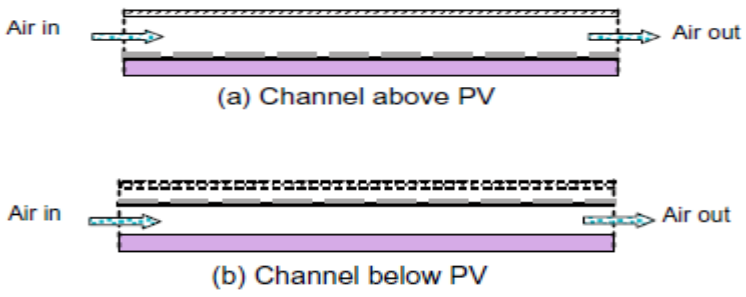

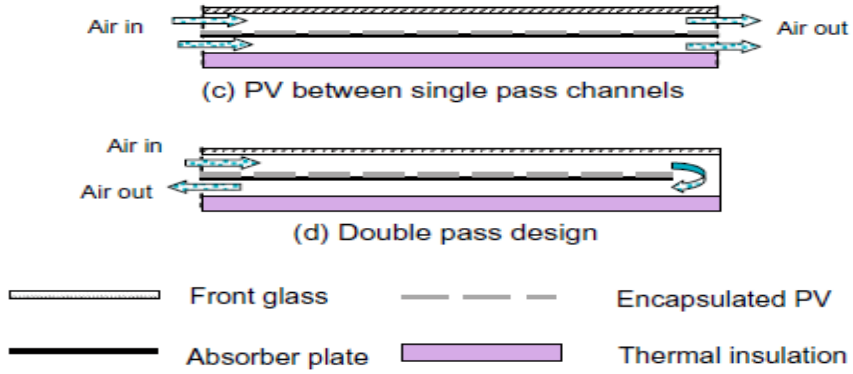

Fig. 2.6: Cross-section of some PVT air collector designs (source: Chow, 2010)

Hegazy (2000) investigated the thermal, electrical, hydraulic and overall performance of four types of flat-plate PV/T air collectors namely: channel-above PV, channel-below PV, PV between single-pass channels, and PV with double-pass design as shown in Figure 2.6. Using numerical analysis, it was shown that channel-above PV has the lowest performance, while the other three have comparable energy yields. Also, he observed that the least fan power was consumed by PV between single pass channels. Sopian, Liu, Kakac & Veziroglu (2000) developed a steady–state model for comparing the performance of single and double-pass PVT air collectors. The observed better performance of the double-pass design was attributed to the productive cooling of the solar cells and the reduction in front cover temperature. However, a robust flow channel configuration using a single-pass air collector can also be used in achieving productive cooling of the solar cells as acknowledged in the work of Ibrahim, Othman, Ruslan, Sohif & Sopian (2011).

Solanki, Dubey & Tiwari (2009) performed an indoor simulation and testing of photovoltaic thermal (PV/T) systems. They developed a system for thermal and electrical efficiencies of PV/T solar air heater connected in series. The experimental results show that the thermal efficiency gained is 42% and electrical efficiency is 8.4%.

Ibrahim et al. (2011) carried out some extensive reviews in renewable and sustainable energy. These included the works of Garg and Adhikari (1995), who performed the steady state simulation on the conventional hybrid PV/T collector of single and double-glass covers of PV/T air heating system. They conclude that the parametric studies of PV/T air collector showed that increase in collector length led to an increase in thermal efficiency and a corresponding decrease in electrical efficiency. Also, decrease in duct depth resulted to lower cell temperatures hence improving the electrical efficiency of the system while increase in mass flow rate resulted to an increase in both the electrical and thermal efficiencies of PVT systems.

Hegazy (2000) confirmed that glazed PVT collectors produce more heat but have slightly lower electrical yield, and unglazed PVT collectors produce relatively less thermal energy but show higher electrical performance. Glazed PVT collectors are very similar in appearance to flat-plate solar thermal collectors, consisting of a PV-covered absorber in an insulated collector box having a glass cover. The glass-covered insulation leads to increase in the PV module temperature which leads to high thermal efficiency and a reduced electrical efficiency. Unglazed PVT collectors are similar to regular PV panels. They consist of a PV-covered absorber with no glass cover. The configuration without a glass cover results in lower thermal efficiency and a higher electrical efficiency due to the cooling effect experienced by the PV module.

Ogueke & Anyanwu (2017) in their review of PV/T collectors noted that the outlet fluid temperature of air PV/T system is within 42–55°C, representing an increase of 25°C above the inlet value. Also, they reported that in the work of Kim and Kim (2012), thermal efficiency of glazed PVT collector was found to be 14% higher than that of the unglazed one while the electrical efficiency of the unglazed PVT collector is 1.4% higher than that of its glazed counterpart. Also, the glazed PV/T collectors' overall energy performance was 12.6% higher than that of the unglazed system.

2.8 Air based PV/T system applications

The air based PVT systems have numerous applications which include agricultural produce drying systems, power generation, and also for space heating such as in solar ventilation systems, air pre-heating systems, building integrated photovoltaic thermal (BIPVT) systems and other applications.

2.8.1 PVT systems in space heating

PVT systems can be used for active solar space-heating by absorbing solar radiation from the sun and then transferring the heat directly to the desired space or to a storage system using electric fans or pump. According to US Department of Energy (DOE), space heating is a medium-temperature application and consists of two basic types of active solar space-heating systems which are the air and liquid based systems.

Air-based systems use air as the heat-transfer medium in an air collector while liquid-based systems use water or an antifreeze solution in a hydronic collector as the heat-transfer medium. They can be used for either domestic or commercial applications. PVT systems can be adopted for different types of active solar space-heating applications such as in air

preheating used for ventilation in buildings and in building integrated photovoltaic thermal (BIPVT) collectors.

2.8.1.1 Building integrated photovoltaic thermal (BIPVT) systems

Active solar space-heating systems are faced with the challenges of more sophisticated design, installation, and maintenance techniques hence the initiative of PVT research in the 1990s was apparently a response to the global environmental deterioration and the growing interest in building-integrated photovoltaic (BIPV) designs in other to solve these challenges (Chow, Tiwari & Menezo, 2013). Building-integrated photovoltaic thermal (BIPVT) collectors involves the use of the entire façade or roof of a building to absorb solar radiation with the heat recovered converted to meaningful use such as in domestic hot water and electricity simultaneously, in addition to its function as the building cover. BIPVT are multi-functional and can be used for space heating or cooling, air preheating for ventilation, domestic water heating, electricity etc. In conventional BiPVT systems, an air gap is often provided at the rear of the PV arrays for the air cooling of modules by natural convection.

The versatility and potentials of BIPVT has led to various research works carried out in this field. In a review carried out by Chow et al. (2013), various performance assessment were carried out on BIPVT systems. Such reviews include the works of Bazilian and Prasad (2002) that assess the performance of various operational and control modes on a building equipped with a roof-mounted PVT/air system using ESP-r and TRNSYS simulation tools. The monitored actual energy use data of the building showed very positive results.

Mei et al. (2003) studied the dynamic performance of a BiPVT/air collector system constructed at the Mataro Library in Spain. The heating and cooling loads for various European buildings with and without such a ventilated facade were then evaluated. Using TRNSYS for the modelling, their result was validated against experimental data from a pc-Si PV facade. The simulation results showed that more winter heating energy can be saved by the use of the preheated ventilation in a building located in Barcelona, but less for Stuttgart in Germany and Loughborough in UK. The higher latitude locations therefore need a higher percentage of solar air collectors in the combined system.

Zogou and Stapountzis (2012) carried out experimental works on a PVT façade in order to have a better understanding of the flow and turbulence with natural and forced convection modes. Using CFD modelling, the results show that the selection of flow rate and the heat-transfer characteristics of the back sheet are very critical.

Jie et al. (2002) studied numerically the energy performance of a ventilated BiPV façade in Hong Kong. It was found that the free airflow gap affects little the electrical performance, but is able to reduce the heat transmission through the PV façade.

Yang et al. (2011) carried out a similar study to that of Jie et al. (2002) using the weather conditions of three cities in China: Hong Kong, Shanghai, and Beijing. It was found that on typical days the ratio of space cooling load reduction owing to the ventilated PV facade is 33–52%.

Chow et al. (2009) investigated the BiPVT options of a hotel building in Macau, with the PVT facade associated with a 24-hour air-conditioned room. The effectiveness of PV cooling by means of natural airflow was investigated with two options: free openings at all sides of the air gap as Case 1 and in Case 2, the enclosed air gap that behaves as a solar chimney for air preheating. These were also compared with the conventional BiPV without ventilation. The ESP-r simulation results showed an insignificant difference in electricity output from the three options. This was caused by a reverse down flow at the air gap at night, owing to the cooling effect of a 24-hour air-conditioned room located behind the PVT facade. It was concluded that both the climate condition and system operating mode affect significantly the PV productivity.

2.8.2 Solar drying using air PV/T collector

Solar dryers are compartments designed to achieve controlled drying of agricultural and other related products within a given period of time. The use of solar dryers aids the storage of quality dried products. Integrating solar dryers with PV/T air collector will enhance the environment, wealth creation and nation building as well as sustainable development for any country (Ibrahim et al., 2011). There are several designs for PV/T air collector systems, however, its application in solar drying has mostly been carried out experimentally with few practical applications available (Jee et al., 2015). Solar drying has a crucial role to play in the agricultural and food industry. Hot and humid weather conditions particularly in Nigeria, presents a very perfect opportunity for air PV/T collectors to be used to obtain good quality dried products.

Ogueke et al. (2017) designed and measured the performance of a PV/T Air solar dryer. In their work, a single pass channel above the absorber plate glazed with a 4mm plain glass and a DC fan attached to the drying chamber was used to achieve the desired drying effects. The results obtained showed a maximum drying chamber temperature of 47.9° C and 46.2°C for

the loaded and unloaded tests respectively representing an increase of 11.6°C and 9.2°C, respectively above the ambient temperature. Also, an average thermal PV/T collector efficiency of 18.9% was achieved. Fudholi, Othman, Ruslan, Yahya, & Sopian (2011) developed a model using an excel software in analysing raw data obtained from drying kinetics of seaweed. The setup comprises of a double-pass PV/T collector with finned absorber, a blower for forced convection, an auxiliary heater and the drying chamber. The initial and final moisture content of the seaweed were 94.6% (wet basis) and 10% (product basis) respectively after a drying time of about 7 hours at an average solar radiation of about 600 W/m^2 and air flow rate 0.0613kg/s. overall, an average collector efficiency of 31% was recorded during the experiment. However, although the auxiliary heater improved the collector efficiency, additional cost will be required in powering the auxiliary setup hence making the model not being cost effective for commercial farmers.

Fudholi et al. (2012) using a mathematical model developed in 2011 for the drying kinetics of seaweed, developed an experimental setup for the drying of oil palm fronds. The solar drying system was evaluated for drying 100 kg palm oil fronds with a drying time of about of 3 drying days from an initial moisture content of 60% to the final moisture content of 10% wet basis (wb). It was observed that a temperature of 55°C could be reached at a solar radiation level of 650 W/m^2 and a mass flow rate of 0.13 kg/s giving an overall system efficiency of about 20%.

Sajith and Muraleedharan (2013) carried out a study on the drying of Amla using a hybrid solar dryer and compared it with open sun drying. In the work, an experimental hybrid photovoltaic thermal (PV/T) dryer consisting of a double pass arrangement that produced both electric and thermal energy simultaneously was developed. They concluded at the end of the study that the developed hybrid PV/T drying system produced better quality products in shorter time through the efficient use of solar energy compared to open sun drying.

Tonui, Mutai, Mutulu, Mbuge & Too (2014) designed and evaluated a PVT powered grain dryer having a back-up heater. A forced convection technique was adopted to reduce the drying time. A prototype dryer with minimum collector area of 0.6 m^2 was fabricated and used in the experiment. The dryer efficiencies of the solar and solar assisted dryer were found to be 39.9% and 57.7%, respectively. The back-up heating system improved the efficiency of the dryer by 17.8% and reduced drying time substantially. The setup was able to maintain a consistent air temperature inside the dryer leading to the reduction in maize moisture content from 19.3% to 13.7% in 3 hours. They concluded that the same result will be achieved using solar system alone in 3 days of 4 hours daily drying. However, Tonui et al. (2014) failed to

use the calculated mass flow rate of 271.780Kg/hr (0.0755Kg/s) which should have resulted to a thermal efficiency of 36.73%, rather an assumed mass flow rate of 0.12Kg/s was used which gave a thermal efficiency of 59%. Also, the air flow pattern and collector geometry were not specified in this design. Also, the design will require additional funding due to the inclusion of a back-up heater.

Sajith and Muraleedharan (2014) carried out an economic analysis of a hybrid PV/T solar dryer for drying Amla. They used an annualized cost method to find out the net benefits and simple payback period of the setup. Cost and economic parameters such as capital cost of hybrid dryer, capital cost of electric dryer, life span of the dryers, discount rate, electricity cost, maintenance cost, and salvage value were considered during the analysis. A payback period of 5.66 years was found which is very low compared to the 20 years life span of the system. Poor payback period implies poor overall efficiency of this setup due to thermal and optical losses.

Fterich, Chouikhi, Elloumi, Bentaher & Maalej (2015) studied the performance of an agro-food solar dryer equipped with a PV/T air collector. The dryer was constructed to include two compartments: the first one is a direct dryer while the second one is a mixed dryer. To evaluate the performances of the system, tomatoes cut in thin layers were dried naturally and in the mixed compartment under the climatic conditions of Tunisia. The dryer performance was evaluated for two days with 2kg of tomatoes in each compartment. The mixed solar drying exhibited best thermal and electrical efficiencies of 55% and 12.9% respectively. The best global (total) efficiency was 64%.

2.9 Possible reasons for poor Photovoltaic thermal (PV/T) application in drying

Though quite a number of experimental studies have been carried out using PV/T air collectors, its poor application in drying has been a challenge faced by designers and researchers. Different modifications have been made in designing PV/T setups in order to achieve higher collector efficiency. Also, some key operating parameters such as the mass flow rate, ambient temperature, irradiance etc, have been studied with different solutions proffered in optimizing collector performance.

The possible reasons for poor photovoltaic thermal applications in solar drying can be categorized into two groups, namely,

- Design challenges
- Challenges of varying operating parameters.

2.9.1 Design challenges

Design procedure involves the necessary measures or steps taken in making an efficient and reliable prototype. However, challenges encountered during the design process have largely limited the application of PV/T systems in solar drying. These challenges include

- Configuration of the flow channel
- Effect of collector length

2.9.1.1 Configuration of the flow channel

Improving the general efficiency of PV/T collectors for suitable solar drying and other applications has led to various design modifications of their flow channel thus influencing their air flow pattern. This objective has been achieved by the use of baffles, fins, thin metal sheets, and other materials that are good conductors of heat. These materials are given different shapes with the idea of effectively reducing the PV panel surface temperature by converting it to heat energy through these flow channels and removing heat, thereby improving both electrical and thermal efficiency.

Bhattacharyya, Anandalakshimi & Srinivasan (2017) performed a heat transfer analysis on finned plate air heating PVT collector used in paddy drying. The air heating solar collector with rectangular fins attached was studied theoretically for various controlling parameters such as numbers of fins, height to duct (H/D) ratio and fin thicknesses. Outlet air temperature and pressure drop were considered as controlling parameters to find optimum number of fins, fin height and fin thickness. It was observed that the outlet air temperature first increased and then decreased with number of fins while pressure drop increased with number of fins and fin height. Optimum design of the system produced higher outlet temperature at steady state than required. The analysis showed that finned plate air heating solar collector with 80 fins, 0.6 Height (H) to-Duct length (D) ratio and 2 mm fin thickness yielded best results for paddy drying applications.

Similarly, using a pc-Si PV module with absorber area of 0.4 m^2, Payman et al. (2016) applied computational fluid dynamics to investigate the performance of four different fins geometries (rectangular, trapezoidal, curved, and pin) as shown in Figure 2.7.

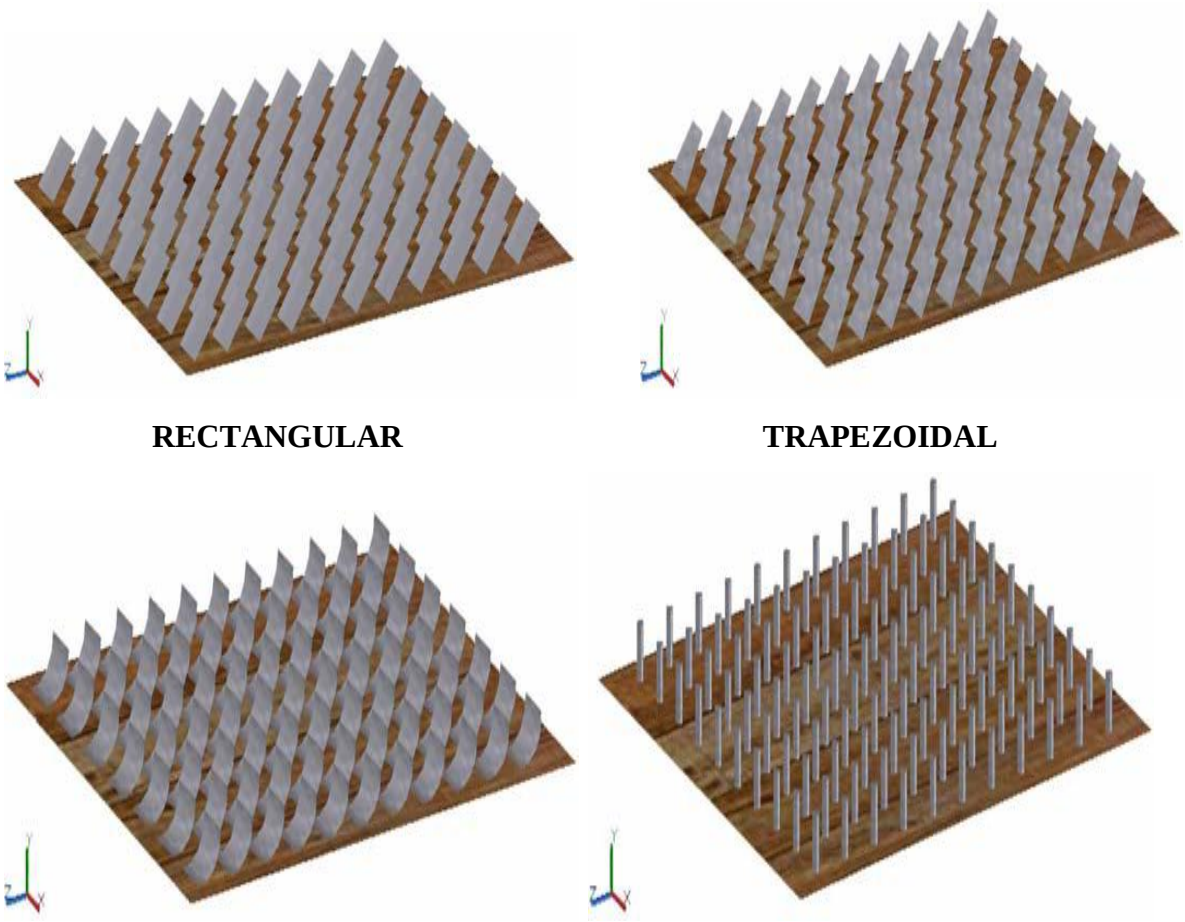

Fig 2.7: Different fins geometries (Source: Payman et al., 2016)

Duct heights of 4, 6, 8, and 10 centimetres and velocity magnitudes of 0.5, 1, 2, and 3 m/s were considered using an air based PV/T system as shown in Table 2.1. The best result was achieved using a 4 cm duct height, rectangular fin and 3 m/s velocity magnitude with a corresponding cell temperature of 33°C.

Table 2.1: Cell temperature at 3 m/s velocity magnitude (Payman et al., 2016)

Duct height / Fin type	4	6	8	10
No fin	36	37	38	39
Rectangular	33	34	35	36
Trapezoidal	34	35	36	36
Curved	34	34	36	37
Pin	35	36	37	38

Pottler, Sippel & Beek (1999) used four different fin configurations shown in Figure 2.8 in optimizing hybrid air PV/T collector performance.

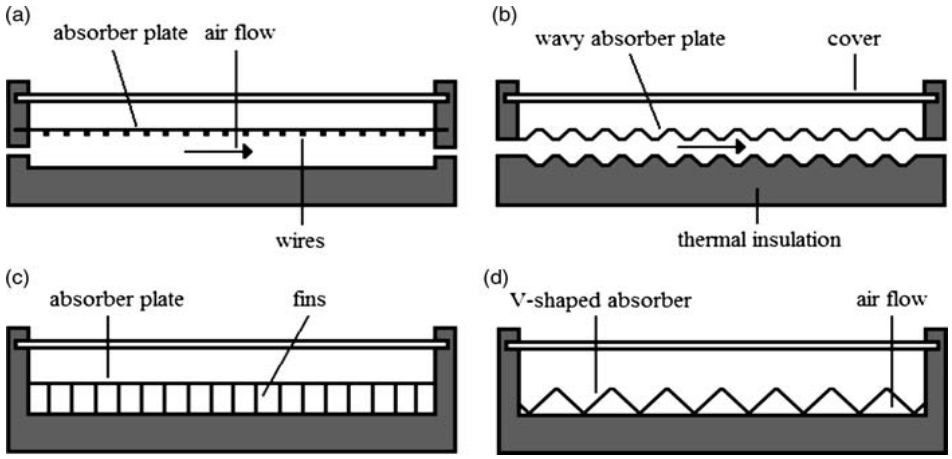

Figure 2.8: (a) Absorber plate augmented with wires, (b) Wavy absorber plate, (c) Absorber plate integrated with rectangular fins and (d) V-corrugated absorber plate (Source: Pottler et al., 1999)

The results indicated that the third setup with continuous rectangular fins had the highest net energy gain. This was achieved with the fins spaced close to each other with an optimal distance between 5–10mm and a laminar optimal flow regime having a low Nusselt number and large heat exchange area.

Alfegi, Sopian & Othman (2007) studied the performance effect of air flow rate for single pass double duct PV/T system with fins. The experiment was performed with PV/T cells placed on top of the fin as depicted in Figure 2.9. Results show that with the fin attached underneath, the PV efficiency increased from 49.135% to 62.823% as mass flow rates varies from 0.0316 to 0.09 kg/s, solar radiation of 600 W/m^2 and inlet temperature of 35°C.

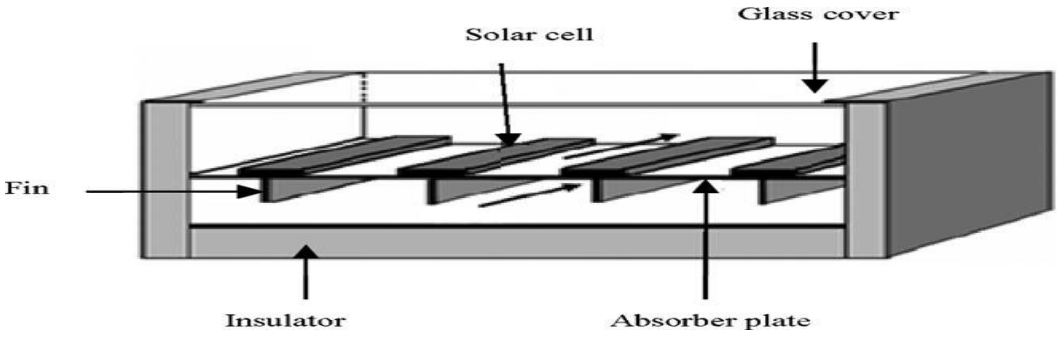

Fig. 2.9: Cross-section of single pass PV/T with finned of double duct PV/T air heaters (Source: Alfegi et al., 2007)

Jin, Ibrahim, Yee & Roonak (2010) simulated the performance of a single-pass photovoltaic-thermal air collector with rectangular tunnel absorber. The tunnel as shown in Figure 2.10 acted as an absorber fixed underneath the photovoltaic panel with the major aim being to identify the suitable air flow for cooling the PV panel. The results showed an electrical

efficiency of 10.02%, a thermal efficiency of 54.70% and a combined PV/T efficiency of 64.72% with solar irradiance of 817.4 W/m^2, mass flow rate of 0.0287 kg/s and an ambient temperature of 25.8°C. They concluded that the hybrid PV/T with rectangle tunnel as heat absorber shows higher performance compared to conventional PV/T system.

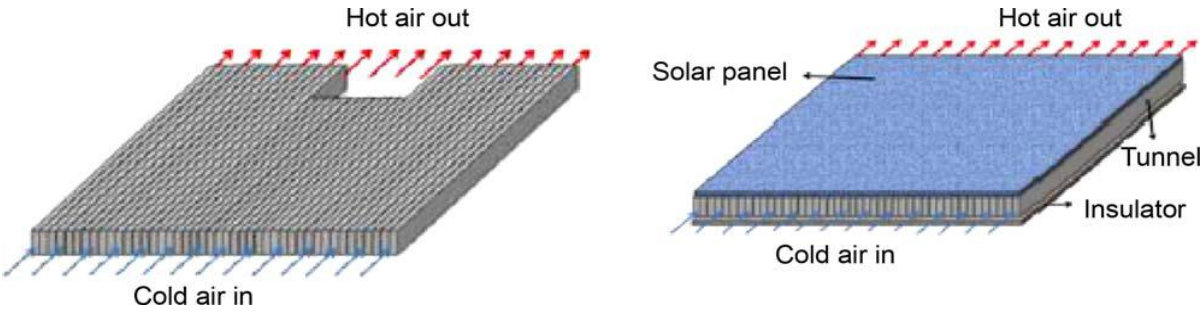

Fig. 2.10: Single-pass PV/T with rectangular tunnel design (Source: Jin et al., 2010)

Ibrahim et al. (2011) carried out comparative study to investigate the effect of mass flow rates on the thermal and electrical efficiencies of the hybrid collectors. As shown in Figure 2.11, a single pass rectangular tunnel absorber collector was designed and compared with spiral flow absorber collector. The single pass rectangular tunnel is designed to generate hot air and electricity while the spiral flow is designed to generate hot water and electricity. Both absorber collectors were fixed underneath the flat plate single glazing sheet of polycrystalline silicon PV module. The experiment results shows that the spiral flow absorber collector generates combined PV/T efficiency of 64% with electrical efficiency of 11% and maximum power output of 25.35 W and single pass rectangular tunnel absorber collector generated combined PV/T efficiency of 55% with electrical efficiency of 10% and maximum power output of 22.45 W.

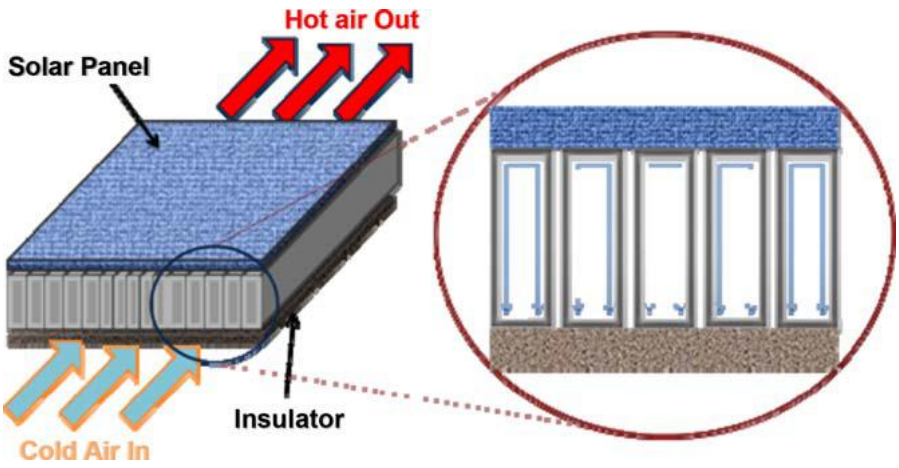

Fig.2.11: Cross-section of PV/T air collector with rectangular shape absorber collector design (Source: Ibrahim et al., 2011)

Ibrahim et al. (2011) cited Othman et al. whose work was based on development of advanced solar assisted drying systems consisting of a single pass PV/T collector. The PV/T collector, as shown in Figure 2.12, was designed with v-groove shape and placed underneath the PV plate. Air was used as the heat transfer medium to transfer heat out. During the experiment, air flow rate ranging from 69.6± 2.2×10^{-4} kg/s to 695.8 ± 2.2×10^{-4} kg/s was passed through the v-groove. The result shows that by adding the v-groove to the design, the PV/T efficiency increased by 30% higher when compared to other type of PV/T collectors.

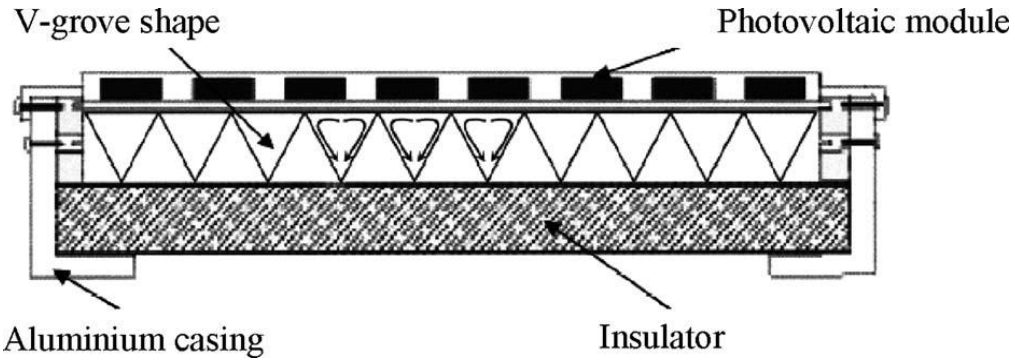

Fig. 2.12: Cross-section of PV/T collector with v-groove (Source: Ibrahim et al., 2011)

Hussain, Othman, Yatim, Ruslan, Sopian, Anuar & Khairuddin (2015) studied an improved air photovoltaic/thermal (PV/T) solar collector combined with hexagonal honeycomb heat exchanger. The honeycomb was installed horizontally into the channel located under the PV module. The system was tested with and without the honeycomb at irradiance of 828 W/m^2 and mass flow rate spanning from 0.02 kg/s to 0.13 kg/s. It was observed that the aluminium honeycomb is capable of enhancing the thermal efficiency of the system efficiently. At mass flow rate of 0.11 kg/s, the thermal efficiency of the system without honeycomb is 27% and 87% with honeycomb. The electrical efficiency of the PV module improved by 0.1% throughout the range of the mass flow rate. The improved design is suitable to be further investigated for solar drying system and space heating.

2.9.1.2 Effect of collector length

The effect of collector length on the system performance is depicted in Figure 2.13. The length of the PV/T air collector was varied while keeping the number of PV cells constant. It was observed that while the thermal efficiency increased, electrical efficiency decreased with an increase in the length of the collector.

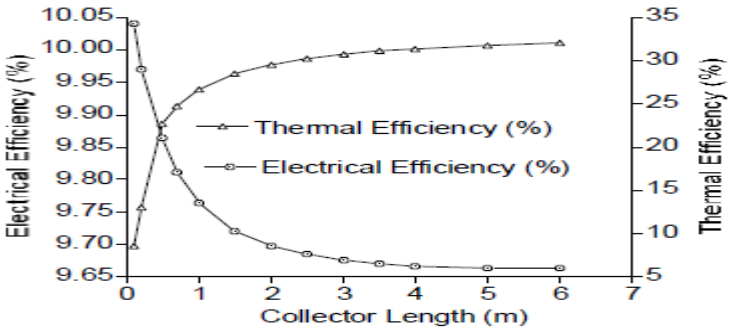

Fig. 2.13: Effect of Collector Length (Source: Koech, Ondieki, Tonui & Rotich, 2012)

This was caused by decreasing packing factor as the length increases resulting in an increase in the amount of solar radiation directly absorbed by the tedlar through the inter-cell spaces. The tedlar layer protects the PV cells from atmospheric elements such as rain due to its low moisture absorption. It also helps to increase the electrical efficiency of the PV module, by reflecting the incoming radiation which has surpassed the PV cells back to the PV module. The variations in the efficiencies, however tend to be very minimal at large collector lengths due to an increase in the amount of heat loss at the top cover (Koech et al., 2012).

2.9.2 Challenges of varying operating parameters

The thermal efficiency of a PV/T system is dependent on the ambient temperature which varies throughout the year and the temperature difference between its inlet and outlet, while the electrical efficiency is largely dependent on the incoming solar radiation and slightly dependent on the temperature of the PV cells (Jee et al., 2015). This shows that the thermal and electrical performances of a PV/T system are largely dependent and affected by a number of operating and design parameters which are not constant all year round. Koech et al. (2012) developed a steady state model of an air PVT single pass channel below the PV configuration and the temperatures of the glass cover, PV cells, the tedlar, the flowing air and the back plate were determined using a FORTRAN95 simulation program. This model was used to investigate the effects of some key operating parameters which include ambient temperature, irradiance and flow rate conditions and the various conclusions reached are highlighted below.

2.9.2.1 Effect of mass flow rate

The effect of mass flow rate on electrical and thermal performance of air PV/T collector is shown graphically in Figure 2.14.

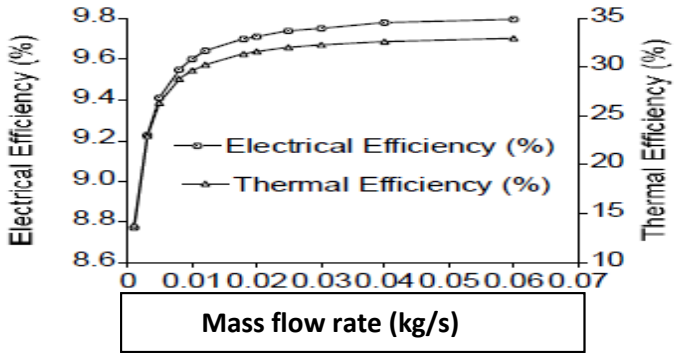

Fig. 2.14: Effects of mass flow rate (Source: Koech et al., 2012)

As observed, the thermal and the electrical efficiencies increased as the mass flow rate increases. However, further increase in mass flow rate above 0.02kg/s resulted to a slight increase in both the electrical and thermal efficiencies. The more the amount of heat extracted by the air, the lower the PV module temperature and the higher electrical and thermal efficiencies (Koech et al., 2012). An optimum flow rate of 0.01kg/s for maximum heat transfer is required for producing higher electrical and thermal efficiencies since it is evident that above a certain value, an increment in mass flow rate has a negligible resultant effect on electrical and thermal efficiencies.

2.9.2.2 Effect of ambient temperature

Koech et al. (2012) observed that an increase in ambient temperature results in a steady decline in electrical and thermal efficiencies of PV/T air systems as shown in Figure 2.15. Higher inlet fluid temperature due to increasing ambient temperature leads to poor heat extraction from the PV cells. There is need for developing techniques for moderating the inlet temperatures of PV/T panels in order to design systems with higher thermal and electrical efficiencies.

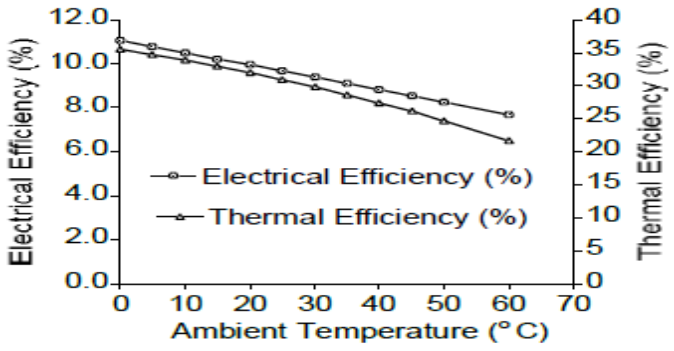

Fig. 2.15: Effect of ambient temperature on electrical and thermal efficiencies (Source: Koech et al., 2012)

2.9.2.3 Effect of irradiance

Solar irradiance is a measure of the amount of solar power received at a particular location. It varies throughout the year and depends on the position of the sun, season of the year, and the weather condition. From the results obtained by Koech et al. (2012), it is observed that the thermal efficiency increases with increasing irradiance whereas the electrical efficiency decreases with increasing irradiance as depicted in Figure 2.16. The increase in thermal efficiency at high irradiance is due to the increase in the temperature of the tedlar and the back plate. This implies that more heat will be transferred to the air in the flow channel. The observed decrease in electrical efficiency is due to the increase in the PV cell operating temperature with irradiance.

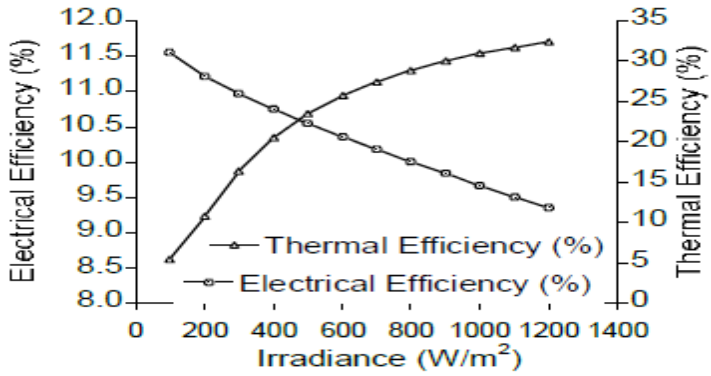

Fig. 2.16: Effect of irradiance on electrical and thermal efficiencies (Source: Koech et al., (2012)

2.10 Observations from literature review / Research gap

(i) Poor implementation of air PV/T systems for drying agricultural products such as cassava, tomatoes, maize etc.

(ii) PVT systems with excellent heat transfer configuration between PV and heat removal media are yet to be established, hence the continuous effort in improving the electrical and thermal efficiencies as observed from the literatures reviewed so far.

(iii) Several material and construction issues are yet to be met eg. Incorporating materials that will improve the heat retention capability of agricultural produce dryers.

(iv) For optimum heat extraction from PV panel, air mass flow rate should be between 0.01-0.03 kg/s.

CHAPTER THREE
MATERIALS AND METHOD

Figure 3.1 shows the schematic diagram of the PVT powered dryer.

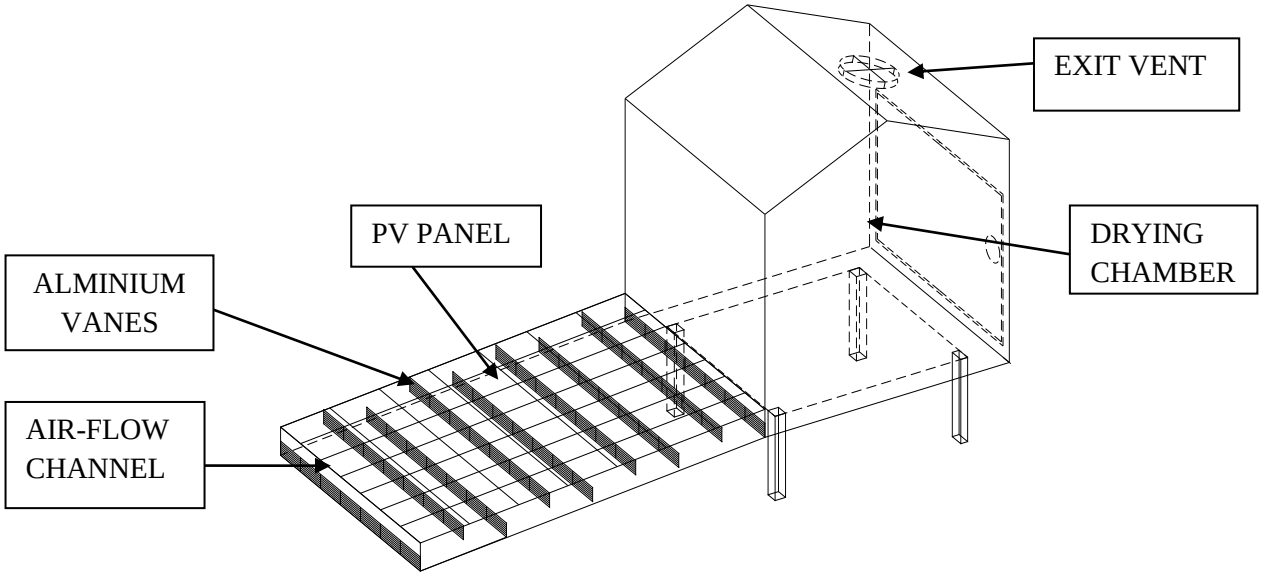

Figure 3.1: Schematic diagram of the PVT powered dryer

3.1 Mode of operation

The PVT powered dryer consists of a drying chamber, a PV panel, a charge controller, a digital thermo-couple temperature reader and air flow system (ducts and fan system). The primary aim of this setup is based on waste heat recovery and electrical energy generation which is to be used in powering peripheral devices such as the charge controller, thermo-couple temperature reader and the DC fan, installed in the PVT dryer. The air flow channel configuration is based on a single pass channel below the PV panel and the assembly of the air flow channel and the PV panel forms the PVT collector. The flow channel is designed such that curved aluminium vanes are uniformly spaced behind the PV panel and on the base of the air-flow channel as depicted in the sectional view in Figure 3.2. The ambient air drawn into the flow channel experiences a serpentine flow pattern as it comes in contact with the aluminium vanes along the channel. This configuration aids the air to absorb more heat as it will be heated for an extended period before exiting the flow channel and entering into the drying chamber, thereby leading to a corresponding cooling effect experienced on the PV panel surface. This in turn improves the quality of hot air delivered into the drying chamber. A DC fan installed at the exit vent of the drying chamber is used to draw air into the drying

chamber. The fan also ensures that the moisture picked up during drying exits the drying chamber without affecting both the content to be dried and the materials used in fabricating the drying chamber. The fan power is stored in a battery which is continuously charged by electrical energy generated from the PVT system using a charge controller. The charge controller also ensures that the battery is not overcharged, thus guarantying optimum performance and extended lifespan of the battery. Also, a digital thermo-couple temperature reader that is powered by an interface of electrical energy generated from the PV panel and the energy stored in the battery is used to display the temperature values for the PV panel surface, the inlet and exit of the flow channel, and also, inside the drying chamber using a five-point switch. The temperature probes inserted at these stated points are connected to the thermo-couple temperature reader. These temperature probes are used for measuring temperature values at their installed positions, which are then transmitted to the digital thermo-couple temperature reader where the numerical values are digitally displayed. A hand-held thermometer is used to compare temperature readings with those displayed on the thermo-couple temperature reader, in particular, the ambient and PV panel surface temperatures. An environmental meter was used to measure real time values for relative humidity of the atmosphere and drying chamber, wind velocity, and ambient temperature. The drying chamber consists of two layers constructed using a wire mesh and a door located behind the chamber. The PVT powered dryer is constructed in consideration that heat loss through the drying chamber is minimal.

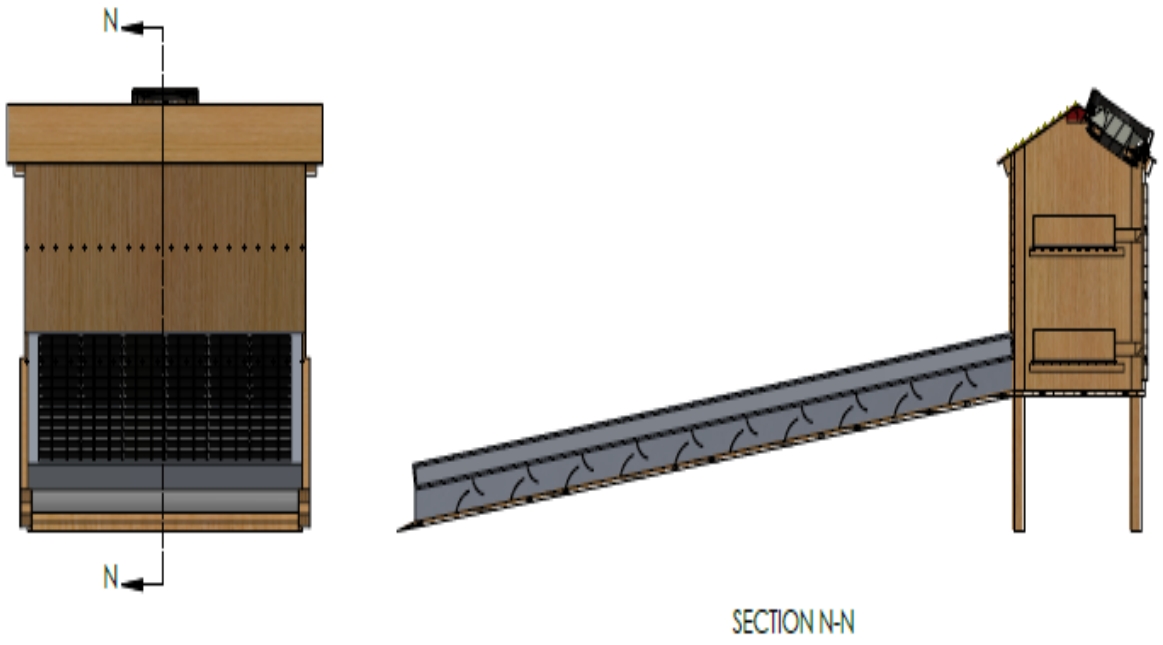

Figure 3.2: Sectional view of the PVT Powered Dryer

3.1.1 Materials

Materials and their description of use in the construction of the PVT powered solar dryer are highlighted in table 3.1.

Table 3.1: Materials used in constructing PVT powered dryer

S/N	MATERIALS	DESCRIPTION OF USE
1	100watts poly crystalline PV panel of dimension 1.476m by 0.670m	Fastened on top of the flow channel using both screws and gum. The gum prevents leakages throughout the flow channel.
2	2 ½ sheet of ½ inch ply wood	Used in constructing both the flow channel and the drying chamber.
3	One lengths of 2x2 inch hard wood	used for the construction of the base columns, flow channel sub-assembly and the roof peak support
4	One Length of 2x2 inch soft wood	Used in the construction of tray support, tray frame and rafter.
5	672x200x5mm stainless steel mesh	Used in the construction of the drying tray by attaching them below the drying tray frame using nails.
6	One DC extraction fan	Attached directly on the exit vent in other to aid the removal of moisture content from the drying chamber
7	Cabinet door hinges	Used to hold the door to the drying chamber in position
8	Two pounds weight of 1 ½ inch nail and screw	Used to assembly all components together
9	Bottle of medium sized wood gum and adhesive gum	For making the entire assembly as air tight as possible. Also, for attaching the aluminium vanes firmly to the flow channel in other to achieve the desired flow configuration.
10	¼ sheet gauge 22 aluminium sheet	Used for the construction of the vanes
11	Wood polish	Used in polishing the entire wooden setup
12	Temperature probes	Used in determining temperatures at the inlet, outlet, lower and upper chamber region
13	Thermo-couple temperature reader	Gives digital reading of the temperature values in the areas stated in 12 above
14	12V DC battery	The fan power is stored in a battery
15	Charge controller	Continuously charges the battery from electrical energy generated from the PVT system
16	Five point fan switch	Used to select the point that the temperature is to be displayed on the thermo-couple temperature reader

3.1.2 Instrumentation

In order to achieve accurate data reading during performance testing of the PVT powered solar dryer, some instruments such as the digital thermo-couple temperature reader, temperature probes, and a charge controller were integrated into the setup. Also, some hand held instruments such as digital pyranometer, environmental meter and an analogue thermometer were also used during the course of this work.

3.1.2.1 Digital thermo-couple temperature reader and temperature probes

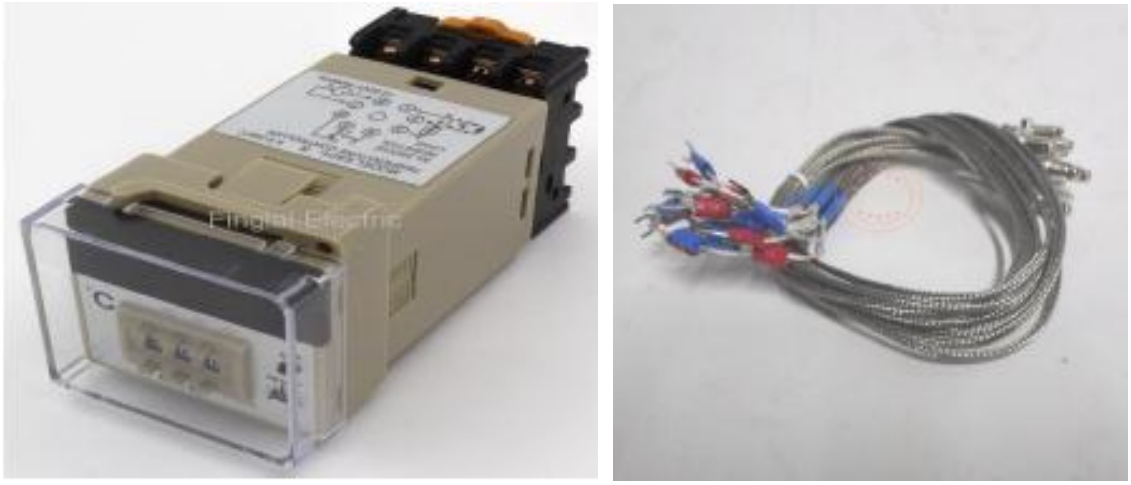

Plate 3.3: Thermo-couple temperature reader and temperature probes

The thermo-couple temperature reader is used to instantly readout temperature values at the various points equipped with temperature probes. The temperature probes are connected to the thermo-couple temperature reader, and they are used for measuring temperature values at their installed positions. During the course of this work, four temperature probes were connected to the PVT powered solar dryer to readout temperatures at the inlet/ambient region, outlet region, lower region of the drying chamber and upper region of the drying chamber respectively.

Due to unavailability of a DC thermo-couple temperature reader within the locality where this work was carried out, an AC thermo-couple temperature reader powered using a locally constructed inverter which converted the electrical input from 220V alternating current (AC) to 12V direct current (DC) was used in the setup.

3.1.2.2 Digital pyranometer

Plate 3.4: Digital pyranometer

This hand-held instrument is used to measure solar intensity at any instant. It can be powered directly by solar energy or using a battery. The device is positioned towards the sky and the value for solar intensity is recorded whenever it becomes relatively steady within a very brief period. This is because the intensity of solar radiation continuously changes while readings are taken.

3.1.2.3 Environmental meter

Plate 3.5: Environmental meter

This is a multi-purpose hand-held device used to measure air velocity, relative humidity, temperature and luminous intensity. It also has a built-in k-type input which allows it to be used for measuring high air and surface temperatures.

In this work, it was used to measure the atmospheric relative humidity, drying chamber relative humidity and air velocity at intervals of 30 minutes during the loaded test experiment. Also, its temperature reading was compared with the one displayed on the thermo-couple temperature reader and the variation between both devices was within 1°C range.

3.1.2.4 Charge controller and analogue thermometer

The charge controller is a device that automatically controls the rate at which electric current is being added or withdrawn from a battery. It protects the battery from being overcharged

thereby preserving the lifespan of the battery. The charge controller used in this work was locally fabricated and performed optimally throughout the experiment.

The analogue thermometer which is a hand-held device used for measuring temperature was used during the cause of this work for measuring the surface temperature of the PV panel.

3.2 Methods

Location analysis with respect to performance evaluation of the PV/T powered drier was carried out at department of Mechanical Engineering, Federal University of Technology Owerri (FUTO). Owerri is a town in the eastern part of Nigeria with latitude of 5.48°N and longitude of 7.03°E. The average wind velocity is in the range of 2.61 - 3.63 m/s while the ambient temperature ranges from 31°C to 35°C. The average daytime relative humidity also ranges from 75% to 90% (Okorafor, Akinbile, & Adebayo, 2018). Table 3.2 depicts the meteorological condition of Owerri which were used in the optimal sizing of the collector.

The month of July was selected as the reference month for this work since it has the lowest insolation value of 13.10MJ/m^{2}daily (Augustine and Nnabuchi, 2010).

Table 3.2: Meteorological condition of Owerri, Imo State

S/N	Parameter	Condition	Reference
1	Longitude and Latitude (ϕ)	7.03°E and 5.48°N	Ogueke et al. (2017)
2	Average monthly wind velocity	2.61 - 3.63 m/s	Ogueke et al. (2017)
3	Date	15th July	Present work
4	Julian day number (n)	196 days	Present work
5	Hours of daily sunshine considering the clearness index obtained during the stated period (8am – 5pm).	9 hours	Present work
6	Average day time temperature	31 - 35°C	Ogueke et al. (2017)
7	Mean daily global solar radiation intensity	13.10 – 17.19MJ/m^{2}day	Ogueke et al. (2017)
8	Average monthly relative humidity	75 – 90%	Okorafor et al. (2018)
9	Mean monthly temperatures	25 - 32°C	Okorafor et al. (2018)

3.2.1 Experimental procedure

The PVT powered dryer is positioned facing due south with the collector section tilted at an angle equal to the latitude of the test location, thus, enabling maximum harvesting of solar radiation at the test location. The experiment is carried out from 8am – 5pm daily with readings for the selected parameters such as solar radiation intensity, relative humidity, PV panel surface temperature, ambient temperature, outlet temperature, wind speed, etc, recorded at intervals of 30 minutes in order to achieve real time statistical data that closely depict the fluctuating meteorological condition of the test location. The experiment is carried out for both loaded and unloaded tests.

However, for optimal sizing/dimensioning of the PVT collector and the drying chamber, a detailed mathematical procedure has to be carried out to determine the following;

1. Positioning of the PVT setup
2. Drying kinetics for the product considered
3. Evaluation of the collector thermal performance
4. Optical properties of the cover material

3.3 Positioning of the PVT dryer for effective operation

Various parameters stated below have to be calculated in determining the positioning of the PVT drier with respect to position of the sun in the sky during daily operations.

3.3.1 Collector slope/tilted angle ($\boldsymbol{\beta}$)

For maximum harvesting of solar radiation at the test location, the installation is positioned facing due south at a collector slope/tilt angle equal to the latitude (ϕ) of the test location plus a 3° (Ogueke et al., 2017).

$$\text{Collector slope } (\beta) = 5.48° + 3° = 8.48° \qquad (3.1)$$

3.3.2 Angle of declination ($\boldsymbol{\delta}$)

The angle of declination (δ) which is the angle made by the incident solar radiation with the horizontal plane given by Duffie and Beckman (2013) as;

$$\text{Angle of declination } (\delta) = 23.45\text{Sin}\left[360 \times \frac{284 + \text{n}}{365}\right] \qquad (3.2)$$

$$(\delta) = 23.45\text{Sin}\left[360 \times \frac{284 + 196}{365}\right] = 21.52°$$

3.3.3 The hour angle (ω)

The angular displacement of the sun east or west of the local meridian due to the rotation of the earth on its axis at an angle of 15° per hour. At solar noon the hour angle is equal to zero while it is negative during morning hours and positive during evening hours.

The hour angle (ω) is given by (Duffie and Beckman, 2013);

$$\omega = 15^\circ \times \text{time before/ after noon} \qquad (3.3)$$

The hour angle at the conclusion of each experiment at 17:00hrs daily is derived from equation (3.3) given as;

$$\omega = 15^\circ \times 5 = 75^\circ$$

The sunset angle (ω_s) is determined by using equation (3.4) (Duffie and Beckman, 2013);

$$\omega_s = Cos^{-1}[-tan\phi tan\delta] \qquad (3.4)$$

$$\omega_s = Cos^{-1}[-tan5.48tan21.52] = 92.17^\circ$$

3.3.4 The incident angle (θ_i)

The incident angle of the sun (θ_i) on the earth's surface tilted towards the equator at an angle with the horizontal is given as (Duffie and Beckman, 2013);

$$\theta_i = Cos^{-1}\,[Cos(\phi-\beta)Cos(\delta)\text{Cos}(\omega) + \text{Sin}(\phi-\beta)Sin(\delta)] \qquad (3.5)$$

$$\theta_i = Cos^{-1}\,[Cos(5.48-8.48)Cos(21.52)\text{Cos}(75) + \text{Sin}(5.48-8.48)Sin(21.52)]$$

$$\theta_i = 77.22^\circ$$

3.3.5 The zenith angle (θ_z)

The zenith angle represents the angle between the sun and the vertical (i.e. the angle of incidence of beam radiation on a horizontal surface). Therefore, the zenith angle (θ_z) is obtained from equation (3.6) given as (Duffie and Beckman, 2013);

$$\theta_z = Cos^{-1}\,[Cos(\phi)Cos(\delta)\text{Cos}(\omega) + \text{Sin}(\phi)Sin(\delta)] \qquad (3.6)$$

$$\theta_z = Cos^{-1}\,[Cos(5.48)Cos(21.52)\text{Cos}(75) + \text{Sin}(5.48)Sin(21.52)]$$

$$\theta_z = 74.06^\circ$$

Considering the incident and zenith angles, the ratio of beam radiation on a tilted surface to that of a horizontal surface (R_b) at any time is given as;

$$R_b = \frac{Cos\theta_i}{Cos\theta_z} \qquad (3.7)$$

$$R_b = \frac{Cos77.22}{Cos74.06} = 0.805$$

3.4 Drying kinetics of the product considered

In designing an efficient drying chamber, Tonui et al. (2014) outlined some design considerations needed to achieve desired results. These considerations include;

- Sizing of the dryer chamber: length and breadth of the drying chamber
- Air vent dimensions
- The amount of moisture to be removed from the product
- Temperature, humidity and the quantity of air needed for drying
- Pressure drop through the drying bed
- Wind speed
- Daily solar radiation to determine energy received by the dryer per day
- The daily sunshine hours for the selection of the total drying time
- Size of the pieces being dried

Fresh cassava is considered for drying in this design. Fresh cassava cannot be stored for a long period as they rot within 3-4 days of harvest. It contains about 50-70% moisture content and can be stored for many months if the water content is reduced to an acceptable level of about 15%, and also, to ensure that the product doesn't get damaged or lose its nutritional value during drying, an optimum temperature of 60°C is recommended to minimize browning of the product (Chappell & Lebel, 2009).

For the purpose of this work, 5kg of freshly peeled cassava having a layer thickness of 2cm will be dried using the solar dryer with an initial moisture content of 65% adopted.

3.4.1 Basic drying principles

The rate of drying is determined by the amount of air being passed over the pieces to be dried. Air containing a certain quantity of water at a low temperature will when heated, have a greater capacity to hold more water. This phenomenon relates directly to the relative humidity (RH) of the air and is defined as the amount of water vapour present in air

expressed as a percentage of the amount needed for saturation at the same temperature. RH is expressed as a percentage and fully-saturated air would have an RH of 100% which implies that it cannot pick up any more moisture. This implies that at lower temperature, relative humidity of air increases while as the air is heated, its relative humidity reduces thereby improving the capacity of air to pick up moisture.

Relative humidity is an important factor in designing a solar dryer considering the fact that most design parameters such as the volume of air required to bring the moisture content to an acceptable value, the amount of moisture to be removed from the product, the final/ equilibrium relative humidity, the mass of the air and the absolute temperature are all dependent on it.

Owerri has an average monthly relative humidity ranging from 75-90% with higher values recorded during the rainy season, and a monthly mean ambient temperature of 25 - 32°C (Okorafor et al., 2018).

3.4.2 Equilibrium relative humidity (ERH) and water activity (a_w)

When the product to be dried is placed in a current of heated air, the product initially loses moisture from the surface. This stage is known as the constant rate period. As drying proceeds, moisture is then removed from inside the product, starting near the outside. Moisture removal becomes more and more difficult as the moisture has to move further from deep inside the product to the surface, with this stage referred to as the falling-rate period. Finally, when no more moisture can be removed from the product, the air is said to attain its final/equilibrium relative humidity (ERH).

Water activity (a_w) of a food is the ratio of the vapour pressure of the food itself, when in a complete undisturbed balance with the surrounding air media, and the vapour pressure of distilled water under identical conditions (https://www.fda.gov/inspection-compliance-enforcement-and-criminal-investigations/inspection-technical-guide/water-activity-aw-foods [accessed 20/07/2021]). Water activity of the product to be dried needs to be reduced in other to reduce the degradation of the product due to physical reactions and microbial growth.
Water activity serves as an indicator of how conducive a given food is for microbial growth, with lower water activity (a_w) levels inhibiting microbial growth. The water activity (a_w) of the dried product serves as an indicator for its equilibrium relative humidity.

3.4.3 Determination of moisture content to be removed

The amount of moisture (m_w) to be removed from the product in other for it to be safely stored can be calculated using the equation (Tonui et al., 2014):

$$m_w = m_p \left[\frac{m_i - m_f}{100 - m_f}\right] \qquad (3.8)$$

Where,

m_p = The initial mass of product to be dried = $5kg$

m_i = Initial moisture content (wet basis) = 65%

m_f = Final moisture content (wet basis) = 15%

$$m_w = 5\left[\frac{65 - 15}{100 - 15}\right] = 2.94kg$$

This implies that 2.94kg of moisture is to be removed from the product in other to store it safely.

In order to reduce degradation of the product due to physical reactions and microbial growth, the water activity (a_w) can be calculated using sorption isotherms equation given as (Tonui et al., 2014):

$$a_w = 1 - \exp[-exp\,(0.914 + 0.5639lnM)] \qquad (3.9)$$

$$M = \frac{m_f}{100 - m_f} \qquad (3.10)$$

Where;

M = Equilibrium moisture content (kg_w/kg_a) dry basis

From equation (3.10)

$$M = \frac{15}{100 - 15}$$

$$M = 0.1765 kg_w/kg_a$$

The water activity value derived from equation (3.9) becomes

$$a_w = 1 - \exp[-exp\,(0.914 + 0.5639ln0.1765)]$$

$$a_w = 0.61 kg_w/kg_a$$

Final or equilibrium relative humidity (ERH) is given by equation (3.11) (Tonui et al., 2014);

$$ERH = 100 a_w\,(\%) \qquad (3.11)$$

$$ERH = 100 \times 0.61(\%) = 61\%$$

3.4.4 Humidity ratio (HR)

Parameters selected for a typical drying day in Owerri are depicted in Table 3.3.

Table 3.3: Typical drying conditions in Owerri

S/N	PARAMETERS	VALUE
1	Relative humidity	75%
2	Ambient temperature (T_a)	30°C
3	Optimum drying temperature for Cassava	55°C
4	Equivalent relative humidity (ERH)	61%

Using a psychometric chart and taking input air temperature (ambient temperature) of 30°C (dry bulb) and a relative humidity of 75%, a humidity ratio (HR_1) of 0.020kg_w/kg_a is achieved.

As the air is heated to the optimum drying temperature of 55°C (dry bulb), the humidity ratio remains constant and corresponds to a wet bulb temperature of 31.5°C and relative humidity of 20%. Drying occurs adiabatically when the hot air is allowed to absorb moisture by passing it through the layers of cassava until its relative humidity is equal to the calculated ERH of 61% at which point no more moisture can be absorbed by the air, the psychometric chart shows a humidity ratio (HR_2) of 0.027kg_w/kg_a and a dry bulb temperature (T_f) of 38.5°C respectively.

This is illustrated in Figure 3.6 with the change in humidity ratio indicating the maximum moisture capacity which the air can hold when leaving the drying chamber at a temperature not below 38.5°C in order to conform to the calculated ERH of 61%.

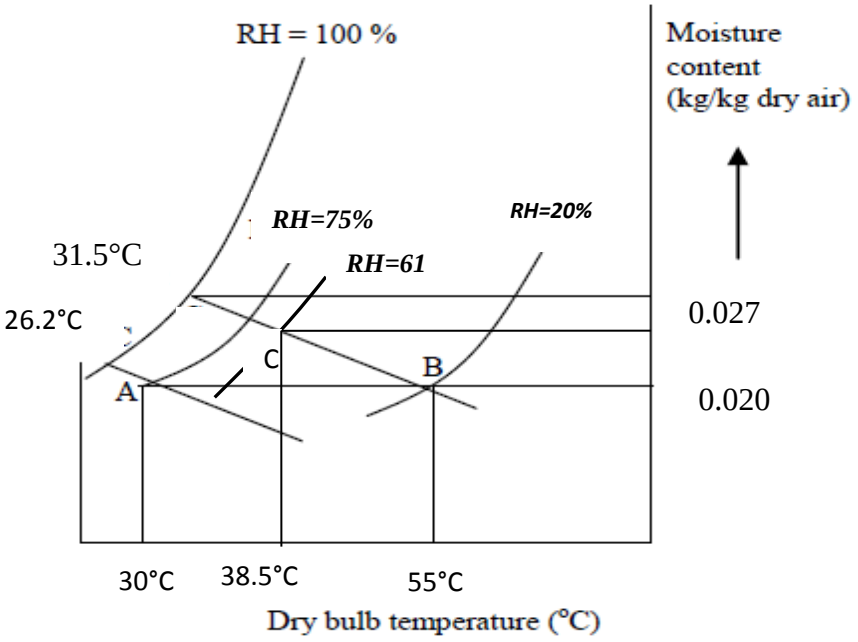

Figure.3.6: Psychometric chart illustrating the drying process

Where;

A: ambient air

B: inlet air to drying chamber

C: outlet air from drying chamber

AB: air heating from solar collector

BC: drying process

Thus, change in humidity ratio $(\Delta HR) = HR_2 - HR_1$ (3.12)

$$\Delta HR = 0.027 - 0.020 = 0.007 kg_w/kg_a$$

3.4.5 Total mass of air (M_T) needed for drying

For each kilogramme of moisture to be removed, the quantity of dry air required is obtained from equation (3.13) below.

$$\text{Dry air required } to\ remove\ 1kg\ of\ moisture = \frac{1}{\Delta HR} \quad (3.13)$$

For a moisture content of 2.94kg to be removed from the product, the total mass of air (M_T) needed is given by:

$$M_T = \frac{2.94}{0.007} = 420kg\ of\ dry\ air \quad (3.14)$$

3.4.6 The average drying air temperature rise

The average drying air temperature rise can be derived from the modified Macedo and Altemani empirical formula in equation (3.15) below (Chappell & Lebel, 2009).

$$\Delta T = 2\mathcal{B}\left(T_b - T_{fr}\right)\frac{I_t}{I_o} \qquad (3.15)$$

Where

$\Delta T =$ Temperature difference between the expected mean temperature of the heated air at the collector outlet and the ambient air temperature.

$\mathcal{B} =$ Dimensionless parameter regulating the temperature difference between the ambient air and the heated air at the outlet of the collector, with values ranging between 0.14 – 0.25. Its increase leads to a corresponding increase in ΔT while its decreases leads to a decrease in ΔT.

$T_b =$ Boiling temperature of water at atmospheric pressure; 100°C

$T_{fr} =$ Freezing temperature of water at atmospheric pressure; 0°C

$I_t =$ Intensity of radiation incident on the plane of the collector [W/m^2]

$I_o =$ Maximum intensity of the solar radiation/solar constant; 1367 W/m^2

Insolation ranging between 420–886 W/m^2 is possible for the test location (Ogueke et al., 2017). An intermediate value of $\mathcal{B} = 0.20$ and a minimum value of $I_t = 420\text{W/m}^2$ are assumed for optimum design purposes.

Hence, from equation (3.15)

$$\Delta T = 2 \times 0.20(100 - 0)\frac{420}{1367}$$

$$\Delta T = 12.3°C$$

This implies that a minimum average drying air temperature rise of 12.3°C is expected all through the year.

3.4.7 The volume of air required for drying

The volume of air required to effect the removal of 2.94kg of moisture from the cassava is calculated from equation 3.16 (Chappell & Lebel, 2009).

$$V_a = \frac{m_w L_v R_a T_a}{Cp_a P_a (T_o - T_f)} \qquad (3.16)$$

Where;

$R_a =$ Specific gas constant; 286.9 J/kg K

$P_a =$ Partial pressure of dry air in the atmosphere; 1.018×10^5 N/m^2

$Cp_a =$ Specific heat capacity of air at constant pressure; 1006 J/kg K

$T_f =$ Temperature of air leaving the drying bed; $38.5°C/311.5K$ (psychometric chart)

$T_o =$ Temperature of drying air leaving the air heater and entering the drying chamber given by $(T_a + \Delta T)$

$$T_o = 30 + 12.3 = 42.3°C/315.3K$$

The latent heat of vaporization (L_v) is calculated using equation (3.17) (Chappell & Lebel, 2009).

$$L_v = R_g T_c T_b In\left[\frac{P_c}{10^5}\right]\frac{(T_c - T_{pt})^{0.3}}{(T_c - T_b)^{1.3}} \qquad (3.17)$$

$R_g =$ Gas constant for water vapour; 461.5 J/kg K

$P_c =$ Critical pressure of water; 2.206×10^7 Pa

$T_{pt} =$ Temperature of the product

$T_c =$ Critical temperature of water; 377°C/650K

$$T_{pt} = 0.25(3\,T_o + T_a) \qquad (3.18)$$

$$T_{pt} = 0.25([3 \times 42.3] + 30) = 39.23°C = 312.23K$$

$$L_v = 461.5 \times 650 \times 373 \times In\left[\frac{2.206 \times 10^7}{10^5}\right]\frac{(650 - 312.23)^{0.3}}{(650 - 373)^{1.3}}$$

$$L_v = 2313.43KJ/kg$$

From equation (3.16) the volume of air required to remove 2.94kg of moisture from the cassava is given as;

$$V_a = \frac{m_w L_t R_a T_a}{Cp_a P_a (T_o - T_f)} = \frac{2.94 \times 2313.43 \times 10^3 \times 286.9 \times 303}{1006 \times 1.018 \times 10^5 \times (315.3 - 311.5)}$$

$$V_a = 1519.31m^3$$

3.4.8 Volume flow rate $(\dot{V})$

From Table 3.1, a daily drying period of 9 hour (8am – 5pm) is considered. This is the period in the location when the sun's energy can be harvested. Volume flow rate based on the 9 hour drying period assuming the flow remains constant at all times is obtained from equation (3.19).

$$\dot{V} = \frac{V_a}{t_d} \qquad (3.19)$$

Where;

$t_d =$ Drying time required to dry the cassava to the desired moisture content; 9 hours daily

$$\dot{V} = \frac{1519.31 m^3}{9hrs} = 189.1\, m^3/hr = 0.047\, m^3/s$$

3.4.9 Mass flow rate ($\dot{m}$)

With air density (ρ) of 1.1644kg/m^3, the mass flow rate ($\dot{m}$) of the air can be calculated from equation (3.20).

$$\dot{m} = \rho \times \dot{V} \qquad (3.20)$$

$$\dot{m} = 1.1644\, kg/m^3 \times 0.047\, m^3/s$$

$$\dot{m} = 0.0547 kg/s$$

According to Chappell & Lebel, (2009), the mass flow rate of 0.547 kg/s falls within the recommended range of 0.02-0.9kg/s.

3.4.10 Total drying time (T_t)

Dividing equation (3.14) by equation (3.20) gives the total drying time (T_t) required to remove 2.94kg moisture from the cassava in other to enable safe storage. Hence, the total drying time is given as;

$$T_t = \frac{M_T}{\dot{m}} \qquad (3.21)$$

$$T_t = \frac{420kg}{0.0547kg/s} = 7678.245\, seconds = 2.133\, hours$$

This implies that 2.94kg of moisture will require 2.133 drying hours given that all conditions calculated remain constant for safe storage of the product, which is equivalent to one drying day.

3.5 Evaluation of collector thermal performance

Incident solar energy on the collector surface is converted into useful energy gain with resultant thermal losses. An energy balance is used to indicate the energy distribution with

the useful energy gain (Q_U) of the collector area (A_c), equal to the difference between the absorbed solar radiation and the thermal losses (Nalis, 2012). However, in other to carry out the thermal performance of the PVT collector, some assumptions as specified by Duffie and Beckmann (2013) are listed below;

Assumptions

1. Dust and dirt on the collector surface are negligible.
2. Shading of the PVT collector is negligible.
3. The sky is considered a black-body for long wave radiation at an equivalent sky temperature.
4. Steady state performance is assumed.
5. Perfect insulation is assumed at the rear (bottom) and edges of the collector.

3.5.1 The useful energy gain (Q_U) of the collector

The energy balance for calculating the useful energy gain of the solar collector is shown in equation (3.22) (Nalis, 2012) with the thermal losses represented as the product of the overall heat loss coefficient (U_L) multiplied by the difference between the mean absorber plate temperature (T_{pm}) and the ambient temperature (T_a). In this case, the absorber plate is the PV panel.

$$A_c = \frac{Q_u}{[(S - U_L(T_{pm} - T_a)]} \qquad (3.22)$$

$$\text{Also,} \quad Q_u = \dot{m}C_p(T_o - T_i) \qquad (3.23)$$

Where;

Q_u = The useful energy gain received by the drying air (KJ/s)

$\dot{m}$ = mass flow rate (kg/s); 0.0547kg/s

C_{pa} = specific heat of air (KJ / kgK); 1.006KJ/kgK

A_c = collector area (m^2)

T_i = inlet air temperature (K); 30°C

T_o = outlet air temperature (K)

T_{pm} = Mean absorber plate temperature

T_a = Ambient temperature; 30°C

U_L = Overall heat loss coefficient

S = Average monthly solar radiation absorbed by the collector per unit area of the absorber

For design purpose, the value for the temperature of drying air leaving the air heater and entering the drying chamber (T_o) is increased from 42.3°C (which is the calculated minimum value assuming an ambient temperature of 30°C) $to\ 55°C(328K)$ which is the selected optimum drying temperature for Cassava. Also, $T_i = T_a$ = 30°C (303°K)

Obtaining the useful energy gain from equation (3.23) gives;

$$Q_u = 0.0547 \times 1.006 \times 10^3(328 - 303)$$

$$Q_u = 1.376KJ/s = 1.376KW$$

3.5.2 Average monthly solar radiation absorbed by the collector (S)

The absorbed monthly average daily solar radiation (S), is the global irradiance received by the collector (beam and diffuse) after being reduced by the optical losses and is derived from equation 3.24 given as (Nalis, 2012);

$$S = H_T(\tau\alpha)_{\grave{e}} \qquad (3.24)$$

$(\tau\alpha)_{\grave{e}}$ = The effective transmittance-absorptance coefficient

The term $(\tau\alpha)_{\grave{e}}$ is used to describe optical losses due to absorption and reflection in the cover and absorber material.

3.5.2.1 Monthly average daily solar radiation on a tilted surface (H_T)

In order to determine the monthly average daily solar radiation on a tilted surface, the model is assumed to receive radiation uniformly from every part of the sky dome. Therefore the monthly average daily solar radiation incident on a tilted surface (H_T) and the clearness index (K_T) can be obtained using equations (3.25) and (3.26) respectively given in Duffie and Beckman (2013) as:

$$H_T = H_b R_b + H_d\left[\frac{1 + Cos\beta}{2}\right] + H\rho_g\left[\frac{1 - Cos\beta}{2}\right] \qquad (3.25)$$

$H_b = Beam\ radiation\ on\ a\ tilted\ surface$

$H_d = Diffuse\ radiation$

$H =$ Monthly mean daily global radiation incident on a horizontal surface

$\rho_g = Ground\ reflectance$

This shows that the solar energy incident on a tilted surface consists of beam radiation from the sun, diffuse radiation that is scattered from the sky and ground reflectance radiation that is diffusely reflected from the ground. Table 3.4 shows the ground reflectance value for various materials.

Table 3.4: Ground reflectance values for various materials (Source: www.itacanet.com assessed 26/01/2019)

S/N	GROUND COVER	REFLECTIVITY
1	Dry bare ground	0.2
2	Dry grass land	0.3
3	Desert sand	0.4
4	Snow	0.5 – 0.8
5	Pale soil	0.3
6	Dark soil	0.1
7	Water	0.1

$$K_T = \frac{H}{H_o} \qquad (3.26)$$

Where;

H = Monthly mean daily global radiation incident on a horizontal surface

$H_o =$ Monthly average daily extraterrestrial radiation on a horizontal surface

3.5.2.2 Monthly average daily extraterrestrial radiation on a horizontal surface (H_o)

For the city of Owerri, July and August have the least measured monthly mean daily global radiation incident on a horizontal surface (H) with values of 13.10MJ/m^{2}daily and 13.42MJ/m^{2}daily respectively (Augustine and Nnabuchi, 2010). However, July having the lowest insolation value of 13.10MJ/m^{2}daily is selected as the reference month while the monthly average daily extraterrestrial radiation on a horizontal surface (H_o) is derived using parameters of Table 3.5 and equation (3.27) given in Duffie and Beckmann (2013) as:

$$H_o = \frac{24\times3600\times G_{SC}}{\pi}\left[1 + 0.033Cos\left(\frac{360n}{365}\right)\right]\left[Cos\phi Cos\delta Sinw_s + \frac{\pi}{180}w_s Sin\phi Sin\delta\right] \quad (3.27)$$

Table 3.5: Parameters for evaluating Monthly average daily extraterrestrial radiation on a horizontal surface (H_o)

S/N	PARAMETER	SYMBOL	VALUE	REFERENCE
1	Measured monthly mean daily global radiation	H	13.10MJ/ m^2 daily	Augustine and Nnabuchi, (2010)
2	Latitude	ϕ	5.48°	Table 3.1
3	Angle of declination	δ	21.52	Equation 3.2
4	The ratio of beam radiation on a tilted surface to that of a horizontal surface	R_b	0.805	Equation 3.7
5	Solar constant	G_{SC}	1367W/m^2	Rahman (2013)
6	Sunset angle	w_s	92.17°	Equation 3.4
7	Julian day number	n	196	Table 3.2

Substituting the required parameters from Table 3.5 into equations (3.26) and (3.27) gives the values for clearness index (K_T) and monthly average daily extraterrestrial radiation on a horizontal surface (H_o) as;

$$H_o = \ 35.72MJ/m^2daily$$

$$K_T = 0.3667$$

3.5.2.3 Diffuse radiation (H_d) and beam radiation (H_b)

The chosen location has a sunset angle (w_s) of 92.17° (equation 3.4) and a clearness index (K_T) of 0.3667 (equation 3.26). However, for a sunset angle (w_s) $> 81.4°$ and a clearness index (K_T) < 0.722, the mathematical relationship between the diffuse radiation (H_d), the monthly mean daily radiation (H), and the clearness index (K_T) is given by equation (3.28) (Duffie and Beckman, 2013).

$$\frac{H_d}{H} = 1.0 + 0.2832K_T - 2.5557(K_T)^2 + 0.8448(K_T)^3 \quad (3.28)$$

Substituting K_T values

$$\frac{H_d}{H} = \ 0.8018$$

Introducing the value of H

$$H_d = 0.8018 \times 13.10 = 10.50 MJ/m^2 daily$$

The summation of the beam (H_b) and diffuse (H_d) radiation during the period (month) in view gives the measured monthly mean daily global radiation on a horizontal surface (Duffie and Beckman, 2013). Mathematically,

$$H = H_b + H_d \qquad (3.29)$$

$$H_b = 13.10 - 10.50 = 2.60 MJ/m^2 daily$$

From equation 3.25, H_T becomes;

$$H_T = (2.60 \times 0.805) + \left(10.50 \times \left[\frac{1 + Cos 8.48}{2}\right]\right) + \left(14.37 \times 0.2 \times \left[\frac{1 - Cos 8.48}{2}\right]\right)$$

$$H_T = 12.55 MJ/m^2 daily$$

3.6 Optical properties of the cover material

The optical properties influencing the performance of collectors depend on wavelength of the radiation and the angle of incidence. The transmittance, reflectance and absorptance are functions of the solar radiation which help in determining the performance of a collector. The transmissivity of the collector depends on the angle of incidence since the path traversed by the rays varies with the incidence angle.

3.6.1 Transmittance-absorptance product ($\tau\alpha$)

The transmittance-absorptance product ($\tau\alpha$) is important in determining the optical properties of flat plate collectors. It is considered due to the multiple reflection and absorption between the cover and the absorber material of the collector (Duffie and Beckman, 2013). Fig.3.4 shows the ray diagram for a typical single glazed collector.

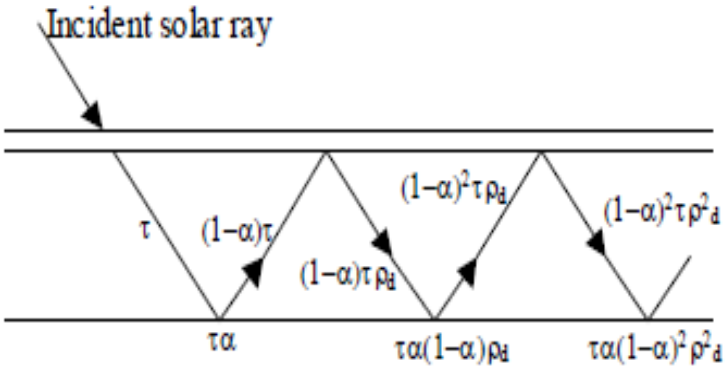

Fig. 3.7: Transmission-absorption process in a flat plate collector (Duffie and Beckman, 2013)

Considering Figure 3.7, the irradiation absorbed by the plate, give as a product of transmittance of the glazing and absorptance of the plate (τα), is reflected back to the cover system as $(\mathbf{1}-\boldsymbol{\alpha})\boldsymbol{\tau}$. However, the reflection from the absorber plate is assumed to be diffuse so that the fraction $(\mathbf{1}-\boldsymbol{\alpha})\boldsymbol{\tau}$ returning to the cover from the absorber plate is diffuse and $(\mathbf{1}-\boldsymbol{\alpha})\boldsymbol{\tau}\boldsymbol{\rho}_{\mathbf{d}}$ is reflected back to the absorber plate. The reflection of the diffuse component of radiation has a multiplying effect such that the fraction of the incident energy absorbed is given as (Duffie and Beckman, 2013);

$$(\tau\alpha) = \tau\alpha\sum_{n=0}^{\infty}[(1-\alpha)\rho_d]^n \quad = \quad \frac{\tau\times\alpha}{1-(1-\alpha)\rho_d} \qquad (3.30)$$

Where;

τ = the transmittance of the cover system at the desired angle of incidence

α = the angular absorptance of the absorber plate of the incident energy

ρ_d = the reflectance of the cover system for diffuse radiation incident from the bottom side

3.6.2 Transmittance due to absorption losses

Considering only the absorption losses, the transmittance becomes (Duffie and Beckman, 2013)

$$\tau_a = exp\left[\frac{-KL}{Cos\theta_2}\right] \qquad (3.31)$$

Where;

K = Extinction coefficient of cover material (glass)

L = glass thickness

τ_a = Transmittance considering absorption losses alone

The coefficient of extinction gives a relative idea of the several different measures of how light is being absorbed in a medium. PV panels are designed such that the photovoltaic cells are protected from mechanical damage and degradation using a highly transparent white tempered glass/low iron glass having an extinction coefficient (K) value of $4m^{-1}$ while the thickness varies from 3.2mm to 4mm (Duffie and Beckman, 2013).

Considering the interfaces and from Snell's law

$$\frac{n_1}{n_2} = \frac{Sin\theta_2}{Sin\theta_1} \qquad (3.32)$$

Where;

$n_1\ and\ n_2 =\ Average\ refractive\ index\ in\ solar\ spectrum$

$\theta_1 = \theta_i = Angle\ of\ incidence$

$\theta_2 = Angle\ of\ refraction$

The average refractive index for ordinary glass in the solar spectrum has a value of 1.526 (Duffie and Beckman, 2013)

Hence, equation (3.32) can be rewritten as

$$\theta_2 =\ Sin^{-1}\left[\frac{Sin\theta_1}{1.526}\right] =\ Sin^{-1}\left[\frac{Sin77.22°}{1.526}\right]$$

$$\theta_2 = 39.72°$$

Considering values of K and L equal to $4m^{-1}$ and 3.2mm respectively (Duffie and Beckman, 2013), equation (3.31) becomes;

$$\tau_a =\ exp\left[\frac{-0.0032 \times 4}{Cos39.72°}\right] =\ \ 0.983$$

3.6.3 Transmittance due to reflection losses

The transmission of radiation through the cover material (glass) experiences reflection losses due to the material having two interfaces. Similarly, if the incidence angle is not at its normal (zero degrees) inclination, the radiation reflected at the interface will be different for each component, hence making the transmitted and reflected radiation become partially polarized

(Duffie and Beckmann, 2013). Therefore, the components (perpendicular and parallel) of polarisation should be accounted for separately.

Hence, the transmittance due to reflection losses, from the glass cover according to Duffie and Beckmann (2013) becomes

$$\tau_r = \frac{1}{2}\left[\frac{1-r_{\parallel}}{1+r_{\parallel}} + \frac{1-r_{\perp}}{1+r_{\perp}}\right] \qquad (3.33)$$

Where;

$r_{\parallel}$ = Parallel component of reflection

$r_{\perp}$ = Perpendicular component of reflection

$$r_{\parallel} = \frac{tan^2(\theta_2 - \theta_1)}{tan^2(\theta_2 + \theta_1)} \qquad (3.34)$$

$$r_{\parallel} = \frac{tan^2(39.72 - 77.22)}{tan^2(39.72 + 77.22)} = 0.1521$$

$$r_{\perp} = \frac{Sin^2(\theta_2 - \theta_1)}{Sin^2(\theta_2 + \theta_1)} \qquad (3.35)$$

$$r_{\perp} = \frac{Sin^2(39.72 - 77.22)}{Sin^2(39.72 + 77.22)} = 0.4663$$

Hence, the transmittance due to reflection losses from equation (3.33) becomes

$$\tau_r = \frac{1}{2}\left[\frac{1-0.1521}{1+0.1521} + \frac{1-0.4663}{1+0.4663}\right] = 0.550$$

Combining the absorptance and reflection losses, the transmittance of the cover becomes (Duffie and Beckmann, 2013);

$$\tau = \tau_a \tau_r \qquad (3.36)$$

$$\tau = 0.983 \times 0.550 = 0.541$$

$$\rho_d = 1 - \tau_r \qquad (3.37)$$

$$\rho_d = 1 - 0.550 = 0.450$$

Crystalline Silicone (c-Si) cells in a PV panel encapsulate which has a tedlar back cover, has an absorptance (α) of 0.905 (Santbergen, & Zalingen 2007).

Equation (3.30) becomes

$$(\tau\alpha) = \frac{\tau \times \alpha}{1 - (1 - \alpha)\rho_d} = \frac{0.541 \times 0.905}{1 - (1 - 0.905)0.450} = 0.5115$$

As reported by Nalis (2012), the effective transmittance-absorptance coefficient$(\tau\alpha)_{\dot{e}}$ can be approximated for ordinary glass by:

$$(\tau\alpha)_{\dot{e}} \cong 1.02(\tau\alpha) \qquad (3.38)$$

$$(\tau\alpha)_{\dot{e}} \cong 1.02 \times 0.5115 = 0.5217$$

From equation (3.24), the value for solar radiation (S) absorbed by the PV panel is estimated as;

$$S = H_T(\tau\alpha)_{\dot{e}}$$

$$S = 12.55 MJ/m^2 daily \times 0.5217 = 6.55 MJ/m^2$$

$$S = \frac{6.55 \times 10^6 J/m^2 daily}{3600s} = 1819.44\, J/sm^2 = 1819.44 W/m^2 daily \qquad (3.39)$$

3.7 Hottel-Whillier-Bliss equation

Considering that average monthly solar radiation absorbed by the collector (S) experiences a reducing effect due to optical losses $(\tau\alpha)_{\dot{e}}$, Hottel and Whillier introduced two efficiency factors for the collector; collector fin efficiency factor (F') and collector heat removal factor (F_R) which account for the temperature distribution in the flow direction by giving the ratio of useful energy to the maximum heat transfer, thus allowing the use of either the mean or inlet fluid temperature in calculating the useful energy gain of the collector. For the purpose of this work, and considering that the aluminium vanes placed in the flow channel increases the surface area available for heat-exchange, the Hottel-Whillier-Bliss equation as reported by Nalis (2012) and shown as equation (3.40) and (3.41) respectively is a more

convenient relation accounting for the collector fin efficiency and collector heat removal factor. The collector fin efficiency factor ($F^{'}$) reflects the quantity that relates the actual useful energy gain of a collector to the useful gain if the whole collector surface was at the average fluid temperature (T_m), as shown in equation (3.40).

$$Q_u = A_c F^{'}[(S - U_L(T_m - T_a)] \qquad (3.40)$$

Similarly, the collector heat removal factor (F_R) is the quantity that relates the actual useful energy gain of a collector to the useful gain if the whole collector surface was at the inlet fluid temperature (T_i), as shown in equation (3.41).

$$Q_u = A_c F_R[(S - U_L(T_i - T_a)] \qquad (3.41)$$

The mean temperature of the fluid (T_m) can be calculated from equation (3.42), given as;

$$T_m = \frac{T_i + T_o}{2} \qquad (3.42)$$

Where;

$F^{'}$ = Collector fin efficiency factor

F_R = Collector heat removal factor

T_m = mean temperature of the liquid

F_R *and* $F^{'}$ can be related by the equation (Gholami, Khalilnejad & Gharehpetian, 2015)

$$F_R = \frac{\dot{m}C_p}{A_c U_L}\left[1 - \exp\left(-\frac{A_c U_L F^{'}}{\dot{m}C_p}\right)\right] \qquad (3.43)$$

According to Gholami et al (2015), the mean plate temperature can be calculated as

$$T_{pm} = T_i + \frac{Q_u(1 - F_R)}{A_c F_R U_L} \qquad (3.44)$$

3.8 The overall collector heat loss coefficient (U_L)

Ease of simplifying any collector model can be achieved using the overall heat loss coefficient. The thermal losses from the solar collector to the surroundings occur through the back, the top and the edges of the collector. The overall heat loss of the collector (U_L) is a

summation of the top (U_t), bottom (U_b) and edges (U_e) losses of the collector. Mathematically,

$$U_L = U_t + U_b + U_e \qquad (3.45)$$

However, if perfect insulation is assumed at the rear surface and edge, and all the energy reaching it by radiation from the front surface is transmitted back into the fluid by convection, then U_b *and* U_e becomes negligible (Koech et al., 2012). Assuming perfect insulation at the rear (bottom) and edges, heat loss will occur only from the top of the collector through convection and radiation. Hence;

$$U_L = U_t \qquad (3.46)$$

Nalis (2012) reported in his work that an empirical equation for the heat loss from the top of a collector for mean plate temperatures range of ambient to 200°C was proposed by Klein (1979) and is given as:

$$U_t = \left[\frac{N}{\frac{C}{T_{pm}}\left[\frac{T_{pm}\_T_a}{(N+f)}\right]^e} + \frac{1}{h_w}\right]^{-1} + \frac{\sigma(T_{pm} + T_a)(T_{pm}^2 + T_a^2)}{(\varepsilon_p + 0.00591Nh_w)^{-1} + \frac{2N + f - 1 + 0.133\varepsilon_p}{\varepsilon_g} - N} \qquad (3.47)$$

Where;

N = Number of glazing (1)

β = Collector tilt angle (8.48°)

ε_g = Emittance of the glass surface (0.88)

$e = 0.430(1 - {}^{100}/_{T_{pm}})$

ε_p = Emittance of the absorber plate/PV panel (0.86)

$f = (1 + 0.089h_w - 0.1166h_w\varepsilon_p)(1 + 0.07866\,N)$

$C = 520(1 - 0.000051\beta^2)$ for $0° < \beta < 70°$. For $70° < \beta < 90°$, use $\beta = 70°$

$\sigma = stefen - Boltzman\ constant\ (5.6697 \times 10^{-8} W/m^2K^4)$

h_w = Wind heat transfer coefficient (W/m^{2}K)

For a forced convection, the wind heat transfer coefficient for the collector can be expressed as (Duffie and Beckman, 2013);

$$h_w = \frac{8.6V^{0.6}}{L^{0.4}} \qquad (3.48)$$

If the characteristic length is not more than 2m, and the wind velocity from Table 3.1 is assumed to be 3m/s then,

$$h_w = \frac{8.6\times3^{0.6}}{2^{0.4}} = 12.6 \text{ W/m}^2\text{K}$$

$$f = (1 + 0.089[12.6] - 0.1166[12.6][0.86])(1 + 0.07866[1]) = 0.925$$

Substituting all the known parameters into equation (3.47) and rewriting the equation, it becomes;

$$U_L = \left[\frac{1}{\frac{518.1}{T_{pm}}\left[\frac{T_{pm}-303}{1.925}\right]^e} + \frac{1}{12.6}\right]^{-1} + \frac{\sigma(T_{pm}+303)(T_{pm}^2+303^2)}{2.388} \qquad (3.49)$$

3.9 The Iterative process

Considering the difficulty in estimating mean plate temperature, an iterative approach proposed by Duffie and Beckman (2013) can be adopted with respect to equation for U_L since it is as well temperature dependent. First, an estimated value for T_{pm} is made from which U_L is calculated with approximate values for A_c and F_R also accounted for. A new T_{pm} is obtained from equation (3.44) and used to find a new value for U_L. The new value for U_L is used to find new values for A_c.

The process is repeated until convergence is achieved. For air heaters, a reasonable first estimate is given as (Duffie and Beckman, 2013); $T_{pm} = T_a + 20°C$.

Hence for the first iteration, the plate mean temperature is assumed to be;

$$T_{pm} = 30°C + 20°C = 50°C \text{ or } 323$$

$$e = 0.430\left(1 - {}^{100}/_{T_{pm}}\right) \qquad (3.50)$$

$$e = 0.297$$

$$U_L = \left[\frac{1}{\frac{518.1}{323}\left[\frac{323-303)}{(1.925)}\right]^{0.297}} + \frac{1}{12.6}\right]^{-1} + \frac{5.6697\times10^{-8}(323+303)(323^2+303^2)}{2.388}$$

$$U_L = 5.476\text{W/m}^2\text{K}$$

From equation (3.22)

$$A_c = \frac{Q_u}{[(S - U_L(T_{pm} - T_a)]} = \frac{1376}{[1819.44 - 5.476(323-303)]} = 0.805m^2$$

From equation (3.40), the fin efficiency factor is with respect to the useful energy gain of the collector can be calculated as;

$$F' = \frac{Q_u}{A_c[(S - U_L(T_m - T_a)]} = \frac{1376}{0.805[1819.44 - 5.476(315.5-303)]}$$

$$F' = 0.976$$

Also, from equation (3.41) the heat removal factor with respect to the useful energy gain of the collector can be calculated as;

$$F_R = \frac{Q_u}{A_c[(S - U_L(T_i - T_a)]}$$

$$F_R = \frac{1376}{0.805[1819.44 - 5.476(303-303)]}$$

$$F_R = 0.933$$

Hence, from equation (3.44), the new value for the plate mean temperature is given as

$$T_{pm} = T_i + \frac{Q_U(1 - F_R)}{A_c F_R U_L}$$

$$T_{pm} = 303 + \frac{1376(1-0.933)}{0.805\times0.933\times5.476}$$

$$T_{pm} = 325.415K$$

Tabulated values for the first iteration are as given in Table (3.6)

Table 3.6: Values from the first iteration using $T_{pm} = 323K$

S/N	PARAMETER	REFERENCE	VALUES
1	Useful heat gain of the collector (Q_u)	Equation (3.23)	$1.376KW$
2	Solar radiation absorbed by the collector (S)	Equation (3.39)	$1819.44W/m^2$
3	$e = 0.430(1 - {}^{100}/_{T_{pm}})$	Equation (3.50)	0.297
4	Overall heat loss coefficient (U_{L1})	Equation (3.49)	5.476W/m^{2}K
5	Collector area (A_c)	Equation (3.22)	$0.805m^2$
6	Collector fin efficiency factor (F')	Equation (3.40)	0.976
7	Collector heat removal factor (F_R)	Equation (3.41)	0.933
8	Plate mean temperature for the first iteration (T_{pm1})	Equation (3.44)	$325.415K$

Using the calculated plate mean temperature (T_{pm1}) value of 325.415K from the first iteration, a second iteration can be performed using a similar approach adopted for the first iteration in other to determine a more suitable value for the collector plate mean temperature. Hence, substituting the value of $(T_{pm1}) = 325.415K$ and solving other relevant equations as done in the first iteration gives the values for the required parameters as highlighted in Table (3.7).

Table 3.7: Values from second iteration using $T_{pm1} = 325.415K$

S/N	PARAMETER	REFERENCE	VALUES
1	Useful heat gain of the collector (Q_u)	Equation (3.23)	$1.376KW$
2	Solar radiation absorbed by the collector (S)	Equation (3.39)	$1819.44W/m^2$
3	$e = 0.430(1 - {}^{100}/_{T_{pm1}})$	Equation (3.50)	0.298
4	Overall heat loss coefficient (U_{L2})	Equation (3.49)	5.5702W/m^{2}K
5	Collector area (A_c)	Equation (3.22)	$0.812m^2$
6	Collector fin efficiency factor (F')	Equation (3.40)	0.968
7	Collector heat removal factor (F_R)	Equation (3.41)	0.931
8	Plate mean temperature for the second iteration (T_{pm2})	Equation (3.44)	$325.547K$

3.10 Collector area (A_c) and its dimensions

Considering both iterations, it is seen that there is no significant difference between the first and second mean plate temperatures compared with the initial assumed value for (T_{pm}). Therefore, an average of the two iterations can be adopted as the effective value for the mean plate temperature and the overall heat loss coefficient (U_L) as shown in equation (3.51) and (3.52) respectively.

$$T_{pm} = \frac{T_{pm1} + T_{pm2}}{2} = \frac{325.415 + 325.547}{2} = 325.481K \quad (3.51)$$

$$U_L = \frac{U_{L1} + U_{L2}}{2} = \frac{5.476 + 5.5702}{2} = 5.523\text{W/m}^2\text{K} \quad (3.52)$$

Substituting $T_{pm} = 325.418K$ and $U_L = 5.523\text{W/m}^2\text{K}$ into equation (3.22)

$$A_c = \frac{Q_u}{[(S - U_L(T_{pm} - T_a)]}$$

$$A_c = \frac{1376}{[1819.44 - 5.523(325.481 - 303)]}$$

$$A_c = 0.812m^2$$

Therefore, the collector area required for drying $5Kg$ of cassava is given as $0.812m^2$.

According to Chappell & Lebel (2009), for optimum performance, the ratio of the collector length(L_c) to width(W_c) of the solar collector is taken to be 1.5, hence;

$$L_c = 1.5W_c \quad (3.53)$$

Since the collector area is given as

$$A_c = L_c \times W_c \quad (3.54)$$

Therefore, the collector length $(L_c) = 1.1073m$ and the collector width(W_c) $= 0.7357m$. However, commercially available PV panel dimensions that is close to the design values achieved is a 100watt poly-crystalline solar panel manufactured by Invensun Sundragon (www.invensun.com) which has a length of 1.476m and a width of 0.670m with a

corresponding area of $0.989m^2$. Other relevant characteristics of the PV panel are shown in Table 3.8.

Table 3.8: Mechanical and Electrical characteristics of the 100watt PV panel (www.invensun.com assessed 9/02/2020)

S/N	MECHANICAL CHARACTERISTICS		ELECTRICAL CHARACTERISTICS	
1	Model name	Sundragon i100P	Model name	i100P
2	Solar cell type	Polycrystalline silicon	Max power at STC (P_{max})	100W
3	Length	1.476m	Optimum operating voltage	17.5V
4	Width	0.670m	Optimum operating current	5.71A
5	Depth	0.040m	Open circuit voltage (V_{oc})	20.5V
6	Operating temperature	-40 to +85°C	Short circuit current (I_{sc})	6.26A

The sundragon i100P model PV panel is adopted for this work since it is commercially available and has dimensions that are within the range of the design calculations. Therefore, the collector length (L_c) and width (W_c) are taken to be 1.476m and 0.670m respectively (Table 3.7).

3.11 Depth of the collector air duct

All the geometries used by Payman et al. (2016) showed acceptable levels of Cell temperature between 4-6cm duct depth, hence an intermediate value of 5cm is adopted during the course of this work considering variations in climatic factors of the test location.

3.11.1 The air-flow channel

The air-flow channel is positioned behind the PV panel with curved aluminium vanes evenly fitted on the opposite sides of the channel. Each vane is considered to have an original height equal to the depth of the air-flow channel (50mm). However, for uniformity, they vanes are experimentally curved into an arc of radius also equal to the depth of the flow channel (50mm), which brings the final height of each curved aluminium vane in the flow channel to 31mm while covering a distance of 37mm from their fixed positions. This modification was carried out in other to generate the required turbulence across the flow channel which will effectively aid the extraction of heat from the back of the PV panel. This is depicted in Figure 3.8.

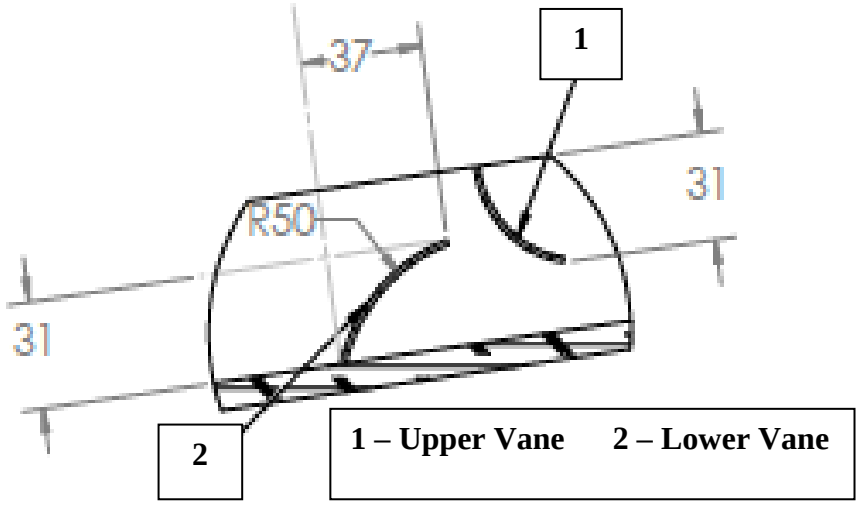

Figure 3.8: Geometry of the aluminium vanes in the air-flow channel

The configuration of the air-flow channel as shown enables the air in the channel to be evenly heated for an extended period thereby absorbing enough heat before exiting the channel and in the process introduces a cooling effect on the PV panel surface.

3.12 Sizing and dimensioning of the drying chamber

Design considerations and assumptions made during material selection and fabrication include;

1. Ply wood is used in fabricating the drying chamber due to its poor heat loss characteristics.
2. The drying chamber is made to be as tight as possible.
3. Uniform temperature distribution within the drying chamber is assumed.

With bulk density of cassava approximately 600kg/m^3, an appropriate drying layer thickness for the cassava is selected as 0.02m as stated earlier (Chappell & Lebel, 2009). Therefore,

$$\text{Loading density of the cassava} = 600\,kg/m^3 \times 0.02m = 12\,kg/m^2 \quad (3.55)$$

Quantity of cassava to be loaded in the drying chamber at a time $= 5kg$

$$\text{Required surface area of drying bed is} = \frac{\text{Quantity of cassava}}{\text{Loading density of cassava}} \quad (3.56)$$

$$= \frac{5}{12} = 0.417m^2$$

For a drying chamber consisting of two drying beds, the surface area required per bed is

$$= \frac{0.417}{2} = 0.2085m^2$$

3.12.1 Length (L_{dc}) and breadth (B_{dc}) of the drying chamber

As specified by Tonui et al. (2014), the breadth (B_{dc}) of the drying chamber is made to be equal to the width of the collector (W_c) and the resulting length of drying chamber is given as;

$$L_{dc} = \frac{A_{dc}}{W_c} \qquad (3.57)$$

$$L_{dc} = \frac{0.2085m^2}{0.670m}$$

$$L_{dc} = 0.311m$$

$A_{dc} = surface\ area\ of\ drying\ bed$

3.12.2 Height of the hot air column

This is the minimum height through which the hot air exits from the drying chamber vent. It is located above the collector inlet and allows for moist air to escape to the surrounding by natural or forced convection. All dryers need ventilation to be able to dry crops effectively.

The following assumptions are made before arriving at the height of the air column (Tonui et al., 2014).

1. the dryer functions under steady state conditions
2. The depth of the drying bed, is small compared to height, H, of the hot air column
3. The whole structure is air tight and ambient air enters through the inlet and the moist warm air escapes through the exit vent
4. The total pressure drop of the system (ΔP_T), is typically twelve times the pressure drop across the drying bed. In calculating the height of the hot air column, the pressure drop across the drying bed which is due to resistance to air flow through a packed bed of food material has to be considered. This resistance is as a result of the density difference between the hot air inside the dryer and the ambient air.
5. The exit air temperature from the dryer at the stated height should not be below 38.5°C as established from the ERH of 61%.

6. The steady state mean values of temperature and density of the hot air inside the dryer are T_{dc} and ρ^*, respectively.
7. The size of the installed DC extraction fan is used to consider the dimensions of the exit vent of the drying chamber.

The pressure drop across the bed can be analysed by adopting the equation given by Chappell & Lebel, (2009);

$$\Delta P_B = \frac{u \times h_L}{a} \qquad (3.58)$$

Where;

u = Superficial air velocity (i.e. the velocity of air across the drying bed at the same volume flow rate).

$a =$ a constant with numerical value of 0.465m^{3}s/kg

$\Delta P_B =$ pressure drop across the bed

$h_L =$ bed thickness equal to the cassava layer thickness of 0.02m

The superficial air velocity can be derived by dividing the volume flow rate (equation 3.19) by the area of the drying chamber (equation 3.56). Therefore,

$$u = \frac{Volume\ flow\ rate\ \ (m^3/s)}{Drying\ area\ (m^2)} \qquad (3.59)$$

$$u = \frac{0.047}{0.2085}$$

$$u = 0.225 m/s$$

Therefore, from equation (3.58), ΔP_B becomes;

$$\Delta P_B = \frac{0.225 \times 0.02}{0.465}$$

$$\Delta P_B = 0.0097 P\text{a}$$

Since the total pressure drop across the system (ΔP_T), is assumed to be twelve times the pressure drop across the bed, hence

$$\Delta P_T = 12 \times .0097 \qquad (3.60)$$

$$\Delta P_T = 0.1164 P\text{a}$$

Apply Bernoulli's equation to the system (Chappell & Lebel, 2009) as shown in equation (3.61);

$$H_{hac} = \frac{\Delta P_T}{g(\rho - \rho^*)} = \frac{\Delta P_T}{g\left({}^{1}/_{T_a} - {}^{1}/_{T_{dc}}\right){}^{P_a}/_{R_a}} \quad (3.61)$$

Where;

g = acceleration due to gravity, which is 9.81m/s^2

P_a = the atmospheric pressure, which is 101325Pa

R_a = the specific gas constant [286.9 J/kg K]

T_a = the ambient temperature [303K]

T_{dc} = the temperature of drying air leaving the air heater [311.5K]

$$H_{hac} = \frac{0.1164}{9.81\left({}^{1}/_{303} - {}^{1}/_{311.5}\right){}^{101325}/_{286.9}}$$

$$H_{hac} = 0.373m$$

Therefore the ideal height of the dryer exit vent for effective drying is 0.373m. This implies that the saturated air which has passed through the product to be dried, needs to be discharged from the exit vent of the drying chamber at a height of 0.373m otherwise condensation of water vapour within the drying chamber will take place. This will largely affect the quality of the product being dried, easy decay of the wood used in fabricating the drying chamber and the overall performance of the PVT powered dryer.

3.12.3 Volume of the solar dryer

The volume of the of the solar dryer is then given as

$$V_{dc} = A_{dc} \times H$$

$$V_{dc} = 0.2085 \times 0.373$$

$$V_{dc} = 0.078m^3$$

3.13 The PVT collector thermal efficiency

The collector thermal efficiency of the PVT can be defined as the ratio of the daily average useful heat gained by the collector to the product of the daily average solar radiation intensity and the collector area. The PVT thermal efficiency is determined from the daily average temperature difference between the ambient and outlet temperatures of the PVT collector during the 5 days unloaded test. The thermal efficiency can be calculated using equation 3.62 (Ogueke & Anyanwu, 2017).

$$\eta_{(c)PVT} = \frac{Q_{g(ave)}}{A_c I_{T(ave)}} \quad (3.62)$$

$$Q_{g(ave)} = \dot{m} C_{pa} (\Delta T_{ave}) \quad (3.63)$$

Were

$I_{T(ave)}$ = Daily average solar radiation intensity (W/m^2)

$Q_{g(ave)}$ = Daily average useful heat gained by the air (KJ/s)

ΔT_{ave} = Daily average temperature difference between the ambient and outlet temperatures of the PVT collector (°C)

$$\Delta T_{ave} = \frac{\Delta T_{1(ave)} + \Delta T_{2(ave)} + \Delta T_{3(ave)} + \Delta T_{4(ave)} + \Delta T_{5(ave)} + \ldots}{Number\ of\ days} \quad (3.64)$$

$$I_{T(ave)} = \frac{I_{T1(ave)} + I_{T2(ave)} + I_{T3(ave)} + I_{T4(ave)} + I_{T5(ave)} + \ldots}{Number\ of\ days} \quad (3.65)$$

3.14 Solar Dryer Efficiency

The solar dryer efficiency can be defined as the ratio of thermal equivalent of the evaporated water plus the quantity of heat used to raise the temperature of the product to the useful heat gained by the drying air from the solar collector. The solar dryer efficiency is given below as (Ogueke et al., 2017)

$$\eta_s = \frac{(M_w \times L_v) + (M_g \times C_{pg} \times \Delta T)}{Q_a} \quad (3.66)$$

Where:

M_w= The mass of moisture content evaporated (kg)

L_v = The latent heat of vaporization: 2313.43KJ/kg (Equation 3.17)

M_g= Mass of product to be dried (5kg)

C_{pg} = Specific heat capacity of fresh cassava (KJ/kgK)

ΔT = Average temperature difference between chamber and ambient air (°C)

Q_a = The useful heat gained by the dry air (KJ)

Also, the useful heat gained by the dry air during the 9 hours of daily drying (8AM – 5PM) is computed from:

$$Q_a = (9 \times 60 \times 60)\left(\dot{m} \times C_{pa} \times [T_{2Ave} - T_{lAve}]\right) \quad (3.67)$$

$\dot{m}_a$ = Air mass flow rate: 0.0547kg/s (Equation 3.20)

C_{pa}= Specific heat capacity of air: 1.006KJ/KgK

$T_{2Ave}\ and\ T_{1Ave}$ = Average temperature change between ambient air and outlet air going into the drying chamber (°C)

The specific heat capacity of cassava (C_{pg}) can be calculated from equation (3.68) given as (Simo-Tagne et al., 2021):

$$C_{pg} = 837 + 3348\left(\frac{H_f}{1 + H_f}\right) \qquad (3.68)$$

H_f = Final moisture content for safe storage of the cassava after drying (db)

From equation (3.8), initial mass of 5Kg of fresh cassava contains 65% moisture. This implies that the 5Kg of fresh cassava contains 3.25Kg of moisture content. However, since it was calculated that during drying, 2.94Kg of moisture content has to be removed from the fresh cassava for safe storage, then the final moisture content (H_f) is the difference between the initial moisture content (3.25Kg) and the calculated moisture content to be removed (2.94Kg).

$$H_f = 3.25Kg - 2.94Kg = 0.31Kg \qquad (3.69)$$

From equation (3.68),

$$C_{pg} = 1.67KJ/KgK$$

CHAPTER FOUR

RESULTS AND DISCUSSION

4.1 Results

The experiment was carried out for a total of thirteen (13) days. The first five days were done without loading the drying chamber (i.e unloaded test) while the remaining tests were done with the drying chamber loaded with the product to be dried (loaded test). The loaded tests were done such that each sample was dried for two days. Thus, four samples were dried in all during the loaded test. Figures 4.1 – 4.5 shows results obtained for the unloaded test while Figures 4.6 – 4.13 shows those of the loaded test.

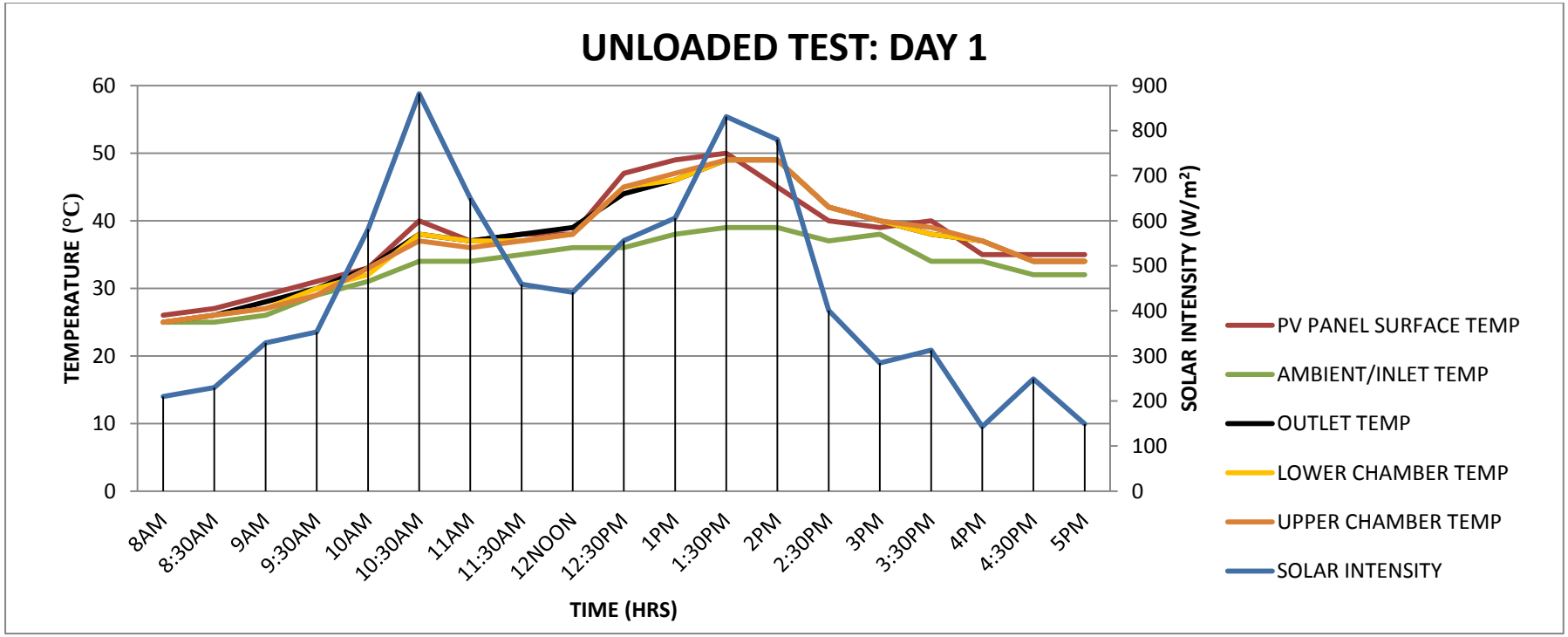

Fig. 4.1: Clear sky PVT solar dryer 1st day unloaded test performance

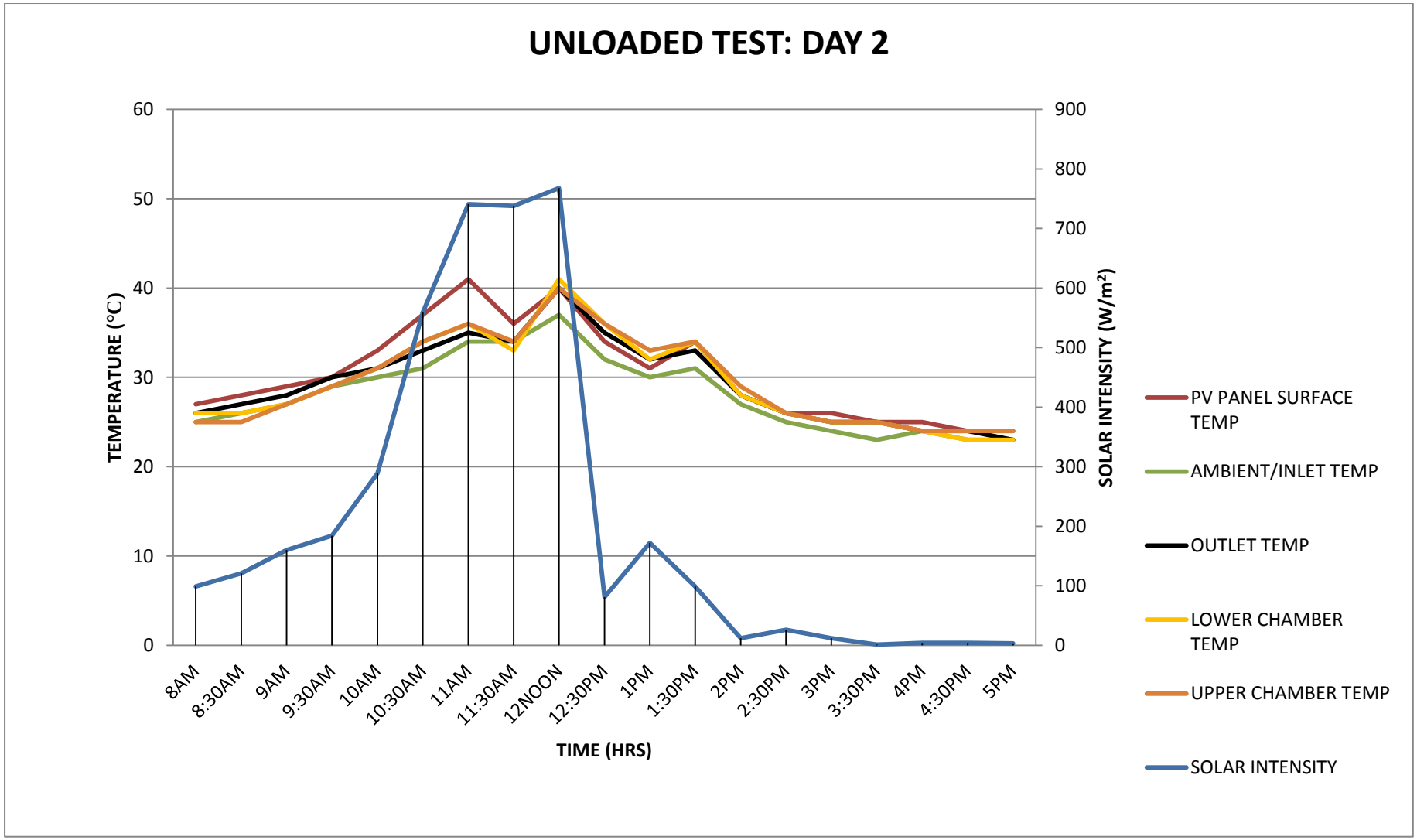

Fig. 4.2: Overcast PVT solar dryer 2nd day unload test performance

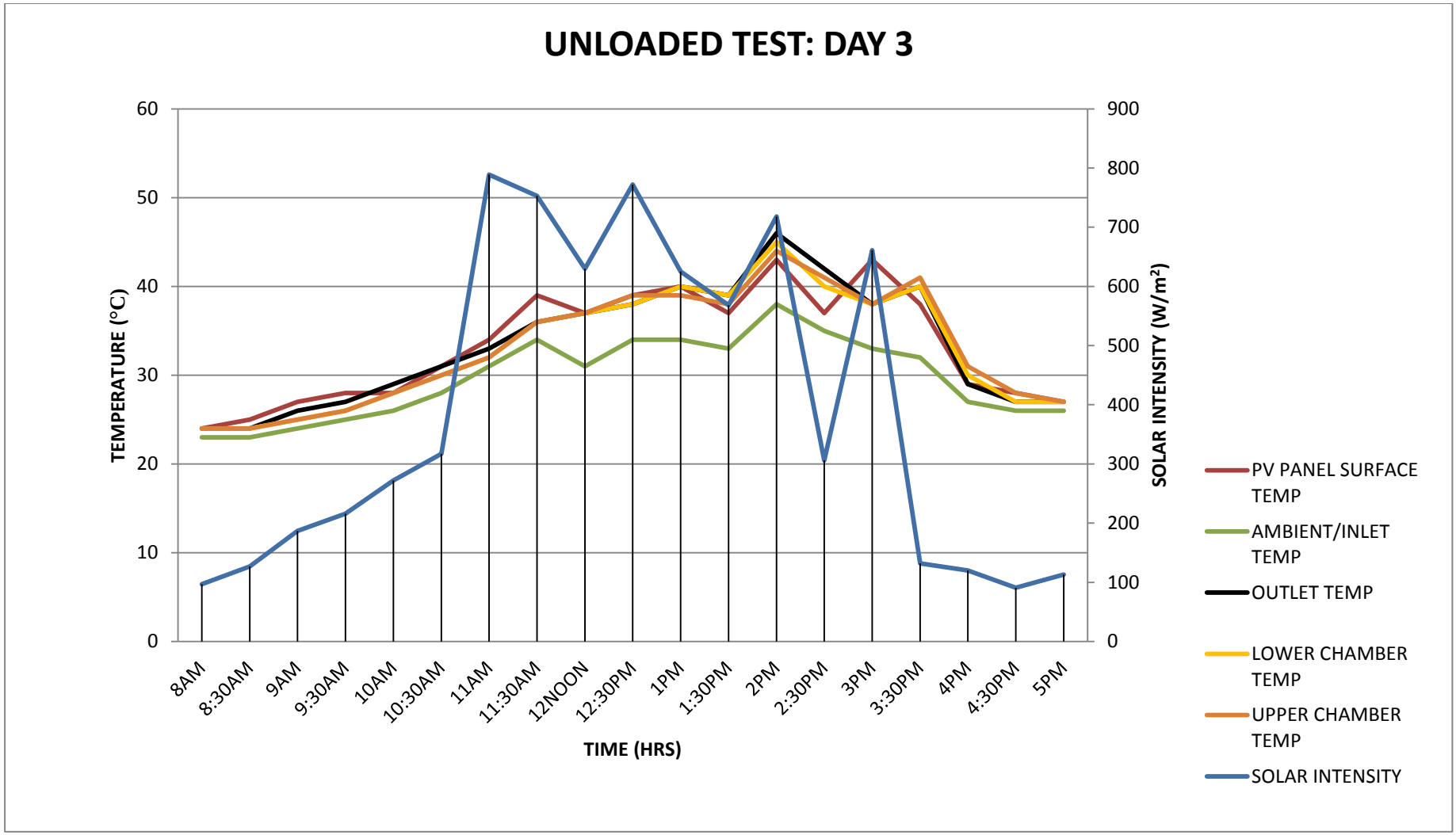

Fig. 4.3: PVT solar dryer 3rd day unloaded test performance

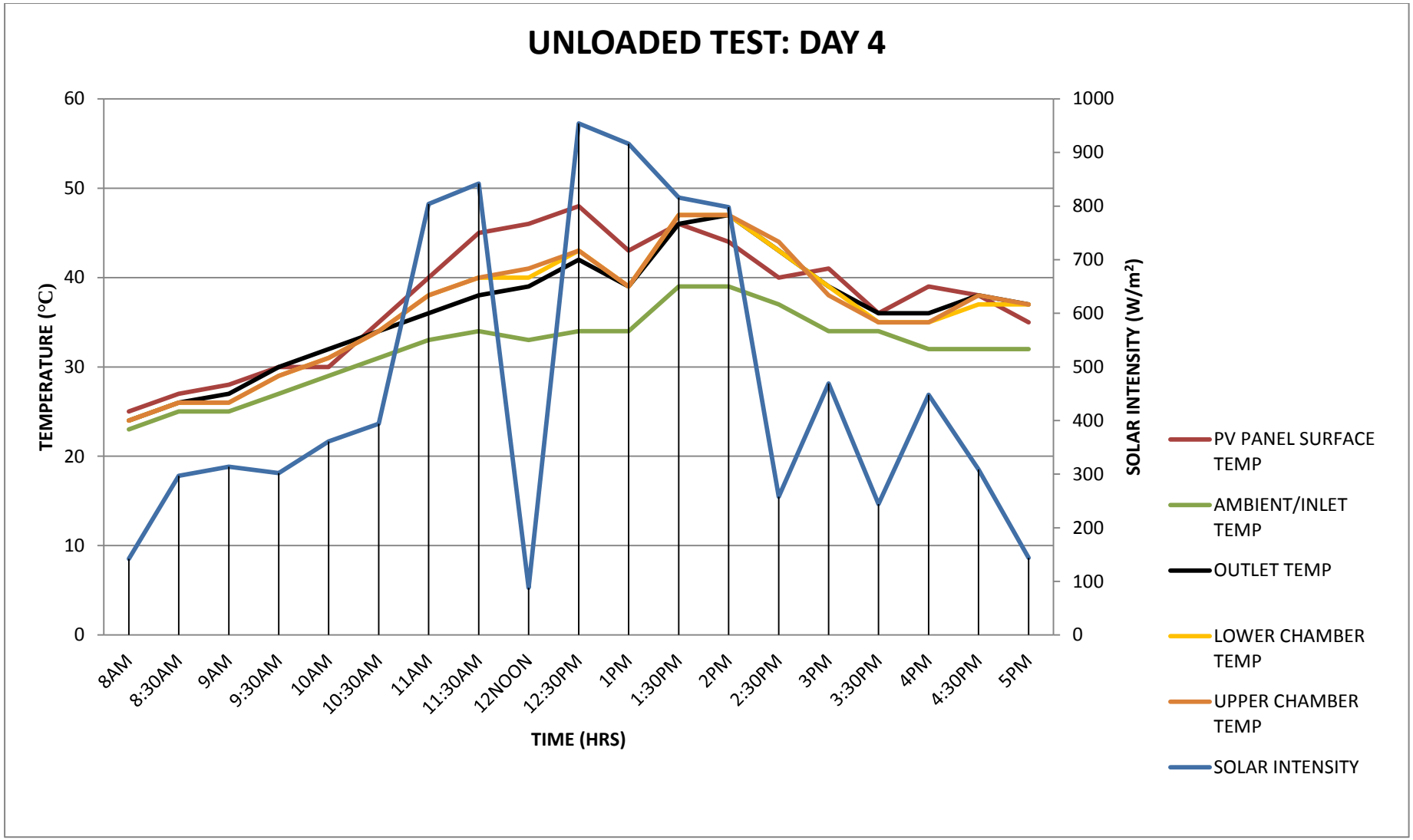

Fig. 4.4: PVT solar dryer 4th day unloaded test performance

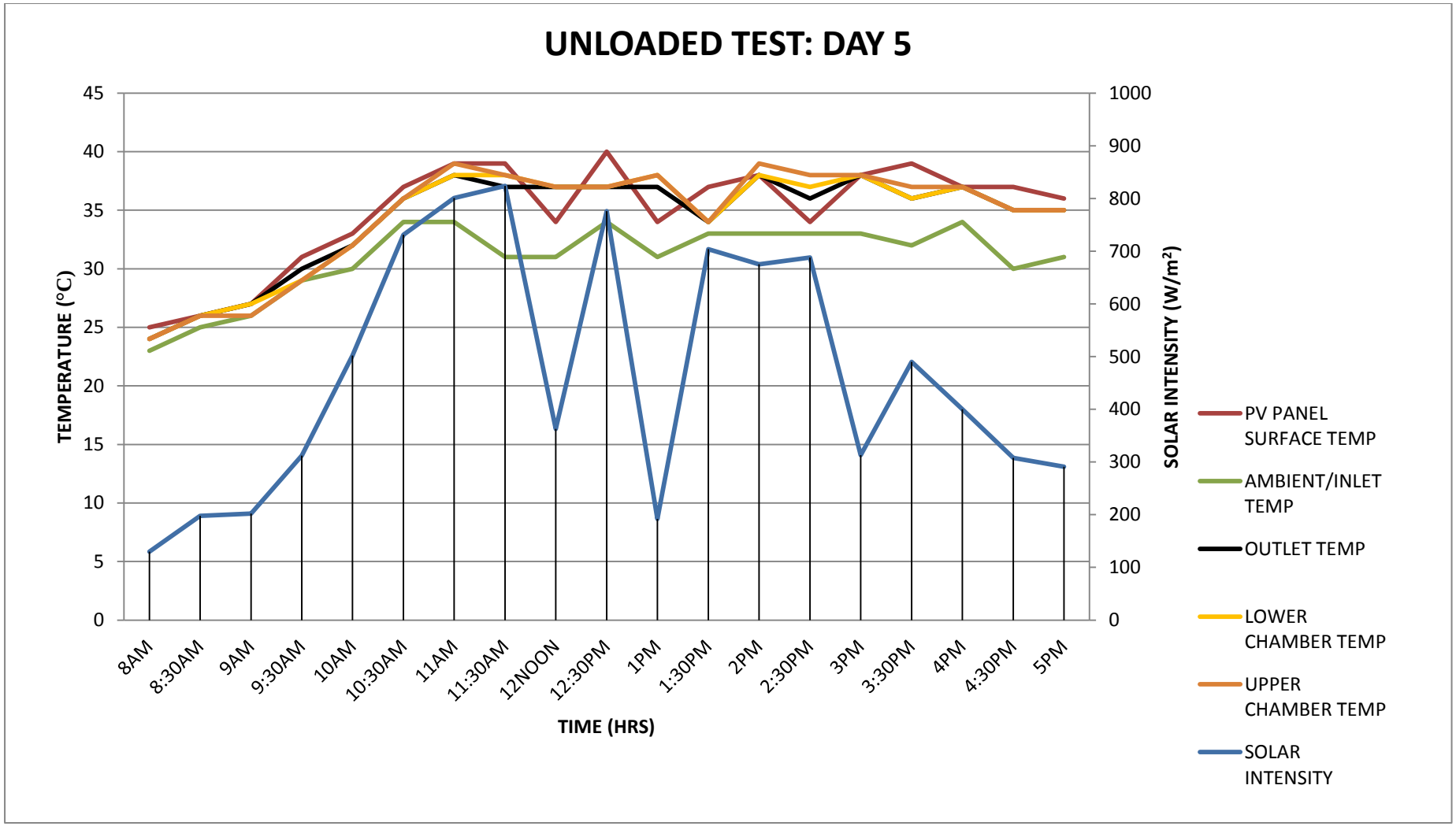

Fig. 4.5: PVT solar dryer 5th day unloaded test performance

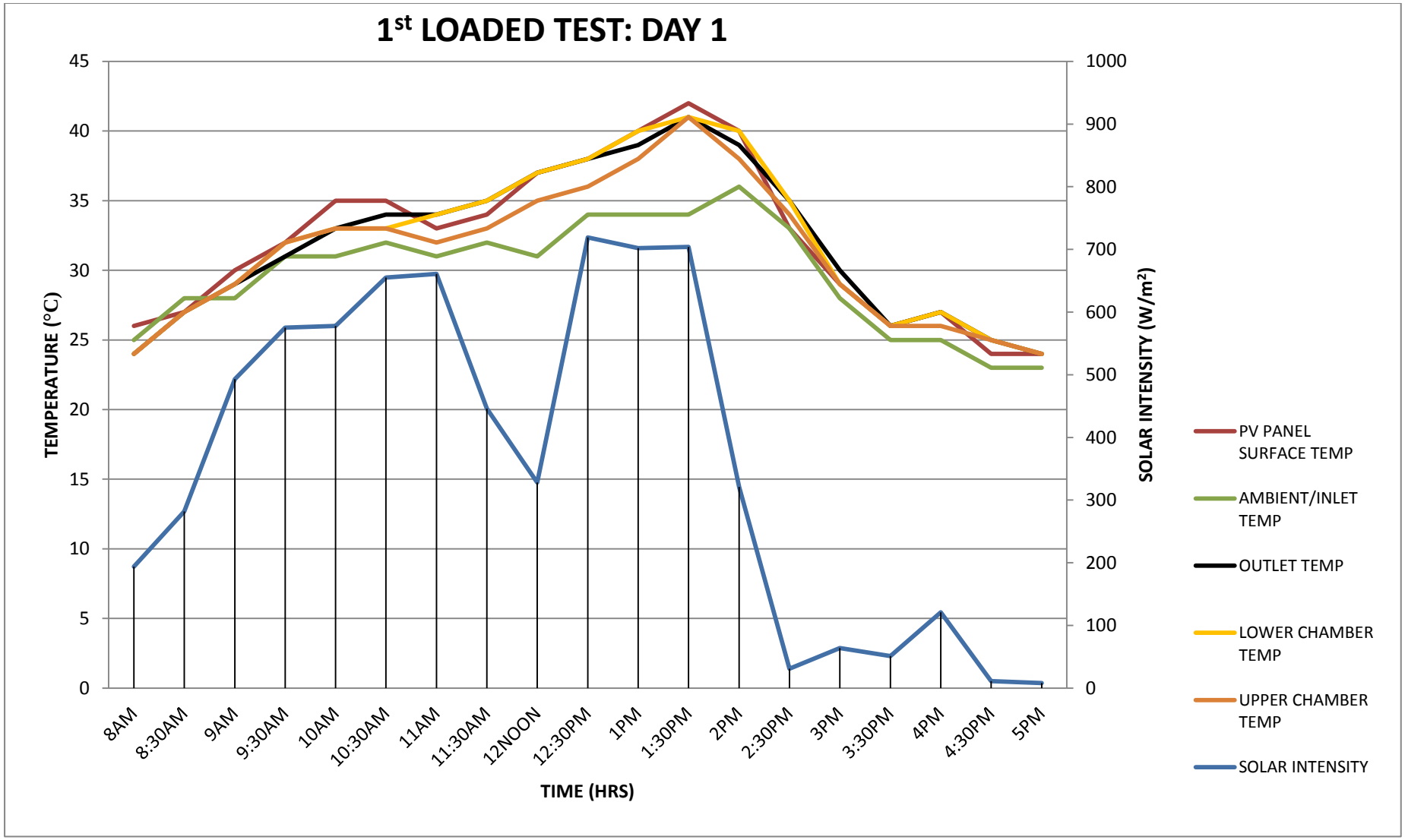

Fig. 4.6: PVT solar dryer 1st loaded test; Day1 performance

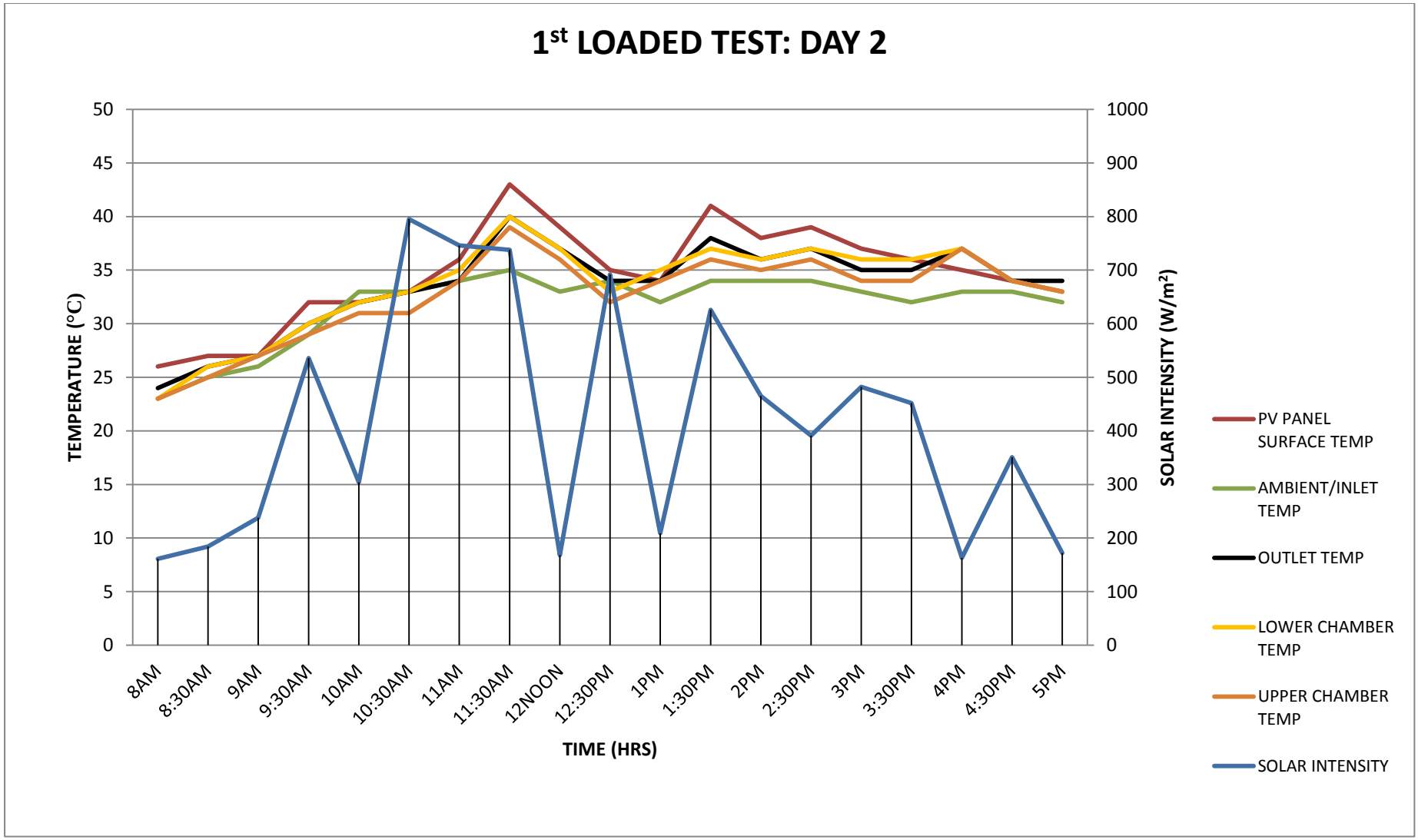

Fig. 4.7: PVT solar dryer 1st loaded test; Day2 performance

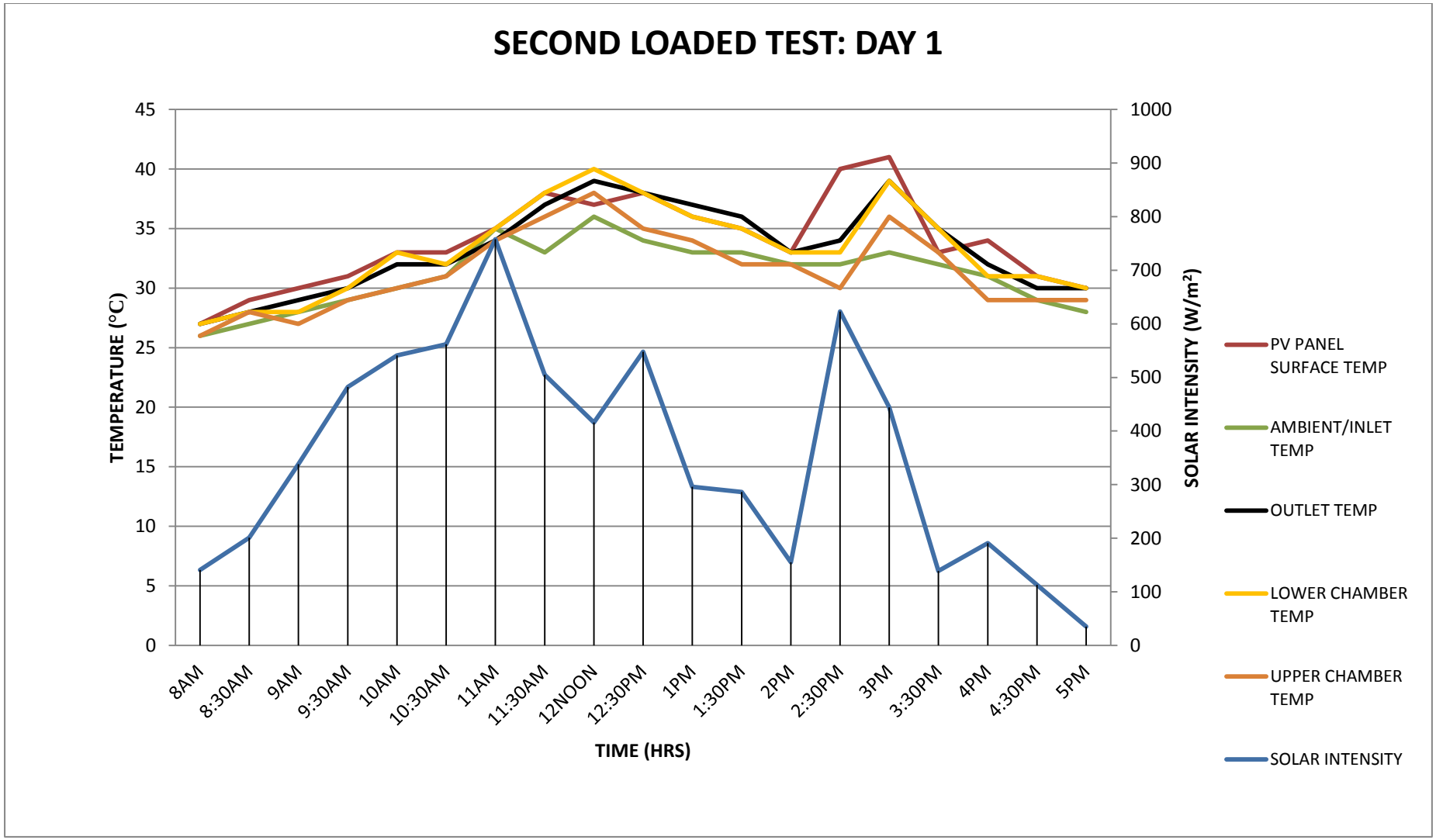

Fig. 4.8: PVT solar dryer 2nd loaded test; Day1 performance

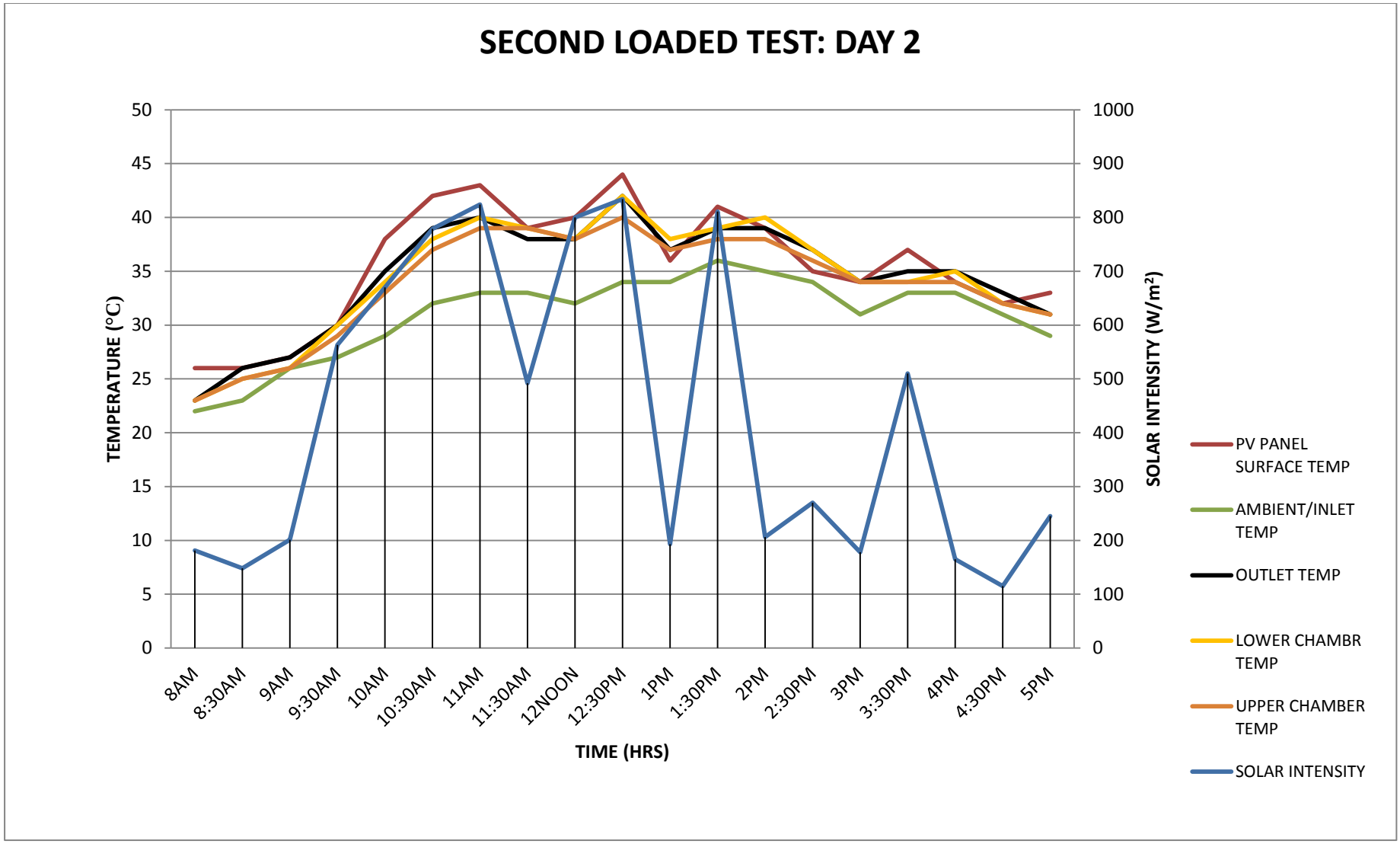

Fig. 4.9: PVT solar dryer 2nd loaded test; Day2 performance

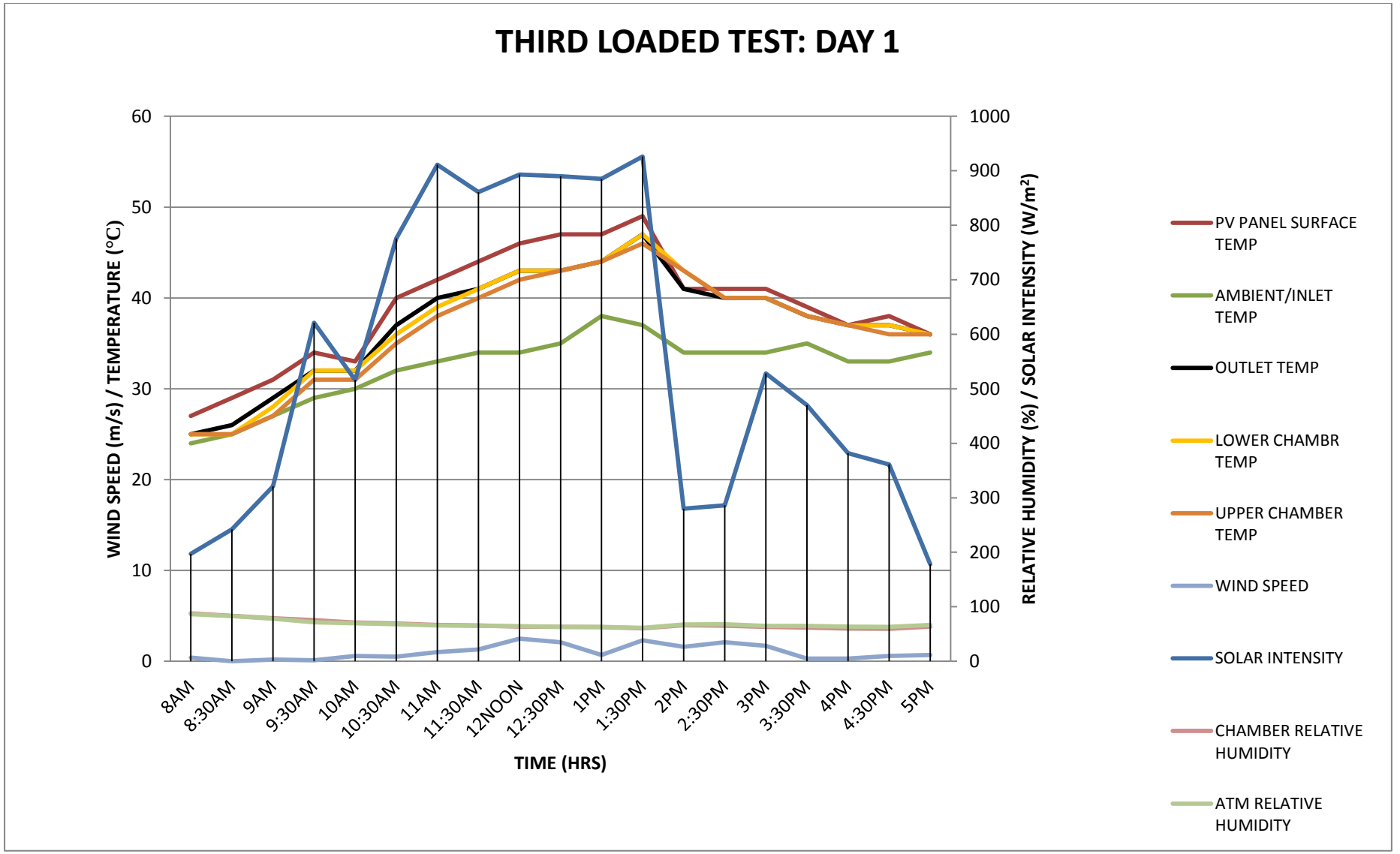

Fig. 4.10: PVT solar dryer 3rd loaded test; Day1 performance

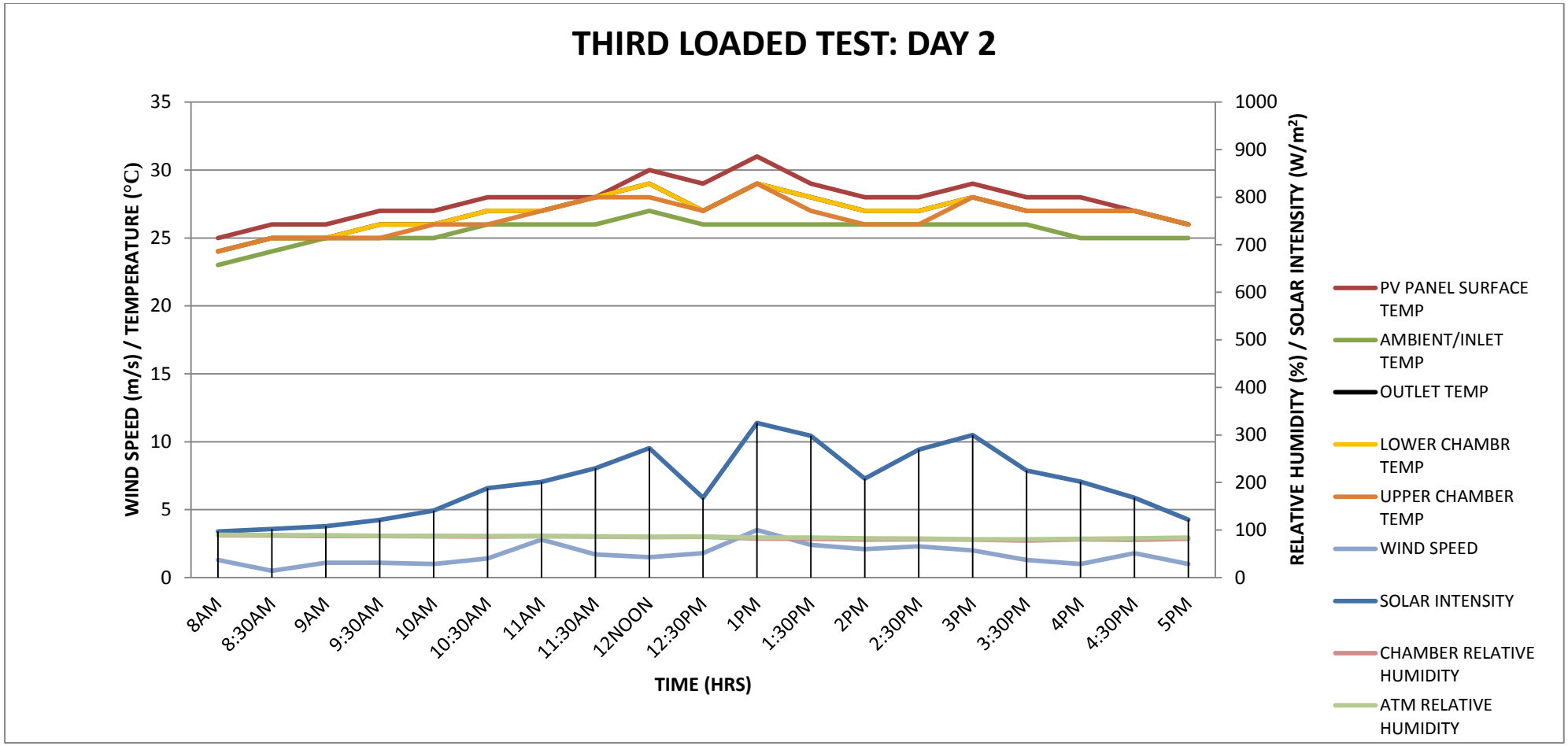

Fig. 4.11: Overcast PVT solar dryer 3rd loaded test; Day2 performance

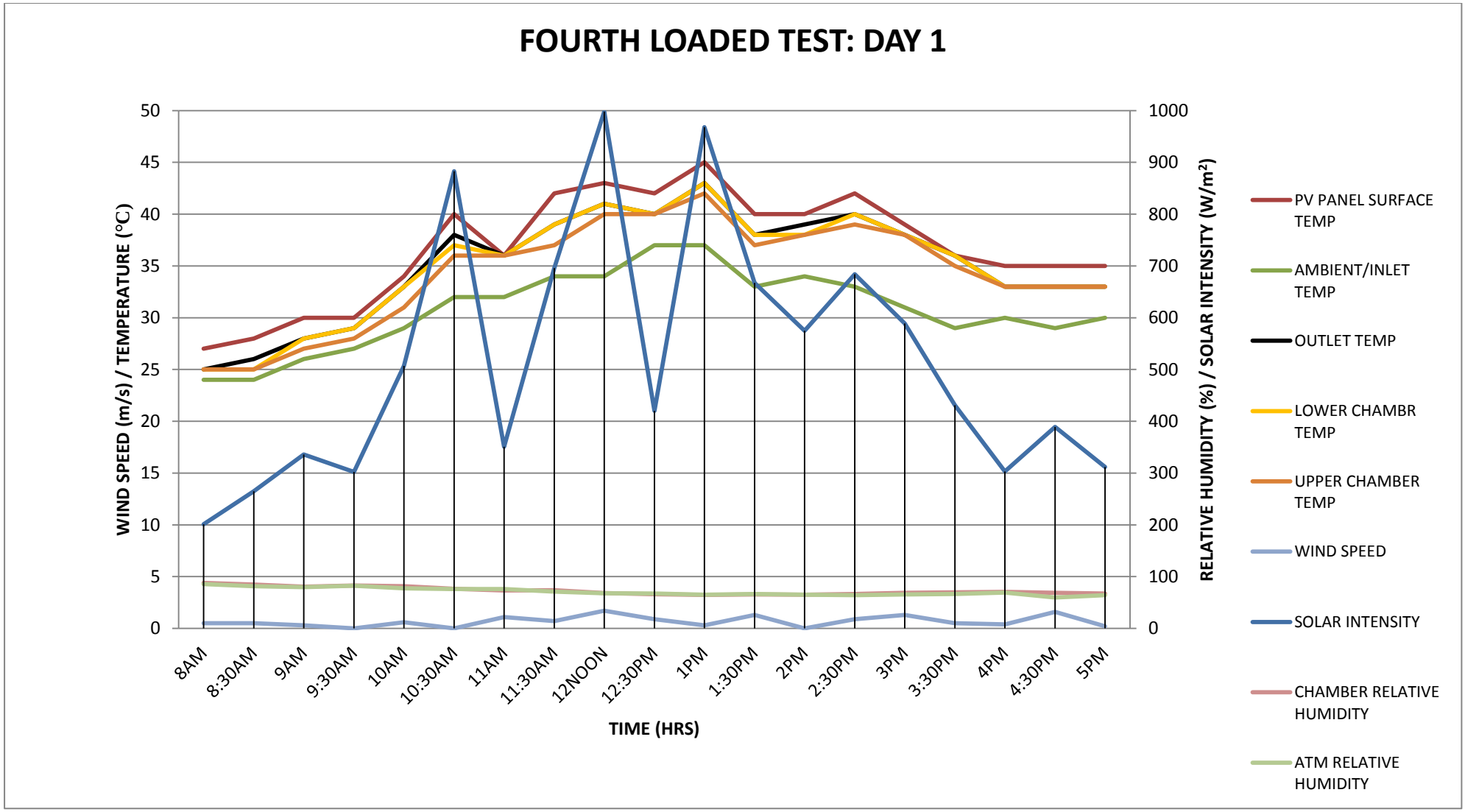

Fig. 4.12: PVT solar dryer 4th loaded test; Day1 performance

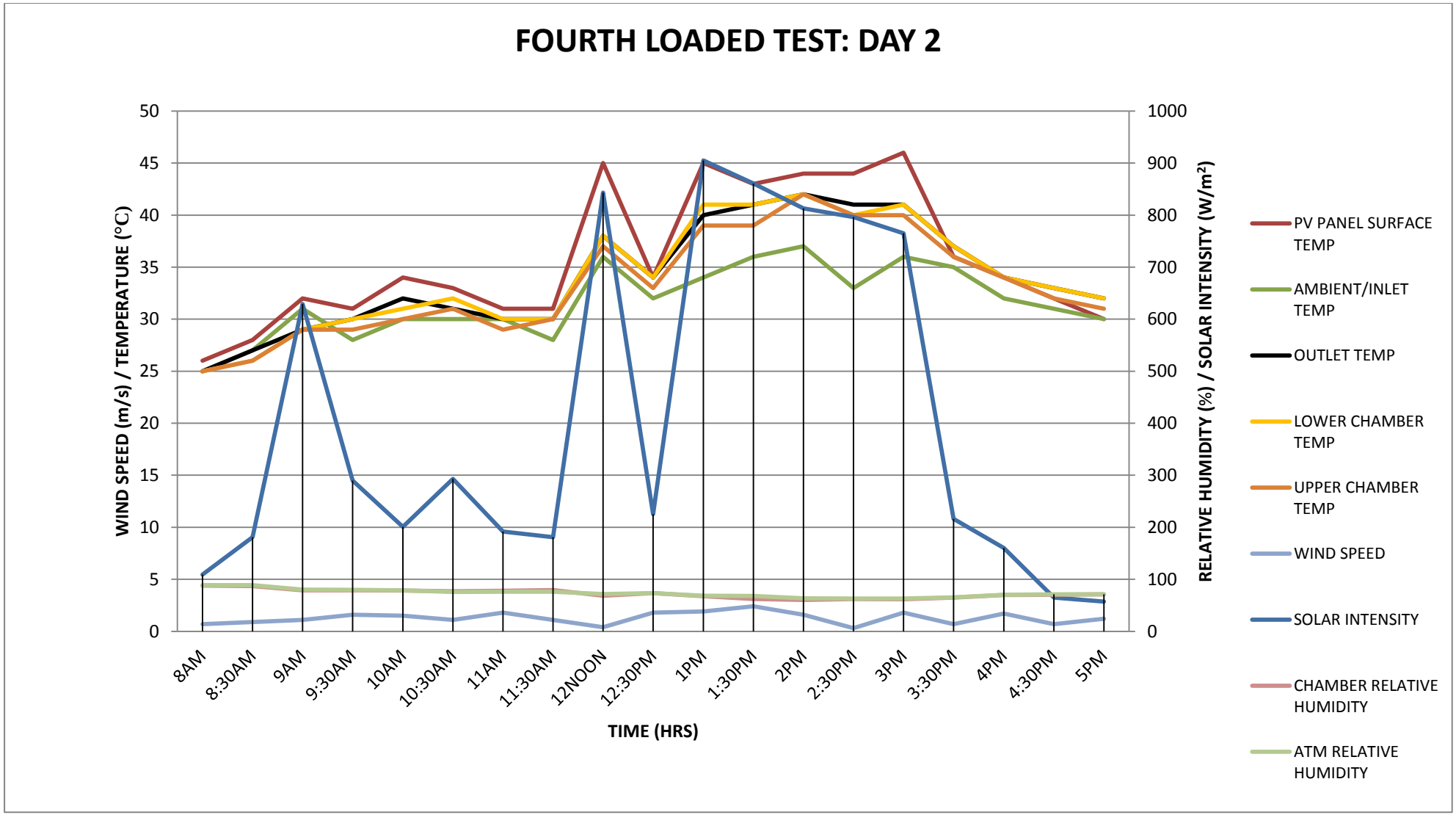

Fig. 4.13: PVT solar dryer 4th loaded test; Day2 performance

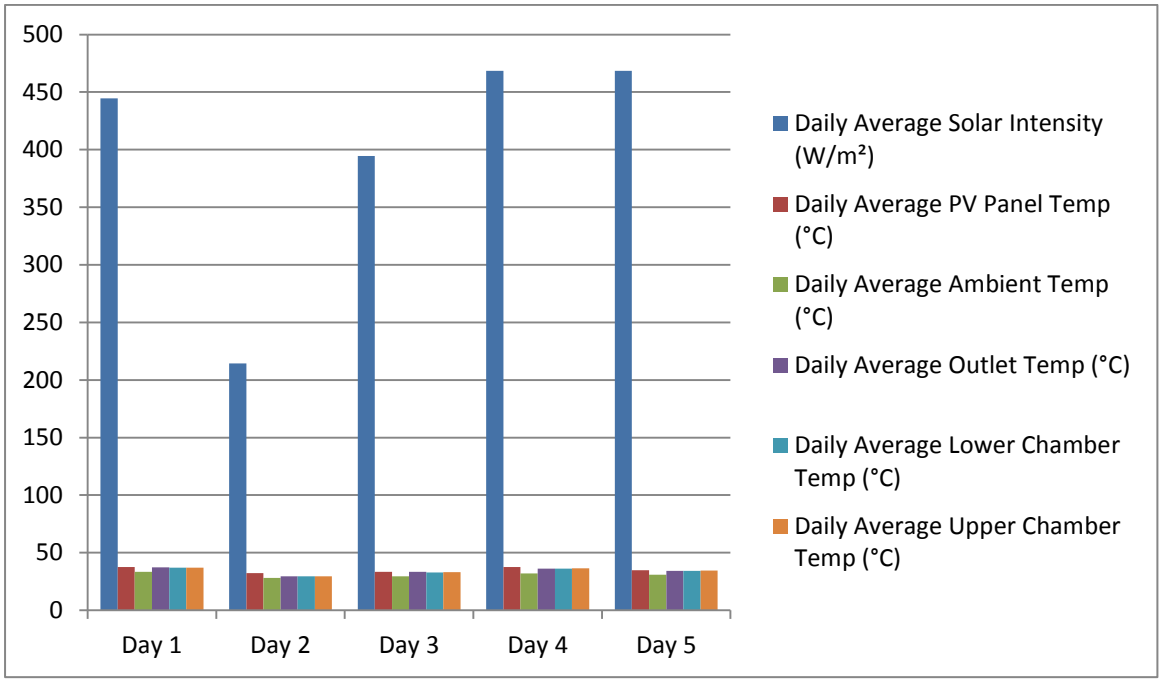

Fig. 4.14: Daily average recorded performance for all parameters (unloaded test)

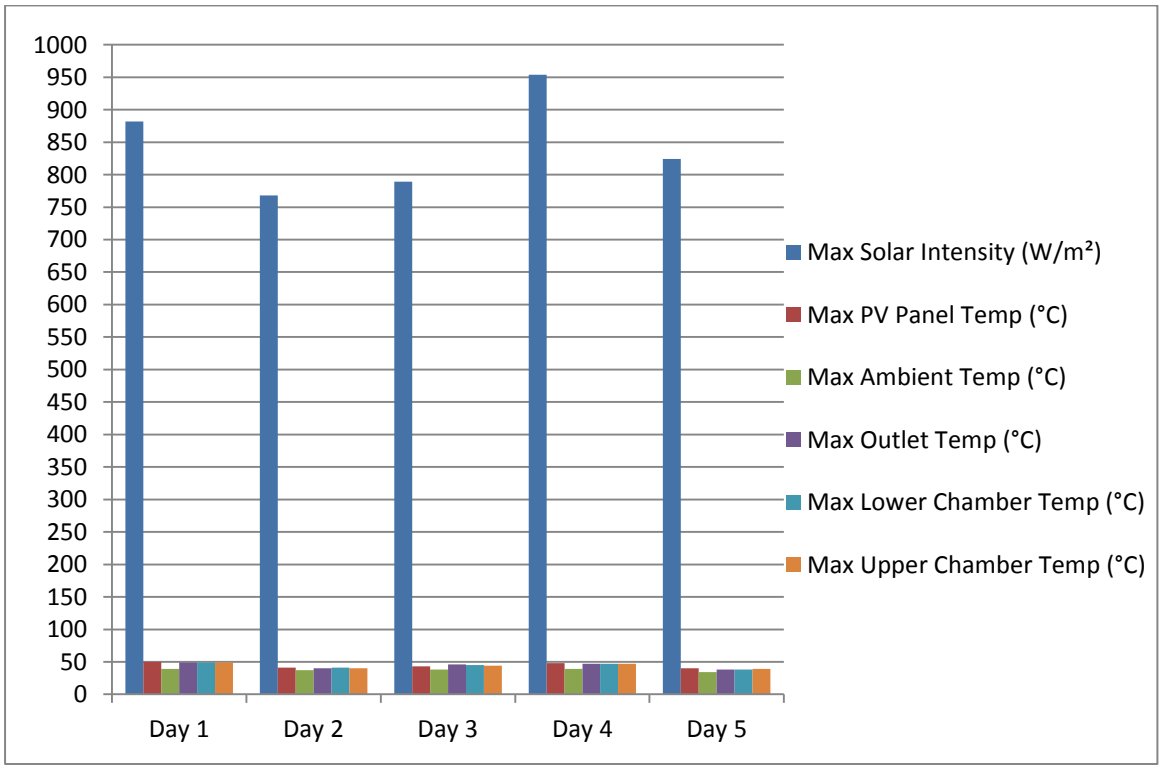

Fig. 4.15: Results for peak periods (unloaded test)

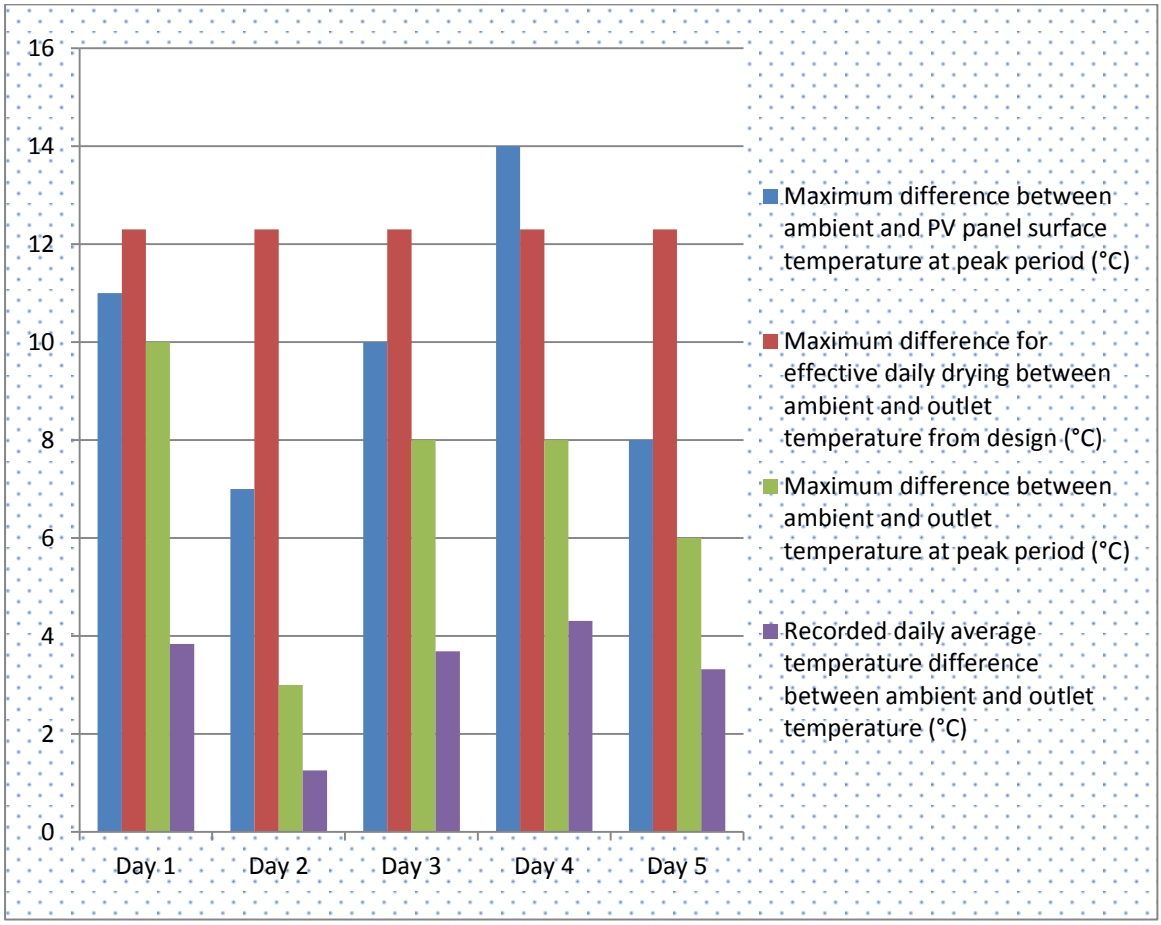

Fig. 4.16: Performance analysis of the PVT section of the setup during unloaded test

Table 4.1: Cumulative average values of parameters during unloaded test

S/N	PARAMETER	REFERENCE	VALUES
1	$\boldsymbol{\Delta T_{ave}}$: Cumulative value for daily average temperature difference between the ambient and outlet temperatures of the PVT collector during the 5 days unloaded test (°C)	Equation (3.64) applied to **Item Number 4 on Table (4. 3)**	3.464°C
2	$\boldsymbol{Q_{g(ave)}}$: Cumulative daily average useful heat gained by the air for the 5 days unloaded test (KJ/s)	Equation (3.63)	$0.191KW$
3	$\boldsymbol{I_{T(ave)}}$: Cumulative value for daily average solar radiation intensity for the 5 days unloaded test (W/m^2)	Equation (3.65) applied to **Table (4. 1)**	$0.398KW/m^2$
4	$\boldsymbol{T_{a(ave)}}$: Cumulative value for daily average inlet/ambient temperature for the 5 days unloaded test (°C)	Table (4.1)	30.8°C
5	$\boldsymbol{T_{o(ave)}}$: Cumulative daily average outlet temperature for the 5 days unloaded test (°C)	Table (4.1)	34.084°C
6	$\boldsymbol{T_m}$: Cumulative value mean temperature of the air for the 5 days unloaded test	Equation (3.42) Applied to **4 and 5 above**	32.44°C
7	$\boldsymbol{C_{pa}}$: Specific heat capacity of air	Given	$1.006KJ/KgK$
8	$(\boldsymbol{\tau\alpha})_{\dot{e}}$: Effective transmittance-absorptance Coefficient	Equation (3.38)	0.5217
9	Overall heat loss coefficient (U_L)	Equation (3.49)	5.5702W/m^{2}K
10	Collector area (A_c) $0.812m^2$ designed value and $0.989m^2$ commercially available value)	Equation (3.22)	$0.989m^2$
11	(F'): Measured cumulative daily average collector fin efficiency factor for the 5 days unloaded test (W/m^2)	Equation (3.40)	97.29%
12	(F_R): Measured cumulative daily average collector heat removal factor for 5 days unloaded test (W/m^2)	Equation (3.41)	93.01%
13	$\eta_{(c)PVT}$: PVT collector thermal efficiency	Equation (3.62)	48.52%

Table 4.2: Assumed and Measured values for fin efficiency and heat removal factors

S/N	PARAMETER	RESULTS FOR ASSUMED VALUES	RESULTS FOR MEASURED VALUES
1	Fin efficiency factor ($F^{'}$)	96.80%	97.29%
2	Heat removal factor (F_R)	93.10%	93.01%

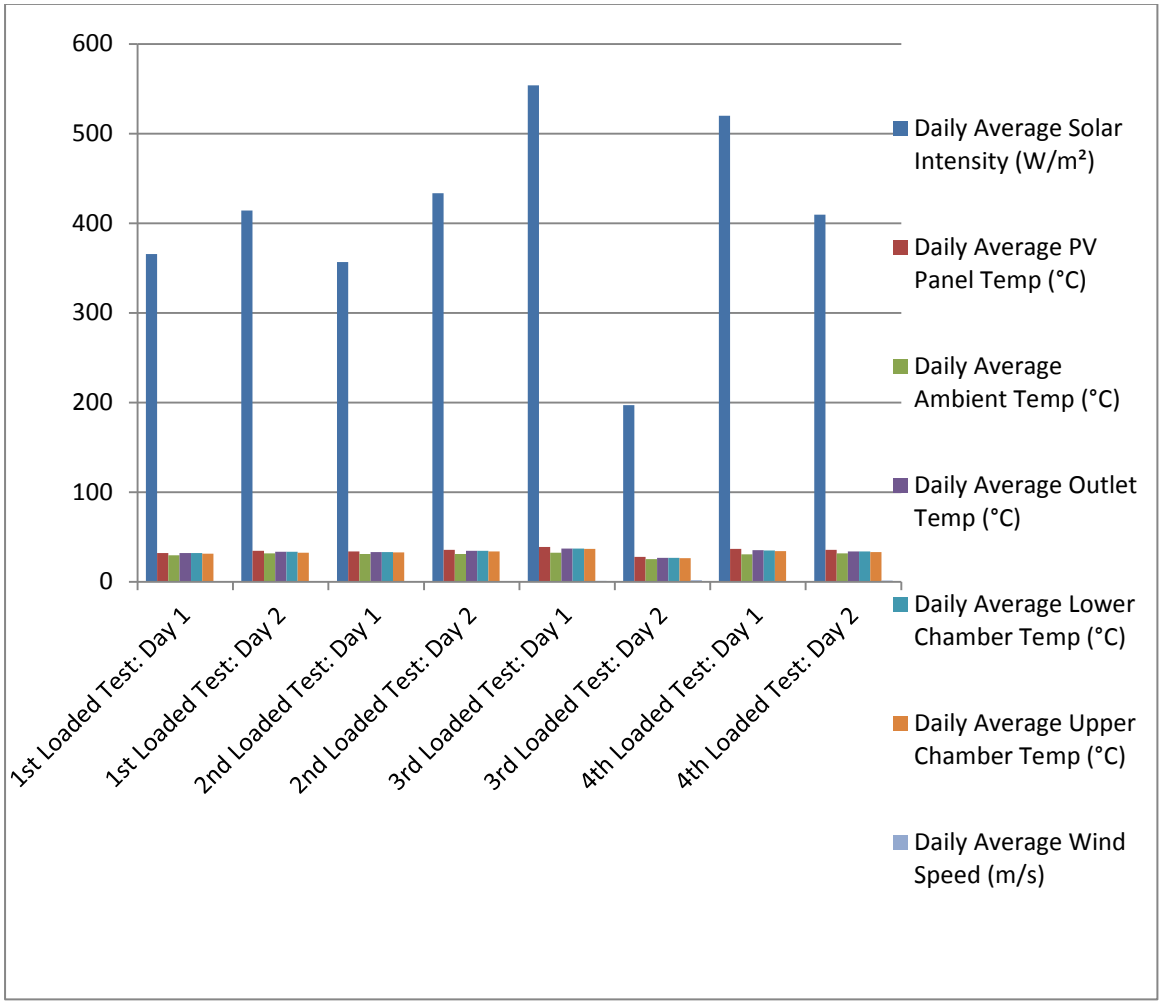

Figure 4.17: Daily average recorded performance for all parameters (loaded test)

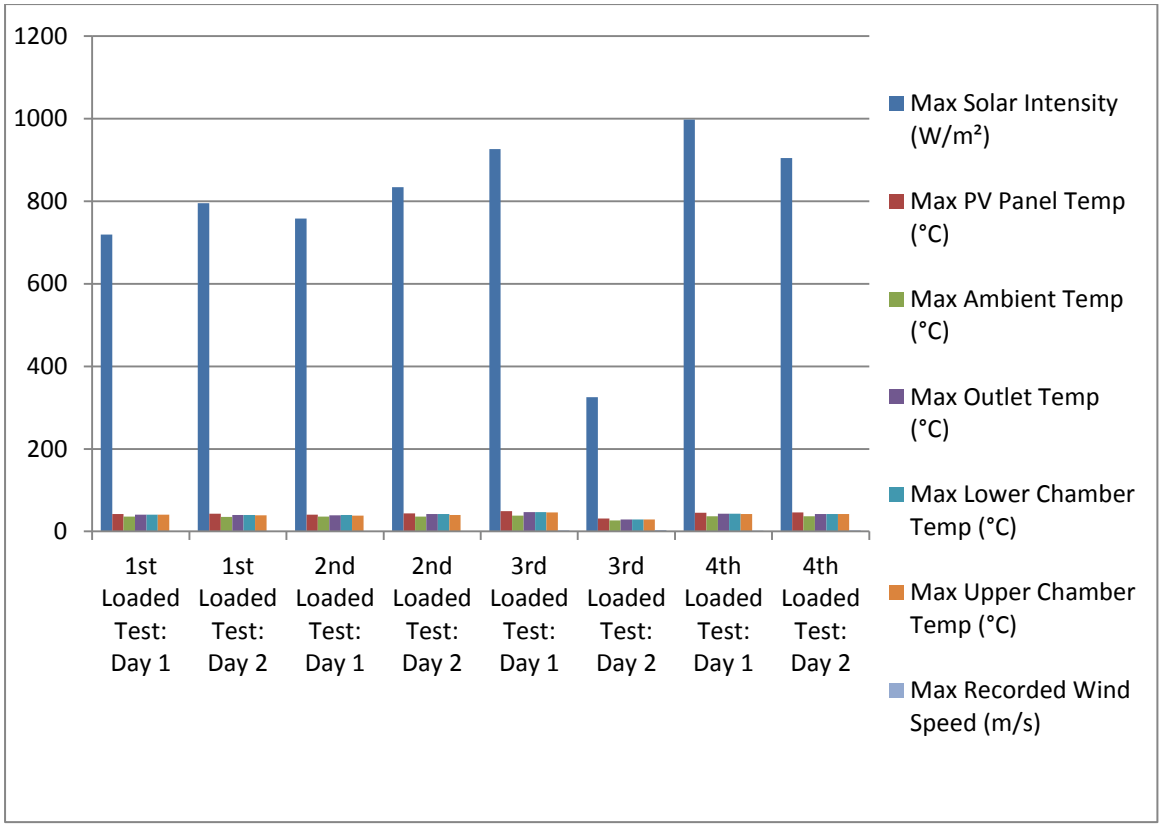

Figure 4.18: Results for peak periods (loaded test)

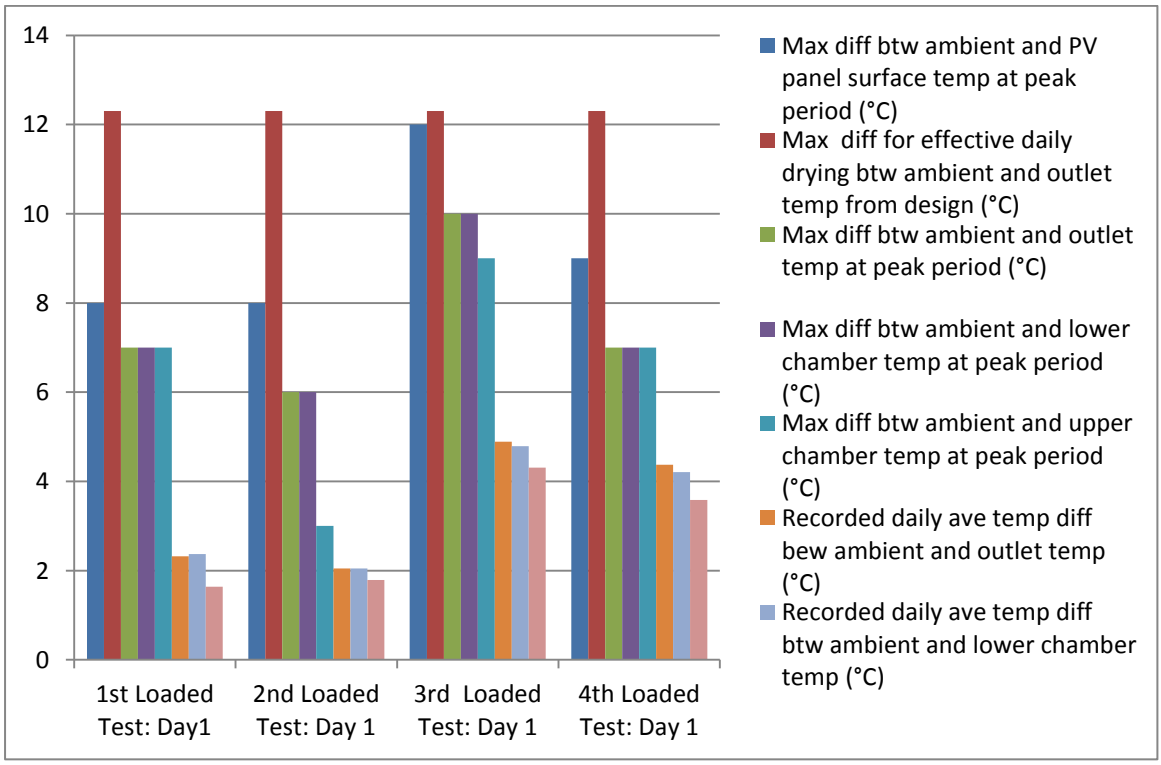

Figure 4.19: Performance analysis of the PVT solar dryer during "Day 1" of 1st to 4th loaded tests

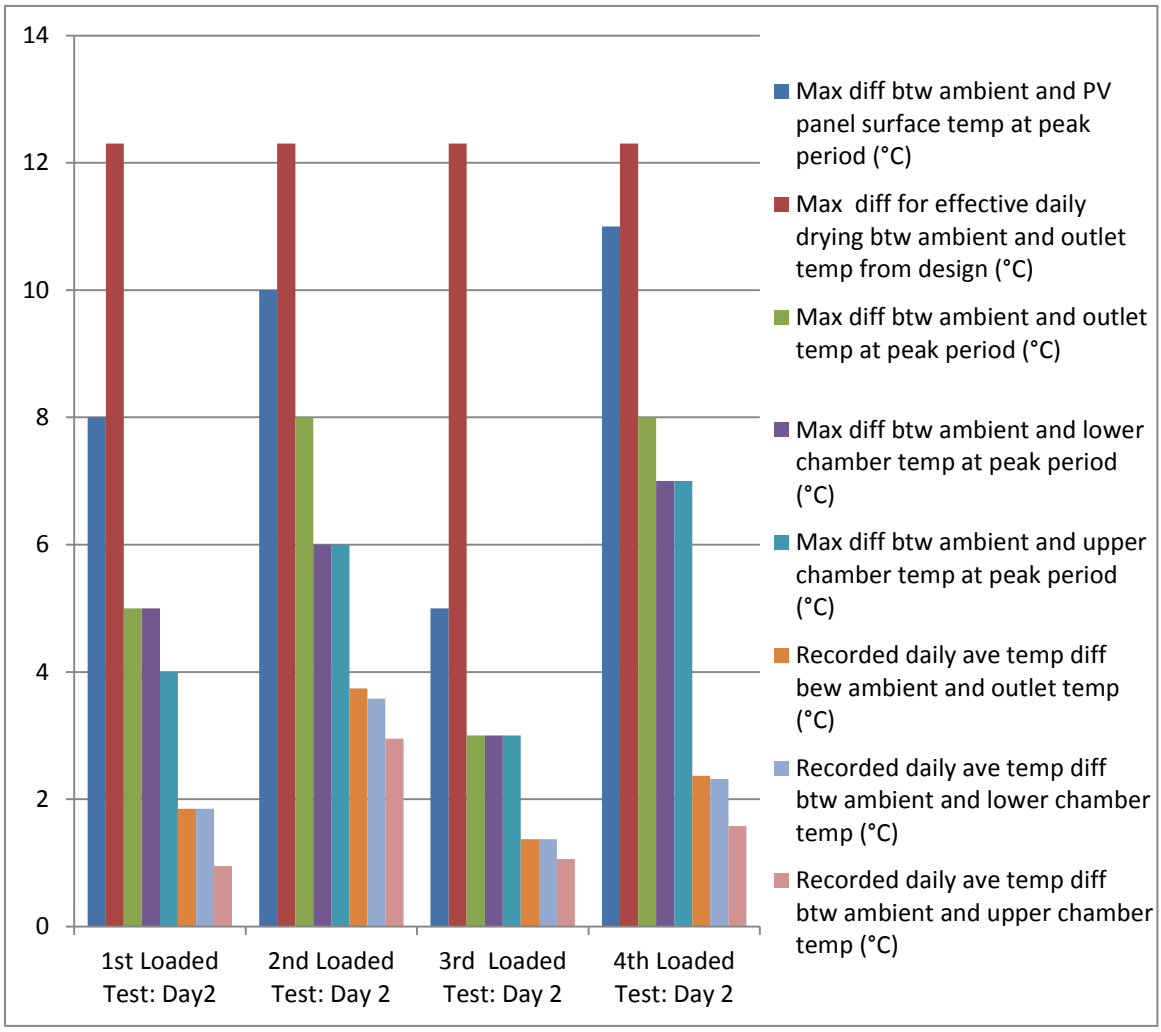

Figure 4.20: Performance analysis of the PVT solar dryer during "Day 2" of the 1st to 4th loaded tests

Table 4.3: Moisture content removed and relative humidity during drying

S/N	DAYS	Moisture Content Removed (kg)	Chamber Exit Relative Humidity (Beginning of the Drying Day) (%)	Atmospheric Relative Humidity (Beginning of the Drying Day) (%)	Chamber Exit Relative Humidity (End of the Drying Day) (%)	Atmospheric Relative Humidity (End of the Drying Day) (%)	Minimum Chamber Exit Relative Humidity Recorded During Drying (%)
1	**1st Loaded Test Day 1**	**1.3**	**--**	**--**	**--**	**--**	**--**
2	**1st Loaded Test Day 2**	**1.1**	**--**	**--**	**--**	**--**	**--**
3	**2nd Loaded Test Day 1**	**1.3**	**--**	**--**	**--**	**--**	**--**
4	**2nd Loaded Test Day 2**	**1.3**	**--**	**--**	**--**	**--**	**--**
5	**3rd Loaded Test Day 1**	**1.9**	**87.7** 8AM	**86.5** 8AM	**63.5** 5PM	**66.8** 5PM	**59.6** 4:30PM
6	**3rd Loaded Test Day 2**	**0.6**	**88.8** 8AM	**89.8** 8AM	**81.3** 5PM	**84.2** 5PM	**78** 3:30PM
7	**4th Loaded Test Day 1**	**1.5**	**87.7** 8AM	**85.8** 8AM	**67.2** 5PM	**64.3** 5PM	**64.6** 1PM
8	**4th Loaded Test Day 2**	**1.2**	**87.8** 8AM	**88.7** 8AM	**71.3** 5PM	**71.3** 5PM	**60.5** 2PM

Table 4.4: Daily Moisture content removed during drying and corresponding daily average drying chamber temperature

S/N	DAYS	Moisture Content Removed (kg)	Moisture Removal Rate Per Hour (kg/hr)	Daily Average Lower Chamber Temperature (°C)	Daily Average Upper Chamber Temperature (°C)	Overall Daily Average Chamber Temperature (°C)	Daily Average Ambient Temperature (°C)
1	**1st Loaded Test Day 1**	**1.3**	0.14	32.05	31.32	**31.69**	29.68
2	**1st Loaded Test Day 2**	**1.1**	0.12	33.53	32.63	**33.08**	31.68
3	**2nd Loaded Test Day 1**	**1.3**	0.14	33.26	33.00	**33.13**	31.21
4	**2nd Loaded Test Day 2**	**1.3**	0.14	34.47	33.84	**34.16**	30.89
5	**3rd Loaded Test Day 1**	**1.9**	0.21	37.16	36.68	**36.92**	32.37
6	**3rd Loaded Test Day 2**	**0.6**	0.07	26.84	26.53	**26.69**	25.47
7	**4th Loaded Test Day 1**	**1.5**	0.17	35.00	34.37	**34.69**	30.79
8	**4th Loaded Test Day 2**	**1.2**	0.13	33.95	33.21	**33.58**	31.63

Table 4.5: Parameters for calculating the efficiency of the solar dryer for each loaded test

S/N	Parameter	1st Loaded Test Day 1	1st Loaded Test Day 2	2nd Loaded Test Day 1	2nd Loaded Test Day 2	3rd Loaded Test Day 1	3rd Loaded Test Day 2	4th Loaded Test Day 1	4th Loaded Test Day 2	REFERENCE
1	η_s: Solar dryer efficiency **(%)**	73.12	77.73	82.72	45.51	50.85	57.23	44.96	66.07	Equation 3.66
2	M_w: The mass of moisture content evaporated daily **(kg)**	1.3	1.1.	1.3	1.3	1.9	0.6	1.5	1.2	Table 4.11
3	ΔT: Daily average temperature difference between chamber and ambient air **(°C)**	2.01	1.4	1.92	3.27	4.55	1.22	3.90	1.95	Table 4.11
4	$(T_{2Ave} - T_{1Ave})$**:** Daily Average difference between Outlet and Ambient Temperature **(°C)**	2.32	1.85	2.05	3.74	4.89	1.37	4.37	2.37	Table 4.6
5	Q_a = The useful heat gained by the dry air during 9 hours of daily drying **(MJ)**	4.136	3.289	3.655	6.668	8.718	2.443	7.791	4.226	Equation 3.67
6	L_v: The latent heat of vaporization **(KJ/kg)**	2313.43								Equation 3.17
7	M_g: Mass of product to be dried **(kg)**	5								Given
8	H_f: Final moisture content for safe storage of the cassava after drying **(kg)**	0.31								Equation 3.69
9	C_{pg}**:** Specific heat capacity of fresh cassava **(KJ/kgK)**	1.67								Equation 3.68
10	M_a**:** Air mass flow rate **(kg/s)**	0.0547								Equation 3.20
11	C_{pa}**:** Specific heat capacity of air **(KJ/kgK)**	1.006								Given

4.2 Discussion

Figures 4.1–4.5 shows the performance of the PVT powered dryer during the unloaded test while Figures 4.6–4.13 shows the performance of the PVT powered dryer during the loaded test. It can be seen that PV surface temperature, outlet air and drying chamber temperatures increase with increase in insolation. In general, the PV surface temperature was generally higher than the exit air and drying chamber temperature. It was observed that there were periods when the drying temperatures were slightly higher than the collector exit/outlet air temperatures at around 12:30PM from Figure 4.1 and 4.2 respectively. This trend can be attributed to the direct heating of the drying chamber by the Sun. Although ply-wood, which is an insulator, was used in constructing the drying chamber, it could not completely eliminate direct drying chamber heating by solar energy. The relative humidity as expected varied with air temperature.

Also, Tables 4.1–4.5 depict the various results recorded for the parameters as shown from Figures 4.1–4.20. These results are achieved during the performance analysis carried out for the unloaded and loaded tests.

Performance analysis carried out during the unloaded and loaded tests include;

1. Daily average values for parameters during the unloaded test
2. Results for peak periods and time of occurrence (unloaded test)
3. Performance analysis of the PVT section of the setup during unloaded test
4. Cumulative average values of parameters during unloaded test
5. Assumed and Measured values for fin efficiency and heat removal factors
6. Daily average recorded performance for all parameters (loaded test)
7. Results for peak periods and time of occurrence (loaded test)
8. Performance analysis of the PVT solar dryer during "Day 1" of 1^{st} to 4^{th} loaded tests
9. Performance analysis of the PVT solar dryer during "Day 2" of the 1^{st} to 4^{th} loaded tests
10. Moisture content removed and relative humidity during drying
11. Daily Moisture content removed during drying and corresponding daily average drying chamber temperature
12. Parameters for calculating the efficiency of the solar dryer for each loaded test

4.2.1 Daily average values for parameters during the unloaded test

Values for solar intensity are plotted on the secondary axis to the right hand side of the graph, while values for PV panel temperature, ambient/inlet temperature, outlet temperature, lower

chamber temperature and upper chamber temperature are plotted on the primary axis to the left hand side of the graph. During the five days unloaded test, a graphical presentation of the daily average reading for the various parameters indicated and their corresponding values are presented in Figure 4.14 and appendix Table B14 respectively while results obtained during peak periods are presented in Figure 4.15 and their corresponding data indicating time of occurrence are stated in appendix Table B15.

Day 4 and **Day 5** recorded the highest daily average solar intensity with an identical value of 468.42W/m^2 which was closely followed by 444.58W/m^2 recorded on **Day 1**. Also, **Day 4** recorded the highest daily average PV panel temperature of 37.68°C which was closely followed by 37.58°C recorded on **Day 1**. However, **Day 1** recorded the highest daily average ambient temperature of 33.58°C which resulted in **Day 1** having the best performance in terms of daily average outlet temperature (37.31°C), daily average lower chamber temperature (37.07°C) and daily average upper chamber temperature (37.07°C). This indicates that the drying chamber temperature profile is more dependent on the ambient air temperature than the solar intensity. Overcast weather conditions for about 7 hours out of the 9 hours of expected sunshine affected the results for **Day 2** with recorded daily average solar intensity of 214.37W/m^2, daily average ambient temperature of 28.16°C and lower and upper chamber temperature of 29.42°C and 29.53°C respectively.

Every parameter considered during the experiment had varying time intervals when they recorded their maximum value as shown in appendix Table B15. Considering the peak periods, it is evident that **Day 1** recorded the best performance in terms of every other parameter assessed apart from maximum solar intensity which **Day 4** performed better with a value of 954(W/m^2) as against 882(W/m^2) recorded for **Day 1**. This can be attributed to **Day 1** having a more consistent and sustained periods of sunshine from 10AM to 2:30PM. It was also observed that **Day 5** had better daily average results than **Day 3** for all parameters considered. However, **Day 3** recorded better results compared to those obtained for **Day 5** for all parameters considered during peak period except for solar intensity**.**

4.2.2 Performance analysis of the PVT section during unloaded test

Performance analysis of the PVT section of the setup during the five days of unloaded test was carried out. Performance analysis for the five days unloaded test is presented in Figure 4.16 while the corresponding values are tabulated in appendix Table B16. The maximum temperature difference between ambient and PV panel surface, and also, the maximum temperature difference between ambient and exit/outlet region during peak periods

for each day were recorded. Similarly, daily recorded average temperature difference between ambient and outlet temperature were recorded.

From Figure 4.16, the designed maximum temperature difference for effective daily drying between ambient and outlet temperatures was calculated as 12.3°C. However, the highest daily average temperature difference recorded during the unloaded test analysis between the ambient and outlet was 4.31°C which was recorded on **Day 4,** followed by 3.84°C recorded on **Day 1**. Also, during peak periods, the maximum temperature difference recorded between the ambient and outlet temperature was 10°C on **Day 1** followed by 8°C recorded on **Day 3** and **Day 4** respectively.

4.2.3 Results for cumulative average values for parameters used during the 5 days unloaded test

Results for cumulative average values recorded across the 5 days of the unloaded test are tabulated in Table 4.1.

The collector thermal efficiency, the fin efficiency factor and the heat removal factor are calculated by substituting these cumulative values into the relevant equations which are also stated in Table 4.1.

4.2.4 PVT collector average thermal efficiency

After 5 days of unloaded test, the thermal efficiency of the PVT collector was determined using equation (3.62) to be 48.52% as tabulated in Table 4.1. The collector thermal efficiency can however be improved by increasing the air mass flow rate required by the drying product.

From the literature reviewed so far, Tonui et al. (2014) failed to use the calculated mass flow rate of 271.780Kg/hr (0.0755Kg/s) which should have resulted to a thermal efficiency of 36.73%, rather an assumed mass flow rate of 0.12Kg/s was used, which gave a thermal efficiency of 59%. Other thermal efficiencies accounted for include Ogueke et al., 2017 (18.9%), Fudholi et al., 2011 (31%) and Fterich et al., 2015 (42.1%).

4.2.5 Assumed and Measured fin efficiency factor and heat removal factor

Measured cumulative average values for parameters used during the five days unloaded test as shown in Table 4.1 were used in calculating the fin efficiency factor and the heat removal factor using equation (3.40) and equation (3.41) respectively. The results recorded were compared with those obtained from the second iterative process given in Table 3.6 where initially assumed plate mean temperature of 50°C was considered. The assumed and measured values are compared in Table 4.2.

The measured value for the fin efficiency factor of the air flow channel was 0.49% higher than the assumed value while the assumed value for the heat removal factor was 0.09% higher that the measured value. These values as tabulated in Table 4.2 shows that results for assumed and measured values are in close agreement. This also indicates that the PVT collector configuration has a high conversion capacity of daily average PV panel temperature into useful energy gain considering the daily average outlet temperature recorded during the 5 days unloaded test.

4.2.6 Daily average values for parameters during the loaded test

Values for solar intensity, atmospheric and drying chamber relative humidity are plotted on the secondary axis to the right hand side of the graph, while values for wind speed, PV panel temperature, ambient/inlet temperature, outlet temperature, lower chamber temperature and upper chamber temperature are plotted on the primary axis to the left hand side of the graph.

Four drying samples requiring two drying days each in other to eliminate the moisture content close enough to the desired value were used during eight days of loaded test.

A scale balance was used to weigh 5kg of freshly peeled cassava which is then loaded into the drying chamber on the first day of each drying. The sample was weighed at the end of each drying day to determine the moisture content removed and then re-weighed the next day before drying commences.

The daily average reading for the various parameters indicated during the loaded test and their corresponding values are presented in Figure 4.17 and appendix Table B17 respectively while results obtained during peak periods of the loaded test are presented in Figure 4.18 and their corresponding data indicating the time of occurrence are stated in appendix Table B18.

Wind speed and relative humidity were not recorded during the first and second loaded test. However, wind speed, atmospheric relative humidity and relative humidity of the drying chamber, were recorded during the third and fourth loaded test.

From Figure 4.17 and appendix B17, the third loaded test (Day 1) recorded the best daily average performance for all results obtained apart from the daily average wind speed which has a value of 1m/s and is bettered by 1.66m/s recorded for the third loaded test (Day 2). It is also observed that the 4^{th} loaded test (Day 1) had the second best performance for all results obtained apart from the daily average wind speed were the least result of 0.67m/s was recorded. Third loaded test (Day 2) having had the best daily average wind speed performance, recorded the least results all through the loaded tests due to overcast weather conditions.

During peak periods, Figure 4.18 and appendix B18 showed that the 4th loaded test (Day 1) had the highest recorded solar intensity of 998W/m^2 which was seconded by 926W/m^2 recorded during the 3rd loaded test (Day 1). Highest PV panel surface temperature of 49°C was recorded during the 3rd loaded test (Day 1), followed by 46°C recorded during the 4th loaded test (Day 2). Ambient temperature recorded during the peak periods varied from 35°C to 38°C with the 3rd loaded test (Day 1) having the highest value of 38°C. However, the 3rd loaded test (Day 2) recorded the least ambient temperature (27°C) due to overcast weather conditions experienced all through the day. The highest outlet, lower chamber and upper chamber temperatures of 47°C, 47°C and 46°C respectively were recorded on the 3rd loaded test (Day 1) and were seconded by 43°C, 43°C and 42°C respectively recorded during the 4th loaded test (Day 1). Maximum wind speed during the peak period was 3.5m/s and was recorded during the 3rd loaded test (Day 2) which was characterised by windy and overcast weather conditions.

However, the maximum temperature difference between the PV panel and the ambient temperature was 20°C when PV panel surface temperature of 50°C was recorded relative to the ambient temperature of 30°C. This shows a higher cooling capacity compared to the one recorded by Ogueke et al., 2017 which recorded maximum temperature difference between the PV panel and the ambient temperature as 35°C when PV panel surface temperature of 65°C was recorded relative to the ambient temperature of 30°C.

4.2.7 Performance analysis of the PVT solar dryer during "Day 1" of 1st to 4th loaded tests and "Day 2" of 1st to 4th loaded tests

Performance analysis of the PVT powered dryer during "Day 1" of each loaded test (1st – 4th loaded test) is shown in Figure 4.19 with the corresponding values tabulated in appendix B19 while the performance analysis during the "Day 2" of the 1st to 4th loaded test is shown in Figure 4.20 with the corresponding values tabulated in appendix B20.

4.2.8 Moisture content removed and relative humidity during loaded test

Moisture content removed from the cassava during each loaded test is shown in table 4.3. However, performance analysis with respect to drying chamber relative humidity and atmospheric relative humidity were introduced during the 3rd (Day 1 and Day 2) and 4th (Day 1 and Day 2) loaded test. This was necessitated in other to observe whether the experiment conformed to the calculated equivalent relative humidity (ERH) of the drying product needed for optimum drying.

As observed from Table 4.3, the 3rd loaded test (Day 1) recorded the best drying day with 1.9kg of moisture removed from the cassava. This also corresponded to the lowest recorded minimum chamber relative humidity of 59.6% likewise the lowest recorded relative humidity of 63.5% from the exit of the drying chamber at the end of the drying day. It was also observed at the end of the experiment that relative humidity is heavily dependent on temperature, hence each time there is an increase in temperature, a corresponding decrease in relative humidity was observed and a decrease in temperature also leads to an increase in relative humidity. Generally, more moisture was removed at lower temperature values during the first day (Day 1) of each loaded test when compared to the second day (Day 2) of each loaded test which required higher temperatures in other to extract the remaining moisture from the product as shown in table 4.4.

The PVT powered solar dryer after 9 hours of daily drying, had moisture removal rates ranging from 0.07 – 0.21kg/hr as observed from table 4.4.

4.2.9 Solar Dryer Efficiency

The solar dryer efficiencies for all the loaded tests likewise all the parameters needed for calculating them are highlighted in Table 4.5. It is however observed that the efficiency of the solar dryer ranges from 44.96 – 82.72% for the eight days of loaded test carried out with an average drying efficiency of 62.27%. These range of values look promising compared to those recorded by by Tonui et al., 2014 (39.9% without backup heater and 57.7% with backup heater), and Ogueke et al., 2018 (72 - 79%).

CHAPTER FIVE

CONCLUSIONS AND RECOMMENDATIONS

5.1 Conclusions

The PVT powered solar dryer has been successfully designed, fabricated and its performance successfully tested during five days of unloaded test and eight days of loaded test. The introduction of a serpentine flow regime by evenly distributing curved aluminium vanes in the flow channel has shown promising results during the performance testing of the solar dryer with an average thermal efficiency of 48.52% recorded. Also, the solar dryer efficiency recorded during loaded tests ranged from 44.96% - 82.72% which corresponded to 0.6 – 1.9kg moisture content removed from the cassava during 9 hours of daily drying. The maximum solar intensity, PV panel surface temperature, drying chamber temperature and ambient air temperature recorded during the performance testing are 998W/m^2, 50°C, 49°C and 39°C respectively. The recorded drying chamber temperature of 49°C represents 89.1% of the expected optimum drying temperature of 55°C needed for effective drying. The PVT powered solar dryer, after 9 hours of daily drying, had moisture removal rates ranging from 0.07 – 0.21kg/hr. Wind speed fluctuated within the range of 0 – 3.5m/s throughout the loaded test while relative humidity showed it was entirely temperature dependent, hence increase in temperature resulted in decrease in humidity while decrease in temperature resulted in increase in humidity.

5.2 Contribution to Knowledge

This work has contributed to improving the thermal performance and also the heat recovery capacity of PVT collectors which can be put to use in various low temperature applications such as in agricultural produce drying and in space heating/cooling.

5.3 Recommendation

The following recommendations are suggested based on the findings made during the course of this work.

1. Due to the ever fluctuating nature of solar insolation all through the drying period, further work needs to be carried out in designing for a more efficient drying chamber, particularly with respect to its heat retention capability.

2. A system of heat storage can be integrated into the setup so that the PVT solar dryer can use the stored heat during periods of low solar insolation. This can also help the setup to perform on a 24 hours basis.
3. Since it has been established that PVT application in solar drying is viable and has the capacity to reduce the wastage of perishable goods due to lack of storage facilities, farmers can be encouraged to increase the production of perishable farm products such as tomatoes, cassava and potatoes, in other to maintain an all year round supply.
4. More work should be carried out on both material selection and configuration of the air flow channel as shown in this work that altering the air flow pattern can improve the thermal performance of the PVT collector.

REFERENCES

Alfegi, M.E.A., Sopian, K., & Othman, M.Y.H. (2007). Transient mathematical model of both side single pass photovoltaic thermal air collector. ARPN J Eng Applied Science, (2), 22-6. ment and performance monitoring of a photovoltaic-thermal (PVT) air collector. Renewable

Aste, N., Giancarlo, C., & Francesco V. (2008). Design, develop Energy, (33), 914–927.

Augustine, C., & Nnabuchi, M. N. (2010). Analysis of some meteorological data for some selected cities in the eastern and southern zone of Nigeria. Afr. J. Environmental Science Technology, IV(2), 92–99.

Bhattacharyya, T., Anandalakshmi, R., & Srinivasan, K. (2017). Heat Transfer Analysis on Finned Plate Air Heating Solar Collector for its Application in Paddy Drying. Energy Procedia, (109), 353 – 360.

Chappell, C., & Lebel, S. (2009). Solar drying shed for Cassava in Malawi. Mc Gill University, department of bio-resource engineering, 21111 lake shoreroad, Quebec, Canada. Design 3 BREE 495.

Chow, T .T. (2010). A review on photovoltaic/thermal hybrid solar technology. Applied Energy, (87), 367–369.

Chow, T. T., Tiwari, G. N., & Menezo, C. (2013) Hybrid Solar: A Review on Photovoltaic and Thermal Power Integration. Building Energy and Environmental Technology Research Unit, Division of Building Science and Technology. City University of Hong Kong, Tat Chee Avenue, Hong Kong. Centre for Energy Studies, Indian Institute of Technology Delhi, Hauz Khas, New Delhi 11 00 16, India.

Deepali, K., & Tiwari, G. N. (2014). Photovoltaic thermal air collectors: A review. Journal of renewable and sustainable energy, (6), 62701-21.

Dissa A.O., Bathiebo, J., Kam, S., Savadogo, P. W., Desmorieux, H., & Koulidiati, J. (2009). Modeling and experimental validation of thin layer indirect solar drying of mango slices. Renewable Energy, (34), 1000-1008.

Dupeyrat, P., Ménézo, C., & Fortuin, S. (2014). Study of the thermal and electrical performances of PVT solar hot water system. Energy and Buildings, (68), 751–755.

Fterich, M., Chouikhi, H., Elloumi, A., Bentaher, H., & Maalej, A. (2015). Performance of an agro-food solar dryer equipped with a pv/t air collector. 6th International Conference on Advances in Mechanical Engineering and Mechanics 20-22 December, 2015, Hammamet, Tunisia. https://www.researchgate.net/publication/287994757

Fudholi, A., Othman, M. Y., Ruslan, M. H., Yahya, M., Zaharim, A., and Sopian, K. (2012). Design and Testing of Solar Dryer for Drying Kinetics of Seaweed in Malaysia. Recent Researches in Geography, Geology, Energy, Environment and Biomedicine, ISBN: 978-1-61804-022-0.

Fudholi, A., Sopian, K., Mohammad H., Yazdi, M. H. R.., Ibrahim, A., and Kazem, H. A. (2014). Performance analysis of photovoltaic thermal (PVT) water collectors. Energy Conversion and Management, (78), 641–651.

Fudholi, A., Sopian, K., Ruslan, M. H., Othman, M. Y., & Yahya, M. (2011). Thermal efficiency of double pass solar collector with longitudinal fins Absorbers. American Journal of Applied Sciences, III(8), 254-260.

Gholami, H., Khalilnejad, A., & Gharehpetian, G. B. (2015). Electrothermal performance and environmental effects of optimal photovoltaic–thermal system. Energy Conversion and Management, (95), 326–333.

Hazi, A., Hazi, G., Grigore, R., & Vernica, S. (2014). Opportunity to use PVT systems for water heating in industry. Applied Thermal Engineering, (63), 151-157.

Hegazy, A. A. (2000). Comparative study of the performances of four photovoltaic/thermal solar air collectors. Energy Conversion and Management, (41), 861-881.

(https://www.fda.gov/inspection-compliance-enforcement-and-criminal-investigations/inspection-technical-guide/water-activity-aw-foods [accessed 20/07/2021])

Hussain, F., Othman, M. Y. H., Yatim, B., Ruslan, H., Sopian, K., Anuar, Z., & Khairuddin, S. (2015). An improved design of photovoltaic/thermal solar collector. Solar Energy, (122), 885–891

Ibrahim, A., Othman, M. Y., Ruslan, M. H., Sohif M., and Sopian, K. (2011). Recent advances in flat plate photovoltaic/thermal (PV/T) solar collectors. Renewable and Sustainable Energy Reviews, (15), 352–365.

Ibrahim, A., Sopian, K., & Daud, W. R. (2009). Study of the drying kinetics of lemon grass. American Journal Of Applied Sciences, (6), 1070-1075.

Jee, J. M., Iniyan, S., & Suganthi, L. (2015). Simulation of the temperature distribution inside a solar photovoltaic thermal collector. Third Southern African Solar Energy Conference.

Jin, G. L., Ibrahim, A., Yee, K. C., & Roonak, D. (2010). Evaluation of a single-pass Photovoltaic-Thermal air collector with a rectangular tunnel absorber. America journal of applied sciences, II(7). DOI: 10.3844/ajassp.2010.277.282

John, H. H. (1984). Solar Absorptance and thermal Emittance of some common spacecraft thermal control coating. NASA reference publication 1121, https://ntrs.nasa.gov.

José T. V., Timo, L., & Kai, S. (2014). Multi-objective optimization of hybrid photovoltaic–thermal collectors integrated in a DHW heating system. Energy and Buildings, (74), 78–90.

Karan, P. (2015). Solar Photovoltaics & Thermal - Hybrid System. DOI: 10.13140/RG.2.1.1435.3443, 3-4.

Kasaeian A. B., Dehghani, M., Golzari, S., & Akhlaghi, M. M. (2013). Energy and Exergy Analysis of Air PV/T Collector of Forced Convection with and without Glass Cover. International Journal of Engineering Journal, (26), 913-926.

Koech, R. K., Ondieki, H. O., Tonui, J. K., & Rotich, S. K. (2012). A steady state thermal model for photovoltaic/thermal (pv/t) system under various conditions. International journal of scientific & technology research, (1), 1-5.

Luuk, V. (2014). Technical and economic evaluation of different utilization options based on combined photovoltaic and solar thermal (PV/T) systems for the residential sector. Utrecht University Master Thesis, Nanosol project.

Mei, L., Infield, D., Eicker, U., Fox, V. (2003). Thermal modelling of a building with an integrated ventilated PV façade. Energy and buildings, (35), 605-17.

Nalis, A. (2012). Quasi-dynamic characterization of hybrid photovoltaic/thermal (pv/t) flat-plate collectors. http://hdl.handle.net/10803/84100

Nayeem-Ur-Rahman, C. (2013). Technical and economic analysis of a novel asymmetric PVT hybrid solar collector. Universitat Politecnica de Catalunya Industrial.

Ogueke, N. V., & Anyanwu, E. E. (2017). Review of photovoltaic-thermal collectors: an overview of the potential beyond experimental testing. International Journal of Energy for a Clean Environment, III(18), 243–273.

Ogueke, N. V., Njokuocha, U. J., & Anyanwu, E. E. (2017). Design and measured performance of a photovoltaic thermal collector-powered dryer. International Journal of Energy for a Clean Environment, II(18), 123–131.

Okorafor, O. O., Akinbile, C. O., & Adebayo, A. J. (2018). Determination of soil erodibility factor (k) for selected sites in Imo State, Nigeria. Resources and environmental, 8), 6-13.

Payman, S., Yahya, A., Shamsollah, A., & Hossein, B. (2016). A comparison among different parameters for the design of a photovoltaic/thermal system using computational fluid dynamics. Engineering, Technology & Applied Science Research, (6), 1119-1123.

Pottler, K., Sippel, C. M., & Beck A. (1999). Optimized finned absorber geometries for solar air heating collector. Solar Energy, (67), 35–52.

Saffa, B., Riffat & Erdem, C. (2011). A review on hybrid photovoltaic/thermal collectors and systems. International Journal of Low-Carbon Technologies, (6), 212–241.

Sajith, K. G., & Muraleedharan, C. (2013). A study on drying of amla using a hybrid solar dryer. International journal of innovative research in Science, Engineering and Technology, (2), 794-799.

Sajith, K. G., & Muraleedharan, C. (2014). Economic analysis of a hybrid photovoltaic thermal solar dryer for drying Amla. International journal of innovative research in Science, Engineering and Technology, (3), 907-910.

Santberg, R., & Van Zalingen, R. J. C. (2007). The absorption factor of crystalline PV cells: A numerical and experimental study. Solar Energy materials and Solar Cells https://doi:10.1016/j.solmat.2007.10.005

Simo-Tagne, M., Tagne, A. T., Ndukwe, M. C., Bennamoun, L., Akong, M. B. O., El-Marouni, M., Rogaume, Y. (2021). Numerical study of the drying of cassava roots chips using indirect solar dryer in natural convection. Agri Engineering https://doi.org/10.3390/agriengineering 2010009.

Solanki, S. C., Dubey, S., & Tiwari, A. (2009). Indoor simulation and testing of photovoltaic thermal (PV/T) air collectors. Applied Energy, (86), 2421–8.

Sopian ,K., Yigit, K. S., Liu, H. Y., Kakac, S., & Veziroglu, T. N. (1996). Performance analysis of photovoltaic thermal air heaters. Energy Conversion Management, XI(37), 1657–70.

Sopian, K., Liu, H. Y., Kakac, S., & Veziroglu, T. N. (2000). Performance of a double pass photovoltaic thermal solar collector suitable for solar drying systems. Energy Conversion Management, (41), 353–65.

Tonui, K. S., Mutai, E. B. K., Mutuli, D. A., Mbuge, D. O., & Too, K. V. (2014). Design and Evaluation of Solar Grain Dryer with a Back-up Heater. Research Journal of Applied Sciences, Engineering and Technology,VII(15), 3036-3043.

Tyagi, V. V., Kaushik, S. C., & Tyagi, S. K. (2012). Advancement in solar photovoltaic/thermal (PV/T) hybrid collector technology: A Review. Sustainable Energy Rev. (16), 1384–1398.

US Department of Energy (2010). Solar energy technologies: Space heating. OpenEI, National Renewable Energy Laboratory.

Uzma, Q., Prashant, B., & Anil, K. (2014). Effect of operating parameters on the performance of the hybrid solar pvt collector under different weather condition. International Journal of Science, Environment and Technology, III(4), 1563 – 1570.

Zondag, H. A. (2008). Flat-plate PV-Thermal collectors and systems: A review. Renewable and Sustainable Energy Reviews, (12), 891–959.

Zondag, H. A., De Vries, D. W., Van Helden, W. G. J., Van Zolingen, R. J. C., & Van Steenhoven, A. A. (2003). The yield of combined PV-thermal collector designs. Solar energy (74), 253-269.

APPENDIX A

THE PVT POWERED DRYER DURING OPERATION

Plate A1: Side view of the PVT powered solar dryer at the test location

Plate A2: Loaded sample at the end of a drying day

Plate A3: Dried cassava at the end of a drying day

Plate A4: Freshly peeled cassava being weighed before commencing drying

Plate A5: Configuration of the flow channel before installing the PV panel

Plate A6: Location of air entrance into the drying chamber

APPENDIX B

TABLE OF VALUES FOR ALL PARAMETERS USED IN GRAPHICAL ANALYSIS

TABLES FOR UNLOADED TEST:

TABLE B1: 1ST DAY UNLOADED TEST

S/N	TIME	SOLAR INTENSITY (W/m^2)	PV PANEL SURFACE TEMP (°C)	AMBIENT/INLET TEMP (°C)	OUTLET TEMP (°C)	LOWER CHAMBER TEMP (°C)	UPPER CHAMBER TEMP (°C)
1	8AM	210	26	25	25	25	25
2	8:30AM	230	27	25	26	26	26
3	9AM	329	29	26	28	27	27
4	9:30AM	353	31	29	30	30	29
5	10AM	581	33	31	33	32	33
6	10:30AM	882	40	34	38	38	37
7	11AM	650	37	34	37	37	36
8	11:30AM	459	38	35	38	37	37
9	12NOON	441	38	36	39	38	38
10	12:30PM	556	47	36	44	45	45
11	1PM	606	49	38	46	46	47
12	1:30PM	831	50	39	49	49	49
13	2PM	780	45	39	49	49	49
14	2:30PM	401	40	37	42	42	42
15	3PM	284	39	38	40	40	40
16	3:30PM	313	40	34	38	38	39
17	4PM	143	35	34	37	37	37
18	4:30PM	249	35	32	34	34	34
19	5PM	149	35	32	34	34	34

TABLE B2: 2ND UNLOADED TEST

S/N	TIME	SOLAR INTENSITY (W/m^2)	PV PANEL SURFACE TEMP (°C)	AMBIENT/INLET TEMP (°C)	OUTLET TEMP (°C)	LOWER CHAMBER TEMP (°C)	UPPER CHAMBER TEMP (°C)
1	8AM	99	27	25	26	26	25
2	8:30AM	121	28	26	27	26	25
3	9AM	160	29	27	28	27	27
4	9:30AM	184	30	29	30	29	29
5	10AM	289	33	30	31	31	31
6	10:30AM	559	37	31	33	34	34
7	11AM	741	41	34	35	36	36
8	11:30AM	738	36	34	34	33	34
9	12NOON	768	40	37	40	41	40
10	12:30PM	81	34	32	35	36	36
11	1PM	172	31	30	32	32	33
12	1:30PM	99	34	31	33	34	34
13	2PM	12	28	27	28	28	29
14	2:30PM	26	26	25	26	26	26
15	3PM	12	26	24	25	25	25
16	3:30PM	1	25	23	25	25	25
17	4PM	4	25	24	24	24	24
18	4:30PM	4	24	23	24	23	24
19	5PM	3	24	23	23	23	24

TABLE B3: 3RD DAY UNLOADED TEST

S/N	TIME	SOLAR INTENSITY (W/m^2)	PV PANEL SURFACE TEMP (°C)	AMBIENT/INLET TEMP (°C)	OUTLET TEMP (°C)	LOWER CHAMBER TEMP (°C)	UPPER CHAMBER TEMP (°C)
1	8AM	97	24	23	24	24	24
2	8:30AM	127	25	23	24	24	24
3	9AM	187	27	24	26	25	25
4	9:30AM	216	28	25	27	26	26
5	10AM	272	28	26	29	28	28
6	10:30AM	317	31	28	31	30	30
7	11AM	789	34	31	33	32	32
8	11:30AM	753	39	34	36	36	36
9	12NOON	630	37	31	37	37	37
10	12:30PM	772	39	34	38	38	39
11	1PM	625	40	34	40	40	39
12	1:30PM	568	37	33	39	39	38
13	2PM	718	43	38	46	45	44
14	2:30PM	306	37	35	42	40	41
15	3PM	661	43	33	38	38	38
16	3:30PM	132	38	32	40	40	41
17	4PM	120	29	27	29	30	31
18	4:30PM	91	28	26	27	27	28
19	5PM	113	27	26	27	27	27

TABLE B4: 4TH DAY UNLOADED TEST

S/N	TIME	SOLAR INTENSITY (W/m^2)	PV PANEL SURFACE TEMP (°C)	AMBIENT/INLET TEMP (°C)	OUTLET TEMP (°C)	LOWER CHAMBER TEMP (°C)	UPPER CHAMBER TEMP (°C)
1	8AM	142	25	23	24	24	24
2	8:30AM	297	27	25	26	26	26
3	9AM	314	28	25	27	26	26
4	9:30AM	302	30	27	30	29	29
5	10AM	361	30	29	32	31	31
6	10:30AM	394	35	31	34	34	34
7	11AM	804	40	33	36	38	38
8	11:30AM	842	45	34	38	40	40
9	12NOON	88	46	33	39	40	41
10	12:30PM	954	48	34	42	43	43
11	1PM	916	43	34	39	39	39
12	1:30PM	816	46	39	46	47	47
13	2PM	798	44	39	47	47	47
14	2:30PM	258	40	37	43	43	44
15	3PM	469	41	34	39	39	38
16	3:30PM	244	36	34	36	35	35
17	4PM	448	39	32	36	35	35
18	4:30PM	309	38	32	38	37	38
19	5PM	144	35	32	37	37	37

TABLE B5: 5TH DAY UNLOADED TEST

S/N	TIME	SOLAR INTENSITY (W/m^2)	PV PANEL SURFACE TEMP (°C)	AMBIENT/INLET TEMP (°C)	OUTLET TEMP (°C)	LOWER CHAMBER TEMP (°C)	UPPER CHAMBER TEMP (°C)
1	8AM	130	25	23	24	24	24
2	8:30AM	198	26	25	26	26	26
3	9AM	202	27	26	27	27	26
4	9:30AM	312	31	29	30	29	29
5	10AM	502	33	30	32	32	32
6	10:30AM	731	37	34	36	36	36
7	11AM	801	39	34	38	38	39
8	11:30AM	824	39	31	37	38	38
9	12NOON	363	34	31	37	37	37
10	12:30PM	776	40	34	37	37	37
11	1PM	192	34	31	37	38	38
12	1:30PM	704	37	33	34	34	34
13	2PM	675	38	33	38	38	39
14	2:30PM	688	34	33	36	37	38
15	3PM	313	38	33	38	38	38
16	3:30PM	490	39	32	36	36	37
17	4PM	400	37	34	37	37	37
18	4:30PM	308	37	30	35	35	35
19	5PM	291	36	31	35	35	35

TABLE FOR LOADED TEST:

TABLE B6: 1ST LOADED TEST: DAY 1

S/N	TIME	SOLAR INTENSITY (W/m^2)	PV PANEL SURFACE TEMP (°C)	AMBIENT/INLET TEMP (°C)	OUTLET TEMP (°C)	LOWER CHAMBER TEMP (°C)	UPPER CHAMBER TEMP (°C)
1	8AM	194	26	25	24	24	24
2	8:30AM	282	27	28	27	27	27
3	9AM	493	30	28	29	29	29
4	9:30AM	575	32	31	31	32	32
5	10AM	578	35	31	33	33	33
6	10:30AM	655	35	32	34	33	33
7	11AM	661	33	31	34	34	32
8	11:30AM	446	34	32	35	35	33
9	12NOON	328	37	31	37	37	35
10	12:30PM	719	38	34	38	38	36
11	1PM	702	40	34	39	40	38
12	1:30PM	704	42	34	41	41	41
13	2PM	321	40	36	39	40	38
14	2:30PM	31	33	33	35	35	34
15	3PM	64	29	28	30	29	29
16	3:30PM	51	26	25	26	26	26
17	4PM	121	27	25	27	27	26
18	4:30PM	11	24	23	25	25	25
19	5PM	8	24	23	24	24	24

TABLE B7: 1ST LOADED TEST: DAY 2

S/N	TIME	SOLAR INTENSITY (W/m^2)	PV PANEL SURFACE TEMP (°C)	AMBIENT/INLET TEMP (°C)	OUTLET TEMP (°C)	LOWER CHAMBER TEMP (°C)	UPPER CHAMBER TEMP (°C)
1	8AM	161	26	23	24	23	23
2	8:30AM	184	27	25	26	26	25
3	9AM	238	27	26	27	27	27
4	9:30AM	536	32	29	30	30	29
5	10AM	304	32	33	32	32	31
6	10:30AM	795	33	33	33	33	31
7	11AM	746	36	34	34	35	34
8	11:30AM	738	43	35	40	40	39
9	12NOON	168	39	33	37	37	36
10	12:30PM	692	35	34	34	33	32
11	1PM	209	34	32	34	35	34
12	1:30PM	626	41	34	38	37	36
13	2PM	465	38	34	36	36	35
14	2:30PM	391	39	34	37	37	36
15	3PM	482	37	33	35	36	34
16	3:30PM	452	36	32	35	36	34
17	4PM	163	35	33	37	37	37
18	4:30PM	351	34	33	34	34	34
19	5PM	172	33	32	34	33	33

TABLE B8: 2ND LOADED TEST: DAY 1

S/N	TIME	SOLAR INTENSITY (W/m^2)	PV PANEL SURFACE TEMP (°C)	AMBIENT/INLET TEMP (°C)	OUTLET TEMP (°C)	LOWER CHAMBER TEMP (°C)	UPPER CHAMBER TEMP (°C)
1	8AM	141	27	26	27	27	26
2	8:30AM	201	29	27	28	28	28
3	9AM	338	30	28	29	28	27
4	9:30AM	482	31	29	30	30	29
5	10AM	541	33	30	32	33	30
6	10:30AM	562	33	31	32	32	31
7	11AM	758	35	35	34	35	34
8	11:30AM	505	38	33	37	38	36
9	12NOON	416	37	36	39	40	38
10	12:30PM	548	38	34	38	38	35
11	1PM	296	36	33	37	36	34
12	1:30PM	286	35	33	36	35	32
13	2PM	155	33	32	33	33	32
14	2:30PM	623	40	32	34	33	30
15	3PM	444	41	33	39	39	36
16	3:30PM	139	33	32	35	35	33
17	4PM	191	34	31	32	31	29
18	4:30PM	113	31	29	30	31	29
19	5PM	35	30	28	30	30	29

TABLE B9: 2ND LOADED TEST: DAY 2

S/N	TIME	SOLAR INTENSITY (W/m^2)	PV PANEL SURFACE TEMP (°C)	AMBIENT/INLET TEMP (°C)	OUTLET TEMP (°C)	LOWER CHAMBER TEMP (°C)	UPPER CHAMBER TEMP (°C)
1	8AM	181	26	22	23	23	23
2	8:30AM	148	26	23	26	25	25
3	9AM	201	27	26	27	26	26
4	9:30AM	563	30	27	30	30	29
5	10AM	670	38	29	35	34	33
6	10:30AM	779	42	32	39	38	37
7	11AM	824	43	33	40	40	39
8	11:30AM	492	39	33	38	39	39
9	12NOON	800	40	32	38	38	38
10	12:30PM	834	44	34	42	42	40
11	1PM	193	36	34	37	38	37
12	1:30PM	811	41	36	39	39	38
13	2PM	206	39	35	39	40	38
14	2:30PM	270	35	34	37	37	36
15	3PM	178	34	31	34	34	34
16	3:30PM	510	37	33	35	34	34
17	4PM	165	34	33	35	35	34
18	4:30PM	115	32	31	33	32	32
19	5PM	245	33	29	31	31	31

TABLE B10: 3RD LOADED TEST: DAY 1

S/N	TIME	SOLAR INTENSITY (W/m^2)	PV PANEL SURFACE TEMP (°C)	AMBIENT/INLET TEMP (°C)	OUTLET TEMP (°C)	LOWER CHAMBER TEMP (°C)	UPPER CHAMBER TEMP (°C)	WIND SPEED (m/s)	CHAMBER RELATIVE HUMIDITY (%)	ATM RELATIVE HUMIDITY (%)
1	8AM	197	27	24	25	25	25	0.4	87.7	86.5
2	8:30AM	242	29	25	26	25	25	0	83.3	83.1
3	9AM	321	31	27	29	28	27	0.2	79.2	78
4	9:30AM	621	34	29	32	32	31	0.1	75.5	71.6
5	10AM	516	33	30	32	32	31	0.6	71.2	69.8
6	10:30AM	776	40	32	37	36	35	0.5	69.4	68.1
7	11AM	911	42	33	40	39	38	1	66.5	65.9
8	11:30AM	861	44	34	41	41	40	1.3	65.9	64.7
9	12NOON	893	46	34	43	43	42	2.5	63.7	64.3
10	12:30PM	890	47	35	43	43	43	2.1	63.1	63.2
11	1PM	885	47	38	44	44	44	0.7	62.6	63
12	1:30PM	926	49	37	47	47	46	2.3	60.3	61.3
13	2PM	280	41	34	41	43	43	1.6	66.1	67.4
14	2:30PM	286	41	34	40	40	40	2.1	65.5	67.9
15	3PM	528	41	34	40	40	40	1.7	63.1	65.1
16	3:30PM	470	39	35	38	38	38	0.3	61.9	64.7
17	4PM	382	37	33	37	37	37	0.3	60.2	63.5
18	4:30PM	361	38	33	37	37	36	0.6	59.6	63.1
19	5PM	178	36	34	36	36	36	0.7	63.5	66.8

TABLE B11: 3RD LOADED TEST: DAY 2

S/N	TIME	SOLAR INTENSITY (W/m^2)	PV PANEL SURFACE TEMP (°C)	AMBIENT/INLET TEMP (°C)	OUTLET TEMP (°C)	LOWER CHAMBER TEMP (°C)	UPPER CHAMBER TEMP (°C)	WIND SPEED (m/s)	CHAMBER RELATIVE HUMIDITY (%)	ATM RELATIVE HUMIDITY (%)
1	8AM	97	25	23	24	24	24	1.3	88.8	89.8
2	8:30AM	102	26	24	25	25	25	0.5	88.4	89.6
3	9AM	108	26	25	25	25	25	1.1	87.5	88.8
4	9:30AM	121	27	25	26	26	25	1.1	87.1	87.9
5	10AM	141	27	25	26	26	26	1	86.8	87.7
6	10:30AM	188	28	26	27	27	26	1.4	86.4	87.1
7	11AM	201	28	26	27	27	27	2.8	87.1	87
8	11:30AM	230	28	26	28	28	28	1.7	86.5	86.8
9	12NOON	272	30	27	29	29	28	1.5	85.1	85.7
10	12:30PM	168	29	26	27	27	27	1.8	85.9	86
11	1PM	325	31	26	29	29	29	3.5	81.9	84.2
12	1:30PM	298	29	26	28	28	27	2.4	81.3	84.4
13	2PM	208	28	26	27	27	26	2.1	79.8	82.6
14	2:30PM	269	28	26	27	27	26	2.3	80.5	82.1
15	3PM	300	29	26	28	28	28	2	79.9	80.6
16	3:30PM	225	28	26	27	27	27	1.3	78	80.3
17	4PM	202	28	25	27	27	27	1	80.4	81.4
18	4:30PM	168	27	25	27	27	27	1.8	79.5	82.6
19	5PM	122	26	25	26	26	26	1	81.3	84.2

TABLE B12: 4TH LOADED TEST: DAY 1

S/N	TIME	SOLAR INTENSITY (W/m^2)	PV PANEL SURFACE TEMP (°C)	AMBIENT/INLET TEMP (°C)	OUTLET TEMP (°C)	LOWER CHAMBER TEMP (°C)	UPPER CHAMBER TEMP (°C)	WIND SPEED (m/s)	CHAMBER RELATIVE HUMIDITY (%)	ATM RELATIVE HUMIDITY (%)
1	8AM	201	27	24	25	25	25	0.5	87.7	85.8
2	8:30AM	265	28	24	26	25	25	0.5	84.6	81.6
3	9AM	336	30	26	28	28	27	0.3	80.7	79.8
4	9:30AM	302	30	27	29	29	28	0	83	82.4
5	10AM	507	34	29	33	33	31	0.6	81.4	77.5
6	10:30AM	883	40	32	38	37	36	0	76.7	76.2
7	11AM	351	36	32	36	36	36	1.1	73.4	76
8	11:30AM	696	42	34	39	39	37	0.7	73.6	71.1
9	12NOON	998	43	34	41	41	40	1.7	68.4	68
10	12:30PM	420	42	37	40	40	40	0.9	66.2	67.2
11	1PM	968	45	37	43	43	42	0.3	64.6	65
12	1:30PM	667	40	33	38	38	37	1.3	65.5	66.3
13	2PM	575	40	34	39	38	38	0	65.1	65.3
14	2:30PM	684	42	33	40	40	39	0.9	66.6	64.3
15	3PM	589	39	31	38	38	38	1.3	68.8	65.5
16	3:30PM	431	36	29	36	36	35	0.5	69.5	66.4
17	4PM	303	35	30	33	33	33	0.4	70.6	69.4
18	4:30PM	389	35	29	33	33	33	1.6	69	59.5
19	5PM	312	35	30	33	33	33	0.2	67.2	64.3

TABLE B13: 4TH LOADED TEST: DAY 2

S/N	TIME	SOLAR INTENSITY (W/m^2)	PV PANEL SURFACE TEMP (°C)	AMBIENT/INLET TEMP (°C)	OUTLET TEMP (°C)	LOWER CHAMBER TEMP (°C)	UPPER CHAMBER TEMP (°C)	WIND SPEED (m/s)	CHAMBER RELATIVE HUMIDITY (%)	ATM RELATIVE HUMIDITY (%)
1	8AM	109	26	25	25	25	25	0.7	87.8	88.7
2	8:30AM	181	28	27	27	26	26	0.9	86.8	88.6
3	9AM	629	32	31	29	29	29	1.1	79	80.3
4	9:30AM	290	31	28	30	30	29	1.6	79	79.9
5	10AM	201	34	30	32	31	30	1.5	78.2	78.7
6	10:30AM	293	33	30	31	32	31	1.1	77.1	75.6
7	11AM	192	31	30	30	30	29	1.8	78.1	76
8	11:30AM	181	31	28	30	30	30	1.1	79.2	76.1
9	12NOON	843	45	36	38	38	37	0.4	68.3	71.7
10	12:30PM	225	34	32	34	34	33	1.8	73.3	73.4
11	1PM	905	45	34	40	41	39	1.9	67.7	68.5
12	1:30PM	861	43	36	41	41	39	2.4	62	68.2
13	2PM	813	44	37	42	42	42	1.6	60.5	63.5
14	2:30PM	796	44	33	41	40	40	0.3	62	63.1
15	3PM	765	46	36	41	41	40	1.8	61.8	63.2
16	3:30PM	216	36	35	37	37	36	0.7	64.7	65.3
17	4PM	160	34	32	34	34	34	1.7	69.8	70.4
18	4:30PM	65	32	31	33	33	32	0.7	70.1	71.1
19	5PM	57	30	30	32	32	31	1.2	71.3	71.3

TABLE B14: Daily average recorded performance for all parameters (unloaded test)

S/N	DAYS	Daily Average Solar Intensity (W/m^2)	Daily Average PV Panel Temperature (°C)	Daily Average Ambient Temperature (°C)	Daily Average Outlet Temperature (°C)	Daily Average Lower Chamber Temperature (°C)	Daily Average Upper Chamber Temperature (°C)
1	**Day 1**	444.58	37.58	33.37	37.21	37.07	37.07
2	**Day 2**	214.37	32.21	28.16	29.42	29.42	29.53
3	**Day 3**	394.42	33.37	29.63	33.32	32.95	33.05
4	**Day 4**	468.42	37.68	31.95	36.26	36.32	36.42
5	**Day 5**	468.42	34.79	30.89	34.21	34.32	34.47

TABLE B15: Results for peak periods and time of occurrence (unloaded test)

S/N	DAYS	Maximum Solar Intensity (W/m^2)	Maximum PV Panel Temperature (°C)	Maximum Ambient Temperature (°C)	Maximum Outlet Temperature (°C)	Maximum Lower Chamber Temperature (°C)	Maximum Upper Chamber Temperature (°C)
1	**Day 1**	**882** 10:30AM	**50** 1:30PM	**39** 1:30PM &2PM	**49** 1:30PM	**49** 1:30PM	**49** 1:30PM
2	**Day 2**	**768** 12NOON	**41** 11AM	**37** 12NOON	**40** 12NOON	**41** 12NOON	**40** 12NOON
3	**Day 3**	**789** 11AM	**43** 2PM & 3PM	**38** 2PM	**46** 2PM	**45** 2PM	**44** 2PM
4	**Day 4**	**954** 12:30PM	**48** 12:30PM	**39** 1:30PM & 2PM	**47** 2PM	**47** 1:30PM & 2PM	**47** 1:30PM & 2PM
5	**Day 5**	**824** 11:30AM	**40** 12:30PM	**34** 10:30AM, 11AM, 12:30PM &4PM	**38** 11AM, 2PM & 3PM	**38** 11AM, 11:30AM, 1PM & 2PM	**39** 11AM & 2PM

TABLE B16: Performance analysis of the PVT section of the setup during unloaded test

S/N	PERFORMANCE ANALYSIS	**DAY1**	**DAY 2**	**DAY 3**	**DAY 4**	**DAY 5**
1	Maximum difference between ambient and PV panel surface temperature (peak period)	**11° C** 1:30PM, 2PM Corresponding temps of 39°C and 50° C respectively	**7° C** 11AM Corresponding temps of 34°C and 41° C respectively	**10° C** 2PM Corresponding temps of 33°C and 43° C respectively	**14° C** 12:30PM Corresponding temps of 34°C and 48° C respectively	**8° C** 11:30AM Corresponding temps of 31°C and 39° C respectively
2	From design: Maximum difference for effective daily drying between ambient and outlet temperature	**12.3° C** Steady difference maintained from 8AM to 5PM daily.	**12.3° C** Steady difference maintained from 8AM to 5PM daily.	**12.3° C** Steady difference maintained from 8AM to 5PM daily.	**12.3° C** Steady difference maintained from 8AM to 5PM daily.	**12.3° C** Steady difference maintained from 8AM to 5PM daily.
3	Maximum difference between ambient and outlet temperature (peak period)	**10° C** 1:30PM, 2PM Corresponding temps of 39°C and 49° C respectively	**3° C** 1 2PM, 12:30PM Corresponding temps of 37°C and 40° C at 12PM and 32°C and 35° C at 12:30PM	**8° C** 2PM Corresponding temps of 38°C and 46° C respectively	**8° C** 2PM Corresponding temps of 39°C and 47° C respectively	**6° C** 11:30AM, 12PM, 1PM Corresponding temps of 31°C and 37° C respectively
4	Recorded daily average temperature difference between ambient and outlet temperature	**3.84° C** 8AM-5PM From Table 4.1	**1.26° C** 8AM-5PM From Table 4.1	**3.69° C** 8AM-5PM From Table 4.1	**4.31° C** 8AM-5PM From Table 4.1	**3.32° C** 8AM-5PM From Table 4.1

TABLE B17: Daily average recorded performance for all parameters (loaded test)

S/N	DAYS	Daily Average Solar Intensity (W/m^2)	Daily Average PV Panel Temperature (°C)	Daily Average Ambient Temperature (°C)	Daily Average Outlet Temperature (°C)	Daily Average Lower Chamber Temperature (°C)	Daily Average Upper Chamber Temperature (°C)	Daily average wind speed (m/s)
1	**1st Loaded Test Day 1**	365.47	32.21	29.68	32.00	32.05	31.32	__
2	**1st Loaded Test Day 2**	414.37	34.58	31.68	33.53	33.53	32.63	__
3	**2nd Loaded Test Day 1**	356.53	33.89	31.21	33.26	33.26	33.00	__
4	**2nd Loaded Test Day 2**	433.63	35.58	30.89	34.63	34.47	33.84	__
5	**3rd Loaded Test Day 1**	553.89	39.05	32.37	37.27	37.16	36.68	1
6	**3rd Loaded Test Day 2**	197.11	27.79	25.47	26.84	26.84	26.53	1.66
7	**4th Loaded Test Day 1**	519.84	36.79	30.79	35.16	35.00	34.37	0.67
8	**4th Loaded Test Day 2**	409.58	35.74	31.63	34.00	33.95	33.21	1.28

TABLE B18: Results for peak periods and time of occurrence (loaded test)

S/N	DAYS	Maximum Solar Intensity (W/m^2)	Maximum PV Panel Temperature (°C)	Maximum Ambient Temperature (°C)	Maximum Outlet Temperature (°C)	Maximum Lower Chamber Temperature (°C)	Maximum Upper Chamber Temperature (°C)	Maximum recorded wind speed (m/s)
1	**1st Loaded Test**	**719**	**42**	**36**	**41**	**41**	**41**	**--**
	Day 1	12:30PM	1:30PM	2PM	1:30PM	1:30PM	1:30PM	
2	**1st Loaded Test**	**795**	**43**	**35**	**40**	**40**	**39**	**--**
	Day 2	10:30AM	11:30AM	11:30AM	11:30AM	11:30AM	11:30AM	
3	**2nd Loaded Test**	**758**	**41**	**36**	**39**	**40**	**38**	**--**
	Day 1	11AM	3PM	12PM	12PM, 3PM	12PM	12PM	
4	**2nd Loaded Test**	**834**	**44**	**36**	**42**	**42**	**40**	**--**
	Day 2	12:30PM	12:30PM	1:30PM	12:30PM	12:30PM	12:30PM	
5	**3rd Loaded Test**	**926**	**49**	**38**	**47**	**47**	**46**	**2.5**
	Day 1	1:30PM	1:30PM	1PM	1:30PM	1:30PM	1:30PM	12PM
6	**3rd Loaded Test**	**325**	**31**	**27**	**29**	**29**	**29**	**3.5**
	Day 2	1PM	1PM	12PM	12PM, 1PM	1PM	1PM	1PM
7	**4th Loaded Test**	**998**	**45**	**37**	**43**	**43**	**42**	**1.7**
	Day 1	12PM	1PM	12:30PM, 1PM	1PM	1PM	1PM	12PM
8	**4th Loaded Test**	**905**	**46**	**37**	**42**	**42**	**42**	**2.4**
	Day 2	1PM	3PM	2PM	2PM	2PM	2PM	1:30PM

TABLE B19: Performance analysis of the PVT solar dryer during "Day 1" of 1st to 4th loaded tests

S/N	PERFORMANCE ANALYSIS	1st Loaded Test DAY1	2nd Loaded Test DAY 1	3rd Loaded Test DAY 1	4th Loaded Test DAY 1
1	Maximum difference between ambient and PV panel surface temperature (peak period)	**8°C** 1:30PM Corresponding temps of 34°C and 42°C respectively	**8°C** 2:30PM Corresponding temps of 32°C and 40°C respectively	**12°C** 12PM, 12:30PM, 1:30PM Corresponding temps of 34°C and 46°C, 35°C and 47°C, 37°C and 49°C respectively.	**9°C** 12PM, 2:30PM Corresponding temps of 34°C and 43°C, 33°C and 42°C respectively.
2	From design: Maximum difference for effective daily drying between ambient and outlet temperature	**12.3°C** Steady difference maintained from 8AM to 5PM daily.	**12.3°C** Steady difference maintained from 8AM to 5PM daily.	**12.3°C** Steady difference maintained from 8AM to 5PM daily.	**12.3°C** Steady difference maintained from 8AM to 5PM daily.
3	Maximum difference between ambient and outlet temperature (peak period)	**7°C** 1:30PM Corresponding temps of 34°C and 41°C respectively	**6°C** 3PM Corresponding temps of 33°C and 39°C at 12PM and 32°C and 35° C at 12:30PM	**10°C** 1:30PM Corresponding temps of 37°C and 47°C respectively	**7°C** 12PM, 2:30PM, 3PM, 3:30PM Corresponding temps of 34°C and 41°C, 33°C and 40°C, 31°C and 48°C, 29°C and 36° C respectively
4	Maximum difference between ambient and lower chamber temperature (peak period)	**7°C** 1:30PM Corresponding temps of 34°C and 41°C respectively	**6°C** 3PM Corresponding temps of 33°C and 39°C respectively.	**10°C** 1:30PM Corresponding temps of 37°C and 47°C respectively	**7°C** 12PM, 2:30PM, 3PM, 3:30PM Corresponding temps of 34°C and 41°C, 33°C and 40°C, 31°C and 48°C, 29°C and 36° C respectively
5	Maximum difference between ambient and upper chamber temperature (peak period)	**7°C** 1:30PM Corresponding temps of 34°C and 41°C respectively	**3°C** 11:30AM, 3PM Corresponding temps of 33°C and 36°C respectively	**9°C** 1:30PM Corresponding temps of 37°C and 46°C respectively	**7°C** 3PM Corresponding temps of 31°C and 38°C, respectively

6	Recorded daily average temperature difference between ambient and outlet temperature	**2.32°C** 8AM-5PM From Table 4.6	**2.05°C** 8AM-5PM From Table 4.6	**4.89°C** 8AM-5PM From Table 4.6	**4.37°C** 8AM-5PM From Table 4.6
7	Recorded daily average temperature difference between ambient and lower chamber temperature	**2.37°C** 8AM-5PM From Table 4.6	**2.05°C** 8AM-5PM From Table 4.6	**4.79°C** 8AM-5PM From Table 4.6	**4.21°C** 8AM-5PM From Table 4.6
8	Recorded daily average temperature difference between ambient and upper chamber temperature	**1.64°C** 8AM-5PM From Table 4.6	**1.79°C** 8AM-5PM From Table 4.6	**4.31°C** 8AM-5PM From Table 4.6	**3.58°C** 8AM-5PM From Table 4.6

TABLE B20: Performance analysis of the PVT solar dryer during "Day 2" of the 1st to 4th loaded tests

S/N	PERFORMANCE ANALYSIS	1st Loaded Test DAY 2	2nd Loaded Test DAY 2	3rd Loaded Test DAY 2	4th Loaded Test DAY 2
1	Maximum difference between ambient and PV panel surface temperature (peak period)	**8°C** 11:30AM Corresponding temps of 35°C and 43°C respectively	**10°C** 10:30AM, 11AM, 12:30PM Corresponding temps of 32°C and 42°C, 33°C and 43°C, 34°C and 44°C respectively	**5°C** 1PM Corresponding temps of 26°C and 31°C respectively.	**11°C** 1PM Corresponding temps of 34°C and 45°C respectively.
2	From design: Maximum difference for effective daily drying between ambient and outlet temperature	**12.3°C** Steady difference maintained from 8AM to 5PM daily.	**12.3°C** Steady difference maintained from 8AM to 5PM daily.	**12.3°C** Steady difference maintained from 8AM to 5PM daily.	**12.3°C** Steady difference maintained from 8AM to 5PM daily.
3	Maximum difference between ambient and outlet temperature (peak period)	**5°C** 11:30AM Corresponding temps of 35°C and 40°C respectively	**8°C** 12:30PM Corresponding temps of 34°C and 42°C respectively	**3°C** 1PM Corresponding temps of 26°C and 29°C respectively	**8°C** 2:30PM Corresponding temps of 33°C and 41°C respectively
4	Maximum difference between ambient and lower chamber temperature (peak period)	**5°C** 11:30AM Corresponding temps of 35°C and 40°C respectively	**6°C** 12:30PM Corresponding temps of 34°C and 42°C respectively.	**3°C** 1PM Corresponding temps of 26°C and 29°C respectively	**7°C** 2:30PM Corresponding temps of 33°C and 40°C respectively
5	Maximum difference between ambient and upper chamber temperature (peak period)	**4°C** 11:30AM Corresponding temps of 35°C and 39°C respectively	**6°C** 12:30PM Corresponding temps of 34°C and 40°C respectively	**3°C** 1PM Corresponding temps of 26°C and 29°C respectively	**7°C** 2:30PM Corresponding temps of 33°C and 40°C, respectively
6	Recorded daily average temperature difference between ambient and outlet temperature	**1.85°C** 8AM-5PM From Table 4.6	**3.74°C** 8AM-5PM From Table 4.6	**1.37°C** 8AM-5PM From Table 4.6	**2.37°C** 8AM-5PM From Table 4.6
7	Recorded daily average temperature difference between ambient and lower chamber temperature	**1.85°C** 8AM-5PM From Table 4.6	**3.58°C** 8AM-5PM From Table 4.6	**1.37°C** 8AM-5PM From Table 4.6	**2.32°C** 8AM-5PM From Table 4.6
8	Recorded daily average temperature difference between ambient and upper chamber temperature	**0.95°C** 8AM-5PM From Table 4.6	**2.95°C** 8AM-5PM From Table 4.6	**1.06°C** 8AM-5PM From Table 4.6	**1.58°C** 8AM-5PM From Table 4.6

APPENDIX C

BILL OF ENGINEERING MEASUREMENT AND EVALUATION (BEME)

S/N	DESCRIPTION	QUANTITY	RATE(N)	AMOUNT (N)
1	100watts poly crystalline PV panel	1	57,000	57,000
2	Sheet of ½ inch ply wood	2 ½	7,200	18,000
3	Length of 2x2 inch hard wood	1	400	400
4	Length of 2x2 inch soft wood	1	300	300
5	672x200x5mm stainless steel mesh	4	4,000	16,000
6	182x182mm stainless steel mesh	2	6,000	12,000
7	DC extraction fan	1	3,000	3,000
8	Cabinet door hinges	1 pair	200	200
9	1 ½ inch nail	2pd weight	400	400
10	Bottle of medium sized wood gum	1	1,500	1,500
11	¼ sheet gauge 22 aluminium sheet	1	2,500	2,500
12	Wood polish	1	2,500	2,500
13	Temperature probes	4	1,200	4,800
14	Thermo-couple temperature reader	1	6,000	6,000
15	12V DC battery	1	3,500	3,500
16	Charge controller	1	3,000	3,000
17	Five point fan switch	1	1,000	1,000
18	Labour aid		25,000	25,000
	TOTAL			**157,100**